

**Essential role of the Notch ligand Delta-like 1
in coronary arteriogenesis and cardiac recovery
after myocardial infarction**

Von der Naturwissenschaftlichen Fakultät
der Gottfried Wilhelm Leibniz Universität Hannover
zur Erlangung des Grades

DOKTORIN DER NATURWISSENSCHAFTEN

Dr. rer. nat.

genehmigte Dissertation

von

MSc Jeanette Woiterski

geboren am 03. August 1981 in Frankfurt (Oder)

2010

Referent: Prof. Dr. Andreas Kispert

Korreferentin: Prof. Dr. Brigitte Schlegelberger

Tag der Promotion: 24. Juni 2010

Dedicated with love

to Roman – without your love, support, and understanding
this thesis would not have been possible.

to Arne – you are the most wonderful son a mother could think of;
your smile makes the sun shine even on the most rainy day.

Hiermit erkläre ich, dass ich die vorliegende Dissertation selbständig verfasst habe. Alle herangezogenen Hilfsmittel, Quellen und Institutionen wurden vollständig an entsprechender Stelle angegeben.

Diese Dissertation wird der Gottfried Wilhelm Leibniz Universität Hannover zur Erlangung des Grades DOKTORIN DER NATURWISSENSCHAFTEN vorgelegt. Die Arbeit wurde nicht schon als Prüfungsarbeit für einen anderen Abschluss an einer anderen Universität oder Institution verwendet.

Jeanette Woiterski

ABSTRACT

The development, homeostasis, and regeneration after injury of the cardiovascular system comprise a huge array of factors and mechanisms which have to work in a temporal and spatial organized fashion. Myocardial infarction is a highly prevalent ischemic disease and multiple studies have demonstrated that only arteriogenesis has considerable ability to fully restore blood flow, which is absolutely critical for the regeneration of all ischemic organs. Notch signalling constitutes an evolutionary conserved pathway and – as activators of the pathway – the Notch ligands play a critical role. The ligand Delta-like 1 (Dll1) has been associated with the maintenance of arterial identity during development and peripheral limb arteriogenesis in the adult. Yet, its function in the coronary vasculature and in cardiac remodelling has not been analyzed to date. This study identifies the Notch ligand Dll1 as critical regulator of developmental/neonatal coronary arteriogenesis and provides evidence that Dll1 is involved in cardiac recovery after myocardial infarction.

To analyse expression and role of Dll1 in adult hearts, Dll1^{+lacZ} reporter mice were the focus of this study, serving as Dll1-lacZ reporter and Dll1 heterozygous strain. In the heart, Dll1 expression was specific for endothelium of coronary arteries >20µm. Coronary artery analysis revealed a reduced number of conductance vessels (>20 µm), but an increased number of arterioles <20 µm. Data suggest a model of the coronary artery phenotype, where reduced levels of Dll1 impairs developmental/neonatal coronary arteriogenesis, becoming evident in the adult by a reduced coronary vessel size in the heart basis and causing a reduced number of vessels reaching more distal heart areas. Altered development of the coronary vasculature caused reduced heart weight and size in Dll1 heterozygous animals, but body weight and size, as well as cardiac function were unchanged. Data demonstrated a relationship where the smaller heart size with concurrent normal body weight is compensated by an elevated ejection fraction, resulting in a normal stroke volume and cardiac output. This finding elucidated the normal 18 month survival of Dll1 heterozygous mice. In addition, monocyte subset analyses demonstrated reduced total monocyte numbers and reduced Ly-6C^{lo} monocytes in Dll1 heterozygous spleen tissue.

To define the role of Dll1 in response to myocardial infarction, mice were subjected to permanent LAD occlusion. Whereas wildtype (WT) control animals demonstrated

functional remodelling and preservation of cardiac function, Dll1 heterozygous animals exhibited features of adverse remodelling: increased inflammation, infarct expansion, progressive dilation and hypertrophy, and complete lack of arteriogenesis, resulting in infarct size enlargement, ventricular dysfunction and progressive mortality. Adverse remodelling in Dll1 heterozygotes was rather based on altered infarct healing mechanisms, than on the extent of the initial ischemic incidence. There is evidence to suggest that impaired arteriogenesis and enhanced inflammation are direct effects of diminished Dll1 levels, whereas infarct expansion, and progressive dilation and hypertrophy are rather downstream effects. These data highlight the importance of Dll1 mediated Notch signalling for correct compensation and functional remodelling to preserve ventricular function after myocardial infarction.

Dll1 was selectively expressed in the heart in arterial endothelium of large coronary arteries and Dll1 expression was upregulated after infarction. However, at least in a setting of myocardial infarction by permanent LAD occlusion, this study provided first evidence that endothelial Dll1 is not the major determinant causing adverse remodelling effects upon absence. Data rather identified an extravascular role of Dll1 in infarct healing, adumbrating a role in the monocyte/macrophage system, but the exact site and mode of action remains an open question which will have to be addressed by future studies.

Keywords: Dll1, arteriogenesis, myocardial infarction

ZUSAMMENFASSUNG

Die Entwicklung, Homöostase und Regeneration des kardiovaskulären Systems umfassen eine enorme Anzahl an Faktoren und Mechanismen, die in zeitlich und räumlich geregelter Art und Weise zusammenwirken müssen. Der Herzinfarkt ist eine weit verbreitete ischämische Erkrankung und vielfache Studien haben belegt, dass Arteriogenese erheblich zur Wiederherstellung des Blutflusses beiträgt. Dies ist absolut kritisch für die Regeneration aller ischämischen Organe. Das Notch Signalsystem ist ein evolutionär erhaltener Signalweg, in dem die Notch Liganden eine kritische Rolle spielen, da sie den Signalweg aktivieren. Der Ligand Delta-like 1 (Dll1) wurde bis jetzt mit der Erhaltung der arteriellen Identität während der Gefäßentwicklung und mit peripherer Arteriogenese im Bein in Verbindung gebracht. Seine Funktion in koronaren Blutgefäßen und im kardialen Remodelling ist bislang noch nicht untersucht worden. Die vorliegende Studie identifiziert den Notch Liganden Dll1 als kritischen Regler in der entwicklungs/neonatalen koronaren Arteriogenese und erbringt Beweise, dass Dll1 an der kardialen Genesung nach einem Herzinfarkt beteiligt ist.

Um die Expression und Rolle von Dll1 im erwachsenen Herzen zu analysieren, standen $Dll1^{+/lacZ}$ Reportermause im Mittelpunkt dieser Studie. Diese fungierten sowohl als Dll1-lacZ Reporter, als auch als Dll1 heterozygoter Mausstamm. Im Herzen wurde die Expression von Dll1 spezifisch im Endothel von Koronararterien nachgewiesen, die größer als 20 μm waren. Eine Analyse der Koronararterien ergab, dass die Anzahl der Konduktanzgefäße ($>20 \mu\text{m}$) signifikant verringert war, während die Anzahl der Widerstandsgefäße ($<20 \mu\text{m}$) erhöht war. Die Daten legen ein Modell des koronaren Phänotyps nahe, in dem verringerte Pegel von Dll1 die koronare Arteriogenese während der Entwicklung und postnatal beeinträchtigen. Dies wird im Erwachsenenalter ersichtlich durch eine reduzierte Größe der Koronararterien in der Herzbasis und hat zur Folge, dass eine verringerte Anzahl an Gefäßen distale Herzareale erreichen. Die beeinträchtigte Entwicklung der Koronargefäße bewirkte eine Reduktion des Herzgewichts und der Herzgröße in Dll1 heterozygoten Tieren, während Körpergröße und -gewicht, sowie Herzfunktion unverändert waren. Daten zeigen einen Zusammenhang in dem das geringere Herzgewicht bei gleichbleibendem Körpergewicht ausgeglichen wird durch eine Erhöhung

der Ejektionsfraktion. Dies führt zu normalem Schlagvolumen und Herzminutenvolumen und erklärt das normale Überleben der Tiere über 18 Monate. Zusätzlich zeigte die Analyse von Monozyten eine verringerte Gesamtzahl der Monozyten, sowie eine verringerte Anzahl von Ly6C^{lo} Monozyten in der Milz von Dll1 heterozygoten Mäusen.

Um die Rolle von Dll1 während der Reaktion auf einen Herzinfarkt zu bestimmen, wurden Mäuse einer permanenten LAD Ligation unterzogen. Während Wildtypiere (WT) funktionelles Remodelling und Erhaltung der kardialen Funktion aufwiesen, zeigten Dll1 heterozygote Mäuse Merkmale von adversen Remodelling: erhöhte Entzündung, Infarktexpansion, fortschreitende Dilatation und Hypertrophie und komplettes Fehlen von Arteriogenese, was im Ganzen eine Ausdehnung der Infarktgröße, ventrikuläre Dysfunktion und progressive Sterblichkeit zur Folge hatte. Adverses Remodelling in Dll1 heterozygoten Tieren war eher auf veränderte Infarktteilung zurückzuführen, als auf das Ausmaß des ursprünglichen, ischämischen Vorfalls. Vieles weist darauf hin, dass beeinträchtigte Arteriogenese und erhöhte Entzündung direkte Folgen verminderter Dll1 Pegel sind, während Infarktexpansion und progressive Dilatation und Hypertrophie eher nachgeordnete Ereignisse sind. Diese Daten zeigen die Wichtigkeit des Dll1 vermittelten Notch Signalweges in ordnungsgemäßer Kompensation und funktionellem Remodelling zur Erhaltung der ventrikulären Funktion nach einem Herzinfarkt.

Dll1 war spezifisch im Endothel großer Koronararterien nachzuweisen und die Expression von Dll1 war nach einem Herzinfarkt erhöht. Die vorliegende Studie konnte jedoch erste Nachweise erbringen (zumindest im Rahmen eines Herzinfarktes durch permanente LAD Ligation), dass nicht endotheliales Dll1 der bestimmende Faktor ist, der bei Fehlen adverses Remodelling bewirkt. Erste Ergebnisse zeigen eher eine extravaskuläre Rolle von Dll1 in der Infarktteilung und deuten auf eine Funktion im Monozyten/Makrophagensystem hin. Der genaue Wirkungsort und die Funktionsweise bleiben allerdings offene Fragen, die von zukünftigen Studien beleuchtet werden müssen.

Stichwörter: Dll1, Arteriogenese, Herzinfarkt

TABLE OF CONTENTS

	Page
SELBSTÄNDIGKEITSERKLÄRUNG.....	4
ABSTRACT.....	5
ZUSAMMENFASSUNG.....	7
TABLE OF CONTENTS.....	9
LIST OF ABBREVIATIONS.....	12
1. INTRODUCTION.....	15-45
1.1 The cardiovascular system.....	15
1.1.1 Cardiogenesis.....	15
1.1.2 Development of blood vessels.....	16
1.1.3 Coronary vessel development.....	17
1.1.4 The adult cardiovascular system.....	19
1.2 Myocardial infarction.....	23
1.2.1 Healing after myocardial infarction – an overview.....	23
1.2.2 Cardiomyocyte death.....	24
1.2.3 Inflammatory response.....	24
1.2.4 The role of extracellular matrix.....	27
1.2.5 Neovascularization after infarction.....	27
1.2.6 LV remodelling and adverse remodelling.....	28
1.3 Notch signalling.....	31
1.3.1 The Notch signalling pathway.....	31
1.3.2 The role of Notch signalling in the cardiovascular system.....	34
1.3.3 Involvement of Notch signalling in immunity mediated wound repair.....	39
1.4 The Notch ligand Delta-like1 (Dll1).....	40
1.4.1 Dll1 – further insights.....	40
1.4.2 Dll1 in the cardiovascular system.....	41
1.4.3 Dll1 involvement in haematopoiesis.....	43
1.5 Objectives and hypotheses.....	45

2. MATERIALS AND METHODS	46-67
2.1 Materials.....	46
2.1.1 Chemicals, reagents, and buffers.....	46
2.1.2 Antibodies.....	48
2.1.3 Primers.....	50
2.1.4 Microscopes and imaging software.....	50
2.2 Mice handling and animal experiments.....	51
2.2.1 Mouse strains, breeding, and handling.....	51
2.2.2 Genotyping.....	53
2.2.3 Knockout induction.....	54
2.2.4 Echocardiography.....	54
2.2.5 Permanent LAD ligation surgery.....	56
2.2.6 Perfusion fixation, tissue embedding, and cryosectioning.....	56
2.3 Basic methodology.....	57
2.3.1 Staining protocols.....	57
2.3.2 RNA isolation and RT-PCR.....	59
2.3.3 Protein isolation and Western blotting.....	60
2.3.4 FACS analysis.....	61
2.4 Data analyses.....	62
2.4.1 Dll1 positive vessel threshold size.....	62
2.4.2 SMA positive vessel quantification.....	62
2.4.3 LAD domain measurement.....	64
2.4.4 Infarct size and other LV parameters.....	64
2.4.5 CSA, myocyte density, and capillary density.....	66
2.4.6 Apoptosis.....	66
2.4.7 Fibrosis.....	67
2.4.8 CD45 positive area.....	67
2.4.9 Statistics.....	67
3. RESULTS	68-100
3.1 Baseline phenotype of Dll1 ^{+lacZ} mice.....	68
3.1.1 Selective endocardial and coronary endothelial expression of Dll1 in coronary arteries >20 μ m.....	68
3.1.2 Dll1 regulates heart size, but does not impair cardiac function.....	69
3.1.3 Dll1 regulates the coronary artery phenotype.....	71

3.1.4	Decreased numbers of total monocyte and Ly-6C ^{lo} monocytes in Dll1 ^{+lacZ} spleen tissue, but not in blood.....	74
3.2	Healing after myocardial infarction in Dll1 ^{+lacZ} animals.....	76
3.2.1	Reduced expression of Dll1 increases infarct size and impairs cardiac function 4 weeks post MI.....	76
3.2.2	Impaired LV remodelling after infarction in Dll1 heterozygous mice.....	79
3.2.3	Increased inflammatory response to MI in Dll1 heterozygous mice.....	88
3.2.4	Dll1 expression is upregulated after myocardial infarction.....	92
3.2.5	Reduced expression of Dll1 impairs arteriogenesis, but not angiogenesis after myocardial infarction.....	95
3.2.6	Altered mortality of Dll1 heterozygous mice after myocardial infarction.....	97
3.3	Not endothelial Dll1 is the major determinant in infarct healing.....	99
4.	DISCUSSION.....	101-113
4.1	Baseline phenotype of Dll1 ^{+lacZ} mice.....	101
4.1.1	Reduced levels of Dll1 do not cause fatal congenital malformation.....	101
4.1.2	Dll1 regulates a heart and coronary artery phenotype.....	101
4.1.3	Dll1 is involved in monocyte generation in the spleen.....	105
4.2	Healing after myocardial infarction in Dll1 ^{+lacZ} animals.....	106
4.2.1	Functional LV remodelling in WT animals post infarction.....	106
4.2.2	Dll1 is upregulated after myocardial infarction.....	108
4.2.3	Dll1 heterozygous animals exhibit features of adverse remodelling after myocardial infarction.....	109
4.2.4	Not endothelial Dll1 is the major determinant in infarct healing.....	112
5.	CONCLUSION.....	114
6.	REFERENCES.....	115-126
APPENDIX		
	Publications.....	127
	Acknowledgements.....	129
	Curriculum Vitae.....	130

LIST OF ABBREVIATIONS

%	percent
°C	degree Celsius
AAR	area-at-risk
ANK	ankyrin domain
AP	alkaline phosphatase
APS	ammoniumpersulphate
bHLH	basic helix-loop-helix
BL	baseline
bp	base pairs
BPM	beats per minute
BSA	bovine serum albumin
CO	cardiac output
COUP-TFII	chicken ovalbumin upstream promoter-transcription factor II
CSA	cross-sectional area
CSL	CBF/Su(H)/LAG-1
CTRL	control
DAPI	4',6-diamidin-2-phenylindol
ddH ₂ O	double deionized water
Dll1	Delta-like 1
Dll4	Delta-like 4
DMSO	dimethyl sulfoxide
DNA	deoxyribonucleic acid
dNTP	deoxynucleotidtriphosphate
DSL	Delta/Serrate/LAG-2
ECM	extracellular matrix
EDTA	ethylene diamine tetraacetic acid
EGTA	ethylene glycol tetraacetic acid
EF	ejection fraction
EGF	epidermal growth factor

EMT	epithelial-to-mesenchymal transformation
EPCDs	epicardium derived cells
epic. circ.	epicardial circumference
EtOH	ethanol
E x	embryonic day x (mouse)
FACS	fluorescence activated cell sorting
FCS	foetal calf serum
FGF	fibroblast growth factor
FITC	fluorescein isothiocyanate
h	hour
HRP	horseradish peroxidase
ICD	intracellular domain
IF	immunofluorescence
IH	immunohistochemistry
Jag1	Jagged 1
Kdr	=VEGFR2
KO	knockout
LAD	left anterior descending artery
LNR	Lin12/Notch repeats
LV	left-ventricular
LVED	left-ventricular end-diastolic
mA	milliampere
MAML	mastermind-like
MI	myocardial infarction
MI xd	day x after myocardial infarction
min	minutes
MMP	matrix metalloproteinases
MP	milk powder
n=x/y	animal numbers WT vs. Dll1 ^{+lacZ}
NF-κB	nuclear factor – kappa B
NICD	Notch intracellular domain
NLS	nuclear localization sequence
Nrp1	neuropilin-1
NRR	negative regulator region

PAGE	polyacrylamide gelelectrophoresis
PBMC	peripheral blood monocytes
PBS	phosphate buffered saline
PCR	polymerase chain reaction
PDGF	platelet derived growth factor
PE	proepicardium
PFA	paraformaldehyde
RBP-J	= CSL
RNA	ribonucleic acid
ROS	reactive oxygen species
rpm	rounds per minute
RT	reverse transcription
SDS	sodium dodecylsulfate
sec	seconds
SMA	smooth muscle α -actin
SMCs	smooth muscle cells
SV	stroke volume
TAE	tris acetate buffer
TAM	tamoxifen
TBS-T	tris-buffered saline – tween-20
TEMED	N,N,N',N'-tetramethylethylenediamine
TIMP	tissue inhibitors of metalloproteinases
TTC	triphenyltetrazolium chloride
V	volt
VECad	vascular endothelial cadherin
VEGF	vascular endothelial growth factor
VEGFR2	VEGF receptor 2
WB	western blot
WT	wildtype

1. INTRODUCTION

The development, homeostasis, and regeneration after injury of the cardiovascular system comprise a huge array of factors and mechanisms which have to work in a temporal and spatial organized fashion (Darland and D'Amore, 2001). Notch signalling constitutes an evolutionary conserved pathway which plays a pivotal role in the cardiovascular system; as activators of the pathway the Notch ligands play a critical role.

In order to provide the reader with all background information needed for an informed understanding of this dissertation, this chapter will give an overview of the cardiovascular system and healing mechanisms after myocardial infarction. Notch signalling and the ligand Dll1 will be reviewed with more detail to the currently available literature.

1.1 The cardiovascular system

1.1.1 Cardiogenesis

The development of the heart follows the same pattern in all vertebrates. The organ is formed from precardiac cells which are arranged in bilateral clusters in the anterior lateral plate mesoderm. The bilateral fields merge to form the so-called cardiac crescent which then fuses along the midline and forms the primitive heart tube. This straight heart tube contains an external myocardial and an internal endocardial layer and also holds a polarity in which the prospective tissues of the aortic sac, outflow tract, right ventricle, left ventricle, and atria are present in anterior to posterior order along the tube. During the next phase, the heart tube undergoes a rightward looping process (cardiac looping) which is necessary for the alignment of the inflow and outflow tracts. The final 4-chambered structure of the heart is achieved by formation of the valves and septa. These originate from a subset of endocardial cells that line the interior of the heart at specific locations (so-called cardiac cushions). These cells undergo a transition to mesenchymal tissue and differentiate to the fibrous tissue of the valves and septa. The foetal heart is already connected to the pulmonary trunk and aorta to ensure the separate pulmonary and systemic blood circulation after birth (Darland

and D'Amore, 2001; Kirby and Waldo, 2002; Zaffran and Frasch, 2002; Buckingham *et al.*, 2005; Chen *et al.*, 2005).

1.1.2 Development of blood vessels

The vascular system develops in the embryo, when its nutritional needs are not longer met by diffusion. The blood vessels form independently and do not sprout from the heart; in fact, the heart is connected afterwards and it does not begin to pump until the vascular system has established its first circulatory loops (Gilbert, 2006).

Blood vessel formation

During development, blood vessels form by temporally separate processes – vasculogenesis, angiogenesis and arteriogenesis. During vasculogenesis hemangioblasts from the mesoderm congregate in blood islands: the inner cells of the islands differentiate to become hematopoietic cells, while the outer cells become angioblasts. Subsequently, angioblasts multiply and differentiate into endothelial cells which then assemble to form a primary vascular plexus (Figure 1.1 A). Important factors during vasculogenesis include fibroblast growth factor (FGF) and vascular endothelial growth factor (VEGF) which are required for hemangioblast generation from the mesoderm (FGF) and enable angioblast differentiation, and assembly and patterning of vessels (VEGF). In the following, the primary vascular plexus is remodelled by angiogenesis. Through sprouting, intussusception, recruitment of supporting cell types, and selective pruning of some vessel connections, a mature vascular network is generated. Angiogenesis is regulated by a number of signalling pathways, including the VEGF pathway, the TGF- β pathway, the Angiopoietin/Tie receptor pathway, the ephrin/Eph receptor pathway and the Notch signalling pathway (Risau and Flamme, 1995; Risau, 1997; Carmeliet, 2000; Iso *et al.*, 2003; Limbourg *et al.*, 2005; Gilbert, 2006). After the onset of circulation, the vascular system is shaped by physiologic factors (like flow and shear stress). Accordingly, mature arteries are formed by arteriogenesis which includes pericyte and smooth muscle cell migration and differentiation, basal lamina modifications, and elastogenesis in elastic arteries (Risau, 1997; Carmeliet, 2000; Smart *et al.*, 2009).

Angiogenesis

During sprouting angiogenesis endothelial cells are stimulated by growth factors which induces the production of proteases (Figure 1.1 A). The following degradation of the

extracellular matrix (ECM) allows endothelial cells to invade the surrounding tissue, where they migrate and proliferate to form a sprout. The sprout then elongates and a lumen is formed, followed by the recruitment of periendothelial cells as pericytes and smooth muscle cells (SMCs) which is critical for vessel stability. The process of non-sprouting angiogenesis – or intussusception – describes the splitting of pre-existing vessels to form new vessels. The emerging vascular plexus is remodelled to a system with small and large vessels, resulting in a pattern resembling a tree - therefore, this process is called pruning (Risau, 1997; Gerwins *et al.*, 2000).

Angiogenesis is characterized by strict regulation. The vessels develop in an organized fashion to the need of nutrients and oxygen in a tissue. Once the need is met, production of the stimulatory factor terminates and endothelial cells become quiescent (Gerwins *et al.*, 2000).

Arterial/venous specification

Already before the onset of circulation, blood vessels are specified as artery or vein. Although in the past physiologic factors from the circulation were believed to determine vessel identity, evidence now shows that at least some steps of genetic control precede regulation by hemodynamic factors (Torres-Vásquez *et al.*, 2003; Adams, 2003). Actually, already the primary plexus contains two different kinds of endothelial cells: arterial endothelial cells expressing ephrin-B2 and venous endothelial cells expressing EphB4 (an ephrin-B2 receptor) (Wang *et al.*, 1998), representing precursors of arteries and veins, respectively. Bidirectional signalling of ephrin-B2 – EphB4 interaction facilitates the establishment of an arterial-venous boundary by restriction of endothelial cell migration. Thereby signalling ensures that arterial capillaries connect only to venous ones and that only capillaries of the same type fuse to create larger vessels (Adams, 2003; Torres-Vásquez *et al.*, 2003; Gilbert, 2006; Swift and Weinstein, 2009).

1.1.3 Coronary vessel development

At an early stage of heart development – when the primitive heart tube has been formed, myocardial expansion starts and the heart transitions to form a multilayered organ – diffusion does no longer satisfy tissue needs and the heart requires a committed vascular system. Coronary vessel development (Figure 1.1 C) involves vasculogenesis, angiogenesis and arteriogenesis.

The major origin of the coronary vasculature is the proepicardium (PE), a structure that is formed on the surface of the heart and is composed of PE mesothelial cells. These cells migrate to the developing heart and envelope its surface, forming the epicardium and a matrix-rich subepicardial space. During the process of epicardium expansion and migration over the heart, a subpopulation of the epicardial cells separate and undergo epithelial-to-mesenchymal transformation (EMT). Epicardial EMT starts at the base of the heart and moves towards the apex. The generated epicardium derived cells (EPDCs) populate the subepicardial space and the myocardium; they give rise to coronary SMCs, pericytes, fibroblasts and cardiomyocytes. However, the origin of coronary endothelial cells is controversially discussed: different studies in various model organisms showed endothelial precursors originating not only from EPDCs, but also from angioblasts in the PE and subepicardial space, from invagination of the endocardium, or migratory cell populations coming from another tissue, like the liver. Yet, independent of origin, endothelial precursor cells and EPDCs in the subepicardial space migrate over the heart and into the myocardium. The cells never come into contact with the heart lumen, as coronary vessels will receive blood from the aorta and not from the heart, and as blood flow from the lumen into the developing myocardium without an established vasculature would be disastrous. The endothelial precursors coalesce and form a primary capillary vascular plexus, followed by remodelling and patterning processes to form a network. Vessel growth is directed towards the base of the heart, eventually connecting to the aorta (aorta and the aortic arches are derived from the neural crest) and onset of perfusion. Upon perfusion, capillaries are remodelled to arteries by arteriogenesis: wall matrix enrichment, and EPDC recruitment to form SMCs and pericytes. Recruitment and differentiation proceeds in a proximal-to-distal direction, starting at the coronary ostia (to form the main trunk of the coronary arteries) and progressing towards the heart apex (forming the small precapillary arterioles) (Reese *et al.*, 2002; Luttun and Carmeliet, 2003; Fernández, 2004; Tomanek, 2005; Smart *et al.*, 2009). Furthermore, once flow is established, remodelling of the system has to take place to establish the hierarchy of the arterial tree. Thereby, flow through the coronary arterial system serves as stimulus and initiates the increase of diameter of the main coronary arteries and provokes the regression of selected vascular channels by apoptosis (Figure 1.1 D) (Tomanek, 2005).

The coronary vasculature continues to grow after birth to account for the increasing needs of a still growing heart and organism, until an adult coronary system is established (Luttun and Carmeliet, 2003; Smart *et al.*, 2009).

As described, coronary vasculature formation involves a series of complex processes and a number of molecular factors and mechanisms regulate each of these steps. Among many other factors, Gata4 has been implicated with the formation of the PE (Watt *et al.*, 2004) and mice deficient for Tbx5 or VCAM fail to form the epicardium from the PE (Hatcher *et al.*, 2004; Kwee *et al.*, 1995). Thymosin β -4 is involved in vasculogenesis and EPDC migration (Smart *et al.*, 2007), and FGF-2 and VEGF are the best characterized regulators of coronary angiogenesis (Tomanek and Zheng, 2002; Carmeliet *et al.*, 1999). Principal pathways of coronary arteriogenesis involve PDGF (platelet derived growth factor) and Notch signalling (Smart *et al.*, 2009).

1.1.4 The adult cardiovascular system

Circulation and vessel morphology

The cardiovascular circulation plays a number of roles in the adult: not only does this include blood, metabolite and waste product transport, but also serves hormonal communication and rapid deployment of immune responses throughout the body.

In the adult, deoxygenated blood enters the heart via the right atrium and is pumped by the right ventricle to the lungs through the pulmonary trunk. Oxygenated blood returns to the left atrium and is pumped through the aorta to the systemic circulation by the left ventricle. The following hierarchical system of elastic arteries, muscular arteries, arterioles, capillaries, venules and veins ensures the most effective transport obeying physical laws of fluid movement (Buckingham *et al.*, 2005; Gilbert, 2006; Eble and Niland, 2009).

Arteries and veins are both composed of an inner endothelial layer (tunica intima), internal elastic tissue, smooth muscle cell layer (tunica media), external elastic tissue and fibrous connective tissue (tunica adventitia) (order from inside to outside). While arteries withstand flow forces with thick layers of SMCs and extracellular matrix, veins are adapted to lower pressure with thin walls and valves to prevent backflow of blood. Capillaries are stabilized by pericytes (Adams, 2003; Torres-Vázquez *et al.*, 2003).

Coronary artery anatomy

The coronary arteries originate from the aorta, just above the aortic valve: the left coronary artery and the right coronary artery (Figure 1.1 E). They travel well-defined routes in the epicardium along the heart and give rise to branches that penetrate the myocardium. The left coronary artery supplies blood to the left ventricle and left atrium; it divides into the left circumflex artery and the left anterior descending artery (LAD). The circumflex encircles

the heart muscle, supplying the lateral and back side of the heart, the LAD supplies the front left side of the heart. The right coronary artery supplies blood to the right ventricle, right atrium, sinoatrial node and the atrioventricular node. The venous return courses over the heart surface with accompanying arteries (Reese *et al.*, 2002).

The coronary artery tree of the mouse is different from human, particularly with regard to the blood supply of the septum. Analyses of mice (C57BL6/J background) showed a variable origin of the septal coronary artery from the right coronary artery (55%), the left coronary artery (35%) and dual origins from both (10%) (Salto-Tellez *et al.*, 2004). However, bifurcation of the left coronary artery to the LAD and the circumflex artery was invariant and a constant ligation of the LAD immediately below the left auricular level showed a statistically significant reproducible infarct size (Salto-Tellez *et al.*, 2004).

Neovascularization and arteriogenesis

In contrast to active vessel growth in the embryo and neonate, blood vessels and endothelium acquire a quiescent state in the adult. Only upon stress or pathologic conditions, does the vascular bed expand by vasculogenesis, angiogenesis, and arteriogenesis (meaning in the adult, the maturation of pre-existing arterioles to large muscular collateral arteries) (Luttun and Carmeliet, 2003; Simons, 2005; Stavrou, 2008).

Restoration of blood flow is absolutely critical for regeneration after myocardial infarction and for all ischemic organs in general. Although angiogenesis is induced after ischemia, its contribution to blood flow regeneration is limited as only a 2-3x increase in blood flow can be achieved and as capillaries – lacking a muscular wall – are not designed for long-distance transport tasks. Only arteriogenesis has a considerable ability to fully restore blood flow, achieving a 20-30x increase of flow; it describes an active growth rather than passive dilation due to changed blood pressure (Deindl and Schaper, 2005; Simons, 2005; Heil *et al.*, 2006).

Rather than ischemia, initial triggers of arteriogenesis are physical forces such as increased shear which is induced by redirection of blood flow into pre-existing arteriolar connections that interconnect proximal and distal side branches of an occluded artery (Deindl and Schaper, 2005; Heil *et al.*, 2006). The increased fluid shear stress activates the endothelium which starts to signal (Figure 1.1 B). Signalling promotes adhesion and invasion of monocytes, which then leads to the production of growth factors and proteases. In the following, the ECM is lysed and elastolysis takes place. The corresponding increase in circumferential wall tension provides a proliferative stimulus for SMCs which change their

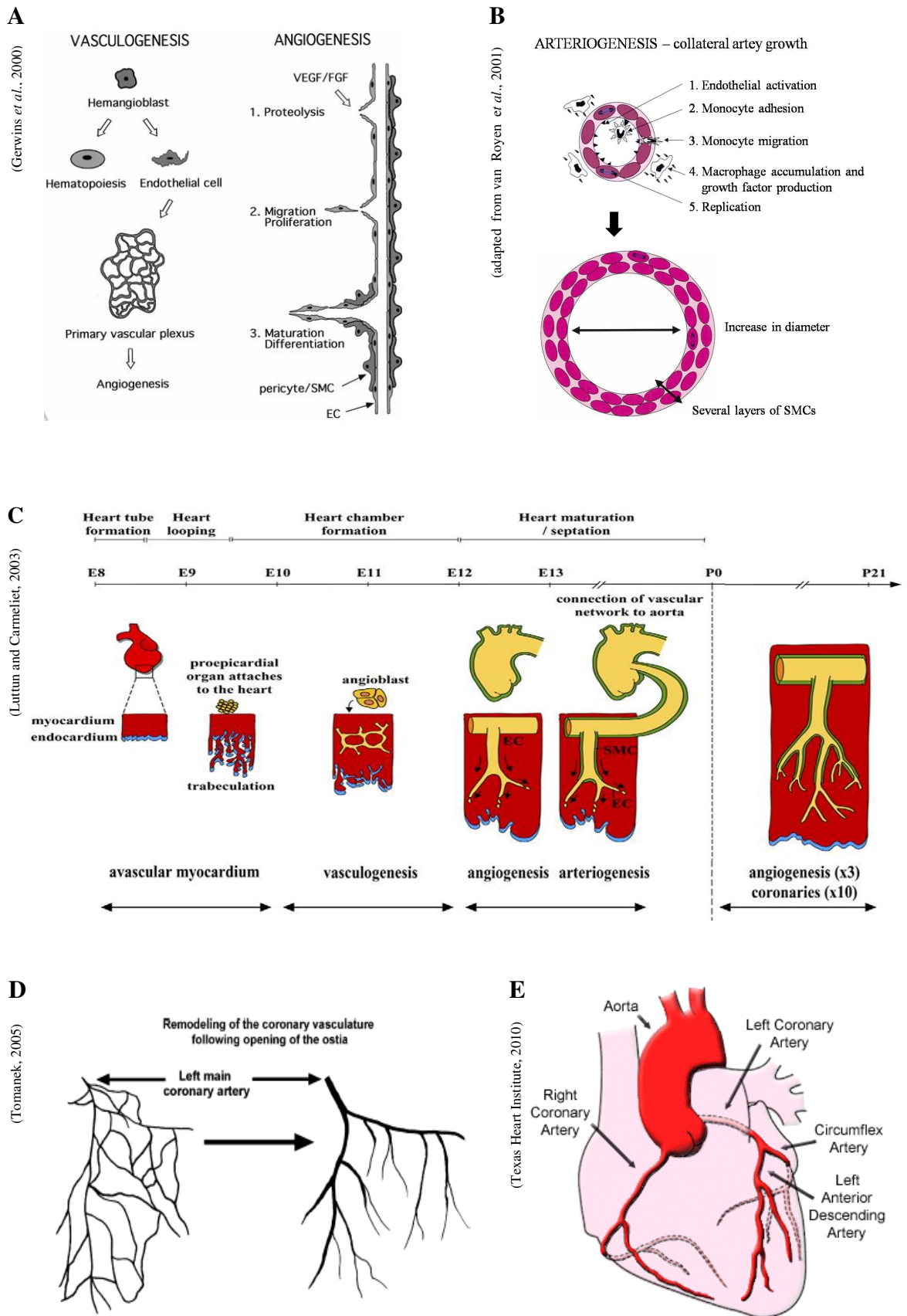
phenotype, become mobile, move towards the intima and proliferate. Proliferation is directed towards the media and outer layers, resulting in a larger vessel. As a consequence of vessel growth, shear stress is reduced and endothelial activation and signalling stops. SMC proliferation continues until wall thickness has reached values comparable with normal circumferential wall tension (Schaper, 2004).

Heart function

Heart function is described by multiple factors. The stroke volume (SV) describes the volume of blood ejected per beat during systole. The stroke volume depends on the force of contraction which itself is influenced by cardiomyocyte contractility. However, the ventricle does not eject the whole blood volume it contains; the portion ejected is called the ejection fraction (EF). The cardiac output (CO) describes the volume of blood flowing through the systemic circulation. It is calculated by multiplication of the heart rate with the stroke volume (Huether and McCance, 2000).

- for figure 1.1 refer to the following page 22 -

Figure 1.1 The cardiovascular system. (A) Schematic outline of vasculogenesis and angiogenesis. In vasculogenesis endothelial cells form the primitive vascular plexus. The following angiogenesis includes protease induction, migration, proliferation and differentiation (adapted from Gerwins *et al.*, 2000). **(B) Schematic outline of arteriogenesis in the adult (growth of collateral arteries).** In the adult, quiescent endothelium in collateral arteriolar connections becomes activated by shear stress and the process of arteriogenesis is activated, forming large collateral conductance arteries with several layers of smooth muscle cells (adapted from van Royen *et al.*, 2001). **(C) Schematic representation of heart and coronary development in the mouse.** The primitive heart tube is supplied with oxygen by diffusion. After heart looping, the epicardium proliferates and migrates over the heart, closely followed by the formation of a primitive vasculature. The primitive vasculature expands by sprouting of new vessels from pre-existing ones and is transformed into a more organized network with smaller and larger vessels. Once the network connects to the aorta, the vessels become invested with a smooth muscle cell coat and a fibroblast-rich adventitia (adapted from Lutun and Carmeliet, 2003). **(D) Remodelling of the coronary vasculature after opening of the ostia.** Prior to formation of the ostia the vasculature consists of endothelial-lined channels with numerous anastomoses (illustration on left). When coronary flow is established, the vasculature remodels by recruiting (1) smooth muscle cells to form arteries; (2) increase the diameters of the main channels, and (3) eliminating many anastomotic channels via apoptosis (illustration on right) (adapted from Tomanek, 2005). **(E) Coronary artery anatomy.** Schematic representation showing the course of the left and right coronary arteries (adapted from Texas Heart Institute, 2010).



1.2 Myocardial infarction

1.2.1 Healing after myocardial infarction – an overview

Myocardial infarction (MI) is induced by coronary artery occlusion, triggering numerous responses at the cellular and molecular level (Tiyyagura and Pinney, 2006). Infarct healing can be divided into three overlapping phases: (1) inflammation, (2) proliferation and (3) maturation (Frangogiannis, 2006). In humans, repair requires up to two months; infarcts in smaller experimental animals such as mice heal substantially faster (Laflamme and Murry, 2005).

The sudden ischemic condition after infarction leads to cardiomyocyte death throughout the region supplied by the affected artery. (1) Cardiomyocyte necrosis triggers a vigorous inflammatory response: activation of chemokines and cytokine cascades leads to the recruitment of leukocytes into the infarcted area, and neutrophils and macrophages clear the wound of cell and matrix debris. (2) In the following, activated macrophages direct the formation of granulation tissue by releasing cytokines and growth factors. At this stage, the inflammatory response is finished and expression of inflammatory mediators is suppressed. The granulation tissue is rich in proliferating fibroblasts and endothelial cells. Consequently, neovasculature is formed and activated myofibroblasts produce ECM proteins. (3) At the end, the granulation tissue matures to form scar tissue; therein the remaining viable myocytes are realigned and attached in the collagen scar matrix (Pfeffer, 1995; Laflamme and Murry, 2005; Frangogiannis, 2006; Frangogiannis, 2008).

In addition, infarct healing is also associated with changes in ventricular architecture and geometry. Cardiac remodelling is initially necessary to compensate for the loss of cardiomyocytes and decrease of contractile function. It describes the normal adaptive changes to preserve ventricular function (i.e. necrosis and apoptosis, inflammation, fibrosis, matrix modulation, hypertrophy and compensating dilation, angiogenesis and arteriogenesis). However, the extent of remodelling is proportional to the mass of infarcted myocardium. Especially after large infarcts profound changes take place, involving massive chamber dilation, wall thinning, cardiac hypertrophy and increased spherical shape of the ventricle, resulting in progressive contractile dysfunction and chronic heart failure. This process of adverse cardiac remodelling is not only influenced by the initial infarct size, but also by alterations in the healing process (Tiyyagura and Pinney, 2006; Whelan *et al.*, 2007; Frangogiannis, 2008).

1.2.2 Cardiomyocyte death

In the mammalian heart, a constant supply of oxygen is essential for the maintenance of cellular processes and, consequently, cardiac function and viability. Thus, an ischemic myocardial insult triggers cardiomyocyte death (Figure 1.2 A) within the infarct zone initially via necrosis. Necrosis describes the death of cells by oxygen/nutrient deprivation so that cellular functions cannot be sustained and a general unorganized breakdown of cell organelles takes place; necrosis initiates a broad inflammatory response. The acute necrotic phase is followed by cycles of cell death in the border zone and the remote myocardium which are mainly attributed to apoptosis, but necrosis and autophagy take place as well. (Apoptosis is an energy requiring process, directed by a highly structured gene program to shut down cellular functions and removal of the cell with minimal consequences for the surrounding tissue. Autophagy is a response to cell starvation under conditions of chronic metabolite or other stress and involves the degradation of most long-lived proteins and some organelles.) The third phase of cell death is characterized by a general loss of cardiomyocytes in the remote myocardium and is predominantly associated with autophagy (Dorn and Diwan, 2008).

1.2.3 Inflammatory response

Innate immunity

After myocardial infarction, the discharge of intracellular components from necrotic cells triggers a profound immune response by activating innate immune processes, including complement activation, reactive oxygen species (ROS) generation, and Toll-like receptor - mediated pathways which initiate the nuclear factor (NF)- κ B system (Frangogiannis, 2008; Frantz *et al.*, 2009).

The NF- κ B system is an essential element in the control of cytokine, chemokine and adhesion molecule expression in the ischemic myocardium. The system is activated by numerous agents including cytokines and ROS. Genes regulated by the NF- κ B family of transcription factors are involved in the inflammatory response, cell adhesion and growth control. Animals studies on mice harbouring different mutations of proteins involved in NF- κ B signalling showed contradictory findings, i.e. an injurious role, as well as a cytoprotective role. These results reflect the diversity of cellular processes and molecular pathways affected by the system. NF- κ B is one of the most important regulator of pro-inflammatory gene expression, but it is also involved in cell survival, has proliferative

effects and influences ECM modulation by regulating MMP (matrix metalloproteinases) synthesis (Frangogiannis, 2008).

After activation of the innate immune system, inflammatory mediators are released and inflammatory cells are attracted to the ischemic zone (Frantz *et al.*, 2009).

Humoral immune response

Cytokine cascades have been shown to be activated in infarcted myocardium and the proinflammatory cytokines TNF- α , IL-1 and IL-6 are consistently found in experimental models of MI. Complement, ROS and NF- κ B stimulate cytokine synthesis in resident and blood-derived cells. TNF- α exhibits various functions, including the suppression of cardiac contractility, enhancement of cardiomyocyte apoptosis and the stimulation of expression of other cytokines and chemokines. It triggers adhesion molecule expression by leukocytes and endothelial cells, and regulates ECM modulation via the reduction of collagen synthesis and enhancement of MMP activity in fibroblasts. IL-1 signalling plays a role in the activation of inflammation and fibrogenic pathways and might be involved in adverse remodelling processes. IL-6 is expressed in mononuclear cells and cardiomyocytes in the infarcted area. It exhibits effects on cardiomyocytes by promoting cardiac hypertrophy, but also by protecting myocytes from apoptosis (Frangogiannis, 2008).

A further feature of the inflammatory phase after MI is the induction of chemokines. Chemokines comprise a family of small polypeptides and are divided into subfamilies based on their cysteine residues (Frangogiannis, 2008). They are synthesized by various cells of the immune system and by non-immune cells including endothelial cells. Chemokines function primarily as chemoattractants for phagocytic cells. Some chemokines appear to be involved in angiogenesis mediation (Frantz *et al.*, 2009).

Cellular immune response

Activated platelets are the first cells to be recruited. They aggregate in the wound, contribute to the formation of the fibrin-based provisional matrix and release various chemokines, cytokines and growth factors. They initiate the complement system and direct the inflammatory response to the site of injury (Frangogiannis, 2008).

Next to the platelets, leukocytes infiltrate the injured myocardium; there exists a correlation between the level of leukocyte infiltration and extension of the infarcted area (Bodi *et al.*, 2008). Neutrophils are recruited early after infarction and release oxidants and proteases, secrete mediators of cell recruitment, and phagocytose cell debris and dead cells (Frantz *et al.*, 2009). In addition, neutrophils contribute to initial ECM degradation by MMP

production. The migration of neutrophils into the infarcted zone is based on adhesive interactions with activated vascular endothelial cells and diapedesis through the vessel wall (Frangogiannis, 2008).

As neutrophil numbers decline, monocytes infiltrate the infarcted myocardium from capillaries and become the predominant phagocytic cell type in the wound. After monocyte recruitment, these blood-derived cells differentiate and mature to macrophages. This process is not well investigated, but probably involves the growth factors M-CSF and GM-CSF. Differentiated macrophages are responsible for the clearance of dead cells and debris, and apoptotic neutrophils and cardiomyocytes. They produce MMPs and TIMPs, and cytokines and growth factors, thereby regulating ECM modulation, growth of fibroblasts and angiogenesis (Frangogiannis, 2008).

Another important finding was that peripheral blood monocytes are a heterogeneous population and two monocyte subsets have been identified (Geissmann *et al.*, 2003) in a murine model which participate in the infarct response (Nahrendorf *et al.*, 2007). The group showed that the modulation of the chemokine expression profile after MI sequentially and actively recruits Ly-6C^{hi} (Gr1^{hi}CCR2⁺CX₃CR1^{lo}) and Ly-6C^{lo} (Gr1^{lo}CCR2⁻CX₃CR1^{hi}) monocytes. (Ly-6C/G (Gr1) is a monocyte marker, CX₃CR1 and CCR2 are chemokine receptors.) Ly-6C^{hi} monocytes dominate early in the inflammatory phase, bringing about phagocytic, proteolytic and inflammatory functions; Ly-6C^{lo} monocytes dominate rather in the proliferative phase and show enhanced healing properties via myofibroblast accumulation, angiogenesis, and collagen deposition (Nahrendorf *et al.*, 2007).

Mast cells are multifunctional resident cells which are mainly localized close to vessels in the heart. Mast cells produce and release a wide variety of inflammatory and pro-fibrotic agents, like TGF- β , FGF, VEGF, and gelatinase A and B; these factors are involved in fibroblast growth, ECM modulation and angiogenesis (Frangogiannis, 2008).

Cardiac fibroblasts are present in normal myocardium and proliferate and infiltrate the wound after MI. Fibroblasts in the infarct undergo a differentiation to myofibroblasts which express contractile proteins (as α -smooth muscle actin (SMA)) and exhibit an enhanced migratory and proliferative activity (Porter and Turner, 2009). Myofibroblasts mediate scar contraction (Jugdutt, 2003) and are the main source of collagen mRNA in the healing infarct; they appear during the formation of the granulation tissue and become apoptotic during maturation of the scar (Frangogiannis, 2008).

Resolution of the inflammatory infiltrate

After the inflammatory phase, chemokine and cytokine synthesis is inhibited, suppressing continuous leukocyte recruitment and injury. This inhibition is crucial for optimal healing which requires the resolution of the inflammatory infiltrate and transition to fibrous tissue deposition (Frangogiannis, 2008).

1.2.4 The role of extracellular matrix

Extracellular matrix proteins not only provide structural and mechanical support, but also modulate cell signalling. After infarction, the ECM undergoes constant changes, thereby modulating the microenvironment and regulating cell behaviour. During the inflammatory phase, normal ECM is degraded and a fibrin-based transient matrix is formed. This matrix enables the migration and proliferation of infiltrating inflammatory, endothelial and stromal cells. Afterwards, the provisional matrix is lysed by proteolytic enzymes which are produced by the cells of the granulation tissue. The formed matrix is an organized network consisting of fibronectin and hyaluronan. As the wound matures, collagen is deposited and cross-linked to stabilize the scar and increasing the strength of the wound (Frangogiannis, 2006). Further to structural matrix proteins (like collagen and fibronectin), matricellular proteins (like tenascin-C, thrombospondins, and osteopontin) are transiently expressed in healing infarcts. They do not have a structural function, but modulate cell behaviour by activating signalling pathways through binding of specific cell-surface receptors (Frangogiannis, 2006).

Remodelling of the ECM is controlled by MMPs, which degrade matrix proteins and are inhibited by TIMPs (tissue inhibitors of metalloproteinases). Latent MMPs are present in normal heart tissue; they are upregulated and activated after infarction. Cytokines play a role in regulating MMP production by inflammatory cells and fibroblasts infiltrating the infarct zone. A balance of MMPs and TIMPs is critical for the modulation of the extracellular matrix (Frangogiannis, 2006).

1.2.5 Neovascularization after infarction

Formation of new blood vessels is critical for supplying the healing myocardium with oxygen and nutrients. Therefore, angiogenesis and arteriogenesis are an essential component of wound healing. After myocardial infarction, a network of neovessels is formed by

angiogenesis in the infarct region, as well as in the border zone to nourish the endangered tissue. In addition, the occlusion of a major artery provokes a change in blood flow, taking the path of lowest resistance via the collateral vessels into the periphery. Corresponding increased blood flow, hydrostatic pressure and shear stress induce arteriogenesis in the collaterals. As mentioned before, even a dense network of capillaries is not sufficient to substitute the flow of an occluded artery, only arteriogenesis can provide adequate perfusion. However, both are needed for infarct healing, as the capillary network in the infarct and border zone requires flow from the larger arteries upstream of the ischemic area, and in turn, large collateral arteries require a functional capillary network for efficient nutrient distribution (Markkanen *et al.*, 2005).

1.2.6 LV remodelling and adverse remodelling

The sudden deprivation of cardiomyocytes after myocardial infarction leads to an abrupt loss of functioning myocardium and, consequently, decline in cardiac function (Figure 1.2 B). In order to preserve ventricular function at least temporarily, acute compensation includes the increase in left-ventricular volume – achieved by cardiomyocyte lengthening – which enhances contractility in the noninfarcted myocardium. This principle is based on the Frank-Starling mechanism which describes a length-tension relationship in the heart and states that the greater the end-diastolic volume, the greater the stroke volume. Increased left-ventricular volume, however, also leads to intensified wall stress. This is counteracted by scar formation in the infarcted area and by cardiomyocyte hypertrophy in the remote myocardium (Whelan *et al.*, 2007). These processes can be considered beneficial or adaptive (Ferrari *et al.*, 2009) in the infarct healing process and are summarized in the term ventricular remodelling (or cardiac remodelling) (Figure 1.2 B).

Nonetheless, progressive – or chronic – remodelling is a key factor in the pathophysiology of ventricular dysfunction after myocardial infarction (Zornoff *et al.*, 2009); in this context the term adverse remodelling is used¹. The major determinant of this process is the initial infarct size (Whelan *et al.*, 2007), but also alterations in the infarct healing process can negatively influence the adaptive processes and cause dilation and dysfunction (Jugdutt, 2003; Ferrari *et al.*, 2009; Hori and Nishida, 2009; Zornoff *et al.*, 2009). One of the first

¹ For clarification of terminology: this thesis will continuously use “remodelling” in connection with beneficial, adaptive processes and “adverse remodelling” with regard to maladaptive processes leading to cardiac dysfunction. However, these terms are not universally applied throughout the literature. Although most studies and reviews confirm that “remodelling” is initially adaptive, the term is rather used to describe the progressive, pathological processes.

changes in adverse remodelling is infarct expansion: during the process of resorption of necrotic tissue and before extensive collagen deposition takes place, the tensile strength of the affected region is transiently reduced and the area most vulnerable. During this period the infarcted area can thin and elongate. This event is not caused by additional myocardial necrosis, but is a consequence of slippage between muscle bundles and cell rupture, leading to reduced myocyte numbers per wall thickness (Pfeffer and Braunwald, 1990; Tiyyagura and Pinney, 2006). Late modulations of adverse remodelling include responses of the remote myocardium. The initial compensative changes of heart architecture also induce increased loading conditions on the viable myocardium. This increase promotes further enlargement and hypertrophy of the healthy myocardium (Pfeffer, 1995). In addition, ECM responds to mechanical overload with an increase in collagen deposition, resulting in increased ventricular stiffness and dysfunction (Jugdutt, 2003; Hori and Nishida, 2009). In consequence, the whole ventricle dilates and a change in shape from ellipsoid to spherical is evident; the ventricle is thin-walled and exhibits poor contractile function. Reduced function becomes apparent by decreased ejection fraction; stroke volume and cardiac output cannot longer be compensated and decline as well. Consequently, adverse remodelling is associated with chronic heart failure in the long run (Whelan *et al.*, 2007; Ferrari *et al.*, 2009; Hori and Nishida, 2009).

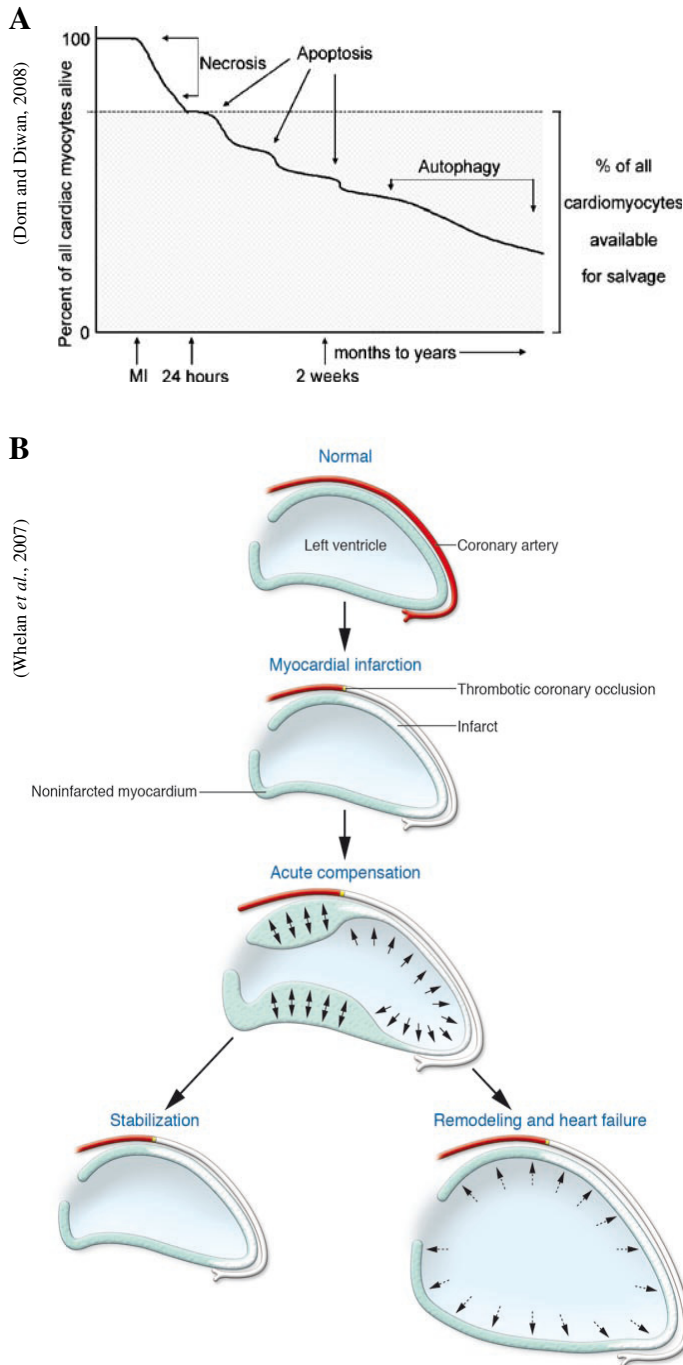


Figure 1.2 Processes involved in myocardial infarction. (A) Schematic depicting cell death after myocardial infarction. Following the ischemic insult in myocardial infarction, necrosis is the predominant form of cell death in the ischemic myocardium, leading to cardiac myocyte loss. This is followed by waves of programmed cell death or apoptosis in the subacute phase as the predominant form of cardiomyocyte loss. In the chronic phase, autophagy emerges as the predominant mechanism of cardiomyocyte loss. The shaded area represents potentially salvageable myocardium by ‘cellular resuscitation’. Timeline for human processes (adapted from Dorn and Diwan, 2008). (B) **Postinfarct myocardial remodelling.** Thrombotic occlusion of a coronary artery leads to myocyte death and the abrupt loss of functioning myocardium decreases contractile function. Acute compensation is provided by increases in left-ventricular volume (arrows) that augment function (the Frank-Starling mechanism) and neurohumoralfactors that increase contractility in the noninfarcted myocardium. Augmented wall stress, a deleterious effect of increased left-ventricular volume, is reduced by myocyte hypertrophy in the noninfarcted myocardium (doubleheaded arrows). Especially after larger infarcts, adverse remodelling (the term remodelling is used in the schematic) takes place where the left ventricle undergoes dilation (dashed arrows), wall thinning, and a change in shape from ovoid to spherical, causing reduced contractile function and chronic heart failure (adapted from Whelan *et al.*, 2007).

1.3 Notch signalling

1.3.1 The Notch signalling pathway

Notch signalling constitutes an evolutionary conserved pathway which plays a pivotal role in a broad spectrum of developmental and physiological processes, including the development of the central nervous system, the vasculature, or the heart, for example. Due to the transmembrane characteristic of both receptor and ligand, signalling requires direct cell-cell interactions and is consequently restricted to adjacent cells. In a context-dependent manner, signals transmitted through the Notch receptor direct cell-fate decisions, thereby promoting or suppressing cell proliferation, differentiation and cell death (Artavanis-Tsakonas *et al.*, 1999; Bray, 2006; Kopan and Ilagan, 2009).

Receptor and ligand basics

In mammals, four Notch receptors (Notch1 – Notch4) and five Notch ligands (Jagged1 and 2, and Delta-like1, 3 and 4) have been identified.

Notch receptors are synthesized as single-chain precursor proteins. The N-terminal part of the extracellular domain of all receptors contains a variable number (29-36) of tandem epidermal growth factor (EGF) –like repeats (Figure 1.3 B). EGF repeats 11-12 mediate ligand interaction in *trans* (neighbouring cell interaction), whereas repeats 24-29 mediate interaction in *cis* (receptor and ligand on the same cell). EGF repeats are followed by a negative regulator region (NRR) which is composed of three Lin12/Notch (LNR) repeats and a heterodimerization domain. The NRR is critical in preventing receptor activation in ligand absence. The intracellular portion of the polypeptide contains the transmembrane domain, a RAM domain responsible for CSL protein interaction, nuclear localization sequences (NLSs), seven ankyrin repeats (ANK) responsible for interaction with other proteins, and a C-terminal PEST sequence necessary for protein degradation. The Notch precursor protein is modified in the endoplasmic reticulum by an O-fucosyl-transferase (fucosylation) and an O-glucosyl-transferase (glycosylation). Glycosylation is completed in the Golgi apparatus by Fringe. Glycosylation is necessary for the ability to bind ligands and for receptor specificity. In addition, in the Golgi the precursor protein is cleaved by Furin protease at the S1 cleavage site located in the heterodimerization domain. This cleavage converts the polypeptide into a NECD-NTMIC (Notch extracellular domain – Notch transmembrane and intracellular domain) heterodimer; the fragments are associated by noncovalent interactions. The functional, glycosylated heterodimer is finally transported to

the plasma membrane (Bray, 2006; Nemir and Pedrazzini, 2008; Niessen and Karsan, 2008; Kopan and Ilagan, 2009; Tien *et al.*, 2009).

The general structure of the Notch ligands includes three related motifs: an N-terminal DSL (Delta/Serrate/LAG-2) domain, specialized EGF repeats called DOS domain, and EGF repeats. Jagged proteins contain a cysteine rich domain in addition. DSL and DOS domains are involved in receptor binding (Bray, 2006; Kopan and Ilagan, 2009). Ligand activity is also modified by glycosylation (Fortini, 2009).

In principle every Notch receptor can be activated by any DSL ligand, but tissue specific expression and posttranslational glycosylation (which modifies binding affinity) results in preferential specific receptor-ligand interaction (McCright, 2003; Nemir and Pedrazzini, 2008; Niessen and Karsan, 2008). For example, modification of Notch by Fringe inhibits the activation by Jagged ligands, but stimulates the response of Notch to Delta ligands (Lai, 2004).

The Notch signalling cascade

Before ligand binding, the Notch receptor is kept in an inactive state by an interaction of the LNR with the heterodimerization domain in the NRR. Ligand binding to the receptor (Figure 1.3 A) results in a conformational change, allowing access for the first proteolytic cleavage event mediated by TACE or Kuzbanian, both members of the ADAM-family of metalloproteases. The corresponding S2 cleavage site is located in the NRR and results in the discharging of the extracellular domain, leaving a membrane-tethered intermediate called Notch extracellular truncation (NEXT); the extracellular domain/ligand complex is transendocytosed into the signal-sending cell. The following cleavage event of NEXT is mediated by γ -secretase (a complex composed of presenilin, Pen-2, Aph-1, and nicastrin) at site S3/4, which is located in the transmembrane domain. This cleavage releases the Notch intracellular domain (NICD) which translocates to the nucleus and interacts with the DNA-binding protein CSL (for CBF1 in humans, Su(H) in *D. melanogaster* and Lag-1 in *C. elegans*; CSL is also known in mice as RBP-J). In the absence of Notch signalling, CBF-1 acts as transcriptional repressor in combination with a co-repressor complex containing SMRT/N-CoR, SHARP/MINT, SKIP, CIR and CtBP; the co-repressor complex is functionally linked to a histone deacetylase, whose activity results in the transcriptionally repressed chromatin state. In the presence of Notch signalling, NICD binds to CBF-1 through its RAM domain, displacing the co-repressor complex and recruiting the transcription coactivator Mastermind-like (MAML) (via the ANK domain). Thus, the transcriptional repressor is converted to a transcriptional activator. This activator complex

of CBF1/NICD/MAML recruits the histone acetyltransferase p300, thereby promoting a transcriptionally active chromatin state, induction of the transcription initiation and elongation complex and, ultimately, activation of Notch target genes (Lai, 2002; Kopan and Ilagan, 2009; Tien *et al.*, 2009).

Target genes of Notch signalling include basic helix-loop-helix (bHLH) transcription proteins of the Hes and Hey family (mammalian homologues of the *Drosophila* Hairy/Enhancer of Split). In mammals, Hes1, Hes5 and Hes7, as well as Hey1, Hey2 and HeyL are under control of Notch signalling and are considered as central regulators of cell fate-specific gene transcription. They act as direct transcriptional repressors by binding to specific DNA sequences on target gene promoters and as indirect repressors by interaction with other transcription factors. Other direct Notch targets include cyclin D1, p21, NF- κ B transcription factors, EphrinB2 and SMA (Miele, 2006; Nemir and Pedrazzini, 2008; Niessen and Karsan, 2008).

Regulation

Notch signalling is regulated at various levels. Influencing availability by regulating expression levels of receptors and ligands is one of the simplest ways and, actually, expression patterns are influenced by other signalling pathways. In addition, surface expression and degradation after signalling are regulated by multiple processes including endocytosis, ubiquitination and proteolysis (Figure 1.3 A). Interestingly, endocytosis of the DSL ligands in the signal-sending cell mediates ubiquitination of the ligand. This ubiquitination is essential for ligand activation. Another example of regulation is control of Notch levels at the cell surface. Several E3 ubiquitin ligases are able to direct Notch receptors to lysosomal degradation or toward endosomal recycling. In addition, control of NICD turnover is critical to prevent prolonged or excessive signalling. In the activator complex, SKIP and MAML recruit kinases which phosphorylate NICD at the PEST domains; the following ubiquitination of the phosphorylated sites triggers NICD degradation (Nemir and Pedrazzini, 2008; Morrow *et al.*, 2008; Fortini, 2009; Kopan and Ilagan, 2009).

Modes of action

Notch signalling acts by different modes of action. During lateral inhibition a group of equipotent cells all expresses equal amounts of both, receptor and ligand. Through a combination of intrinsic and extrinsic signals this balance is shifted and one cell begins to express more ligand. Consequently, Notch signalling is activated in the neighbouring cells.

Thereby, the ligand expressing cell assumes a particular cell fate and inhibits the immediately adjacent cells to assume the same fate. In the mechanism of lateral induction a cell is instructed to adopt a specific cell fate A in the absence of the Notch ligand. In the presence of the ligand provided by a different cell, Notch signalling is activated and the cell adopts another cell fate B. These Notch-mediated interactions segregate specific cell lineages from clusters of cells and induce boundary formation. A third mechanism describes the activation of Notch signalling in stem cells to maintain an undifferentiated state (Artavanis-Tsakonas *et al.*, 1999; Borggreffe and Oswald, 2009).

Non-canonical signalling

The signalling pathway described so far is also known as the classical, canonical cascade. However, non-canonical DSL-independent proteins have also been shown to activate Notch signalling. These proteins include the adhesion molecules F3/Contactin, the EGF-repeat factor DNER, or the mammalian microfibrillar proteins MAGP-1 and MAGP-2 (Fortini, 2009; Kopan and Ilagan, 2009).

1.3.2 The role of Notch signalling in the cardiovascular system

Developmental implications – *heart and vascular morphogenesis*

In the developing heart Notch signalling is engaged in the process of heart looping by interfering in left-right symmetry determining mechanisms (Niessen and Karsan, 2007), cardiomyocyte differentiation (during heart tube formation differentiation is inhibited, but later during ventricular trabeculation differentiation to myocytes is promoted) (High and Epstein, 2008), and in EMT which is essential for valve and septa formation (Karsan, 2005). Expression analysis have revealed Notch1 and Notch2 as predominant receptors in the developing heart (Swiatek *et al.*, 1994; McCright *et al.*, 2001; Nemir and Pedrazzini, 2008). Delta-like 1 (Dll1) is expressed in the endocardium at the base of the trabeculae at E9.5, but not in the distal endocardium (Grego-Bessa *et al.*, 2007; Nemir and Pedrazzini, 2008). Delta-like 4 (Dll4) is expressed around E8 in the cardiac crescent, but is later restricted to the ventricular endocardium (Benedito and Duarte, 2005; Nemir and Pedrazzini, 2008). Jagged 1 (Jag1) is found at E12.5 in the outflow tract, the atrioventricular canal, the ventricular trabeculae and the atrial myocardium (Loomes *et al.*, 1999; Loomes *et al.*, 2002; Nemir and Pedrazzini, 2008).

In addition, a wide variety of studies have proven the essential role of Notch receptors, ligands and downstream targets in vascular development during embryogenesis in mammals. Gene ablation experiments all have in common that Notch inhibition does not influence vasculogenesis, but prevents the conversion of the primary vascular plexus to the hierarchical vascular network of arteries, veins and capillaries. Thus, Notch signalling plays a more important role in angiogenesis. Null mutant mouse models (*Notch1*^{-/-}, *Notch2*^{-/-}, *Notch1*^{-/-}/*Notch4*^{-/-}, *Dll1*^{-/-}, *Dll4*^{-/-} and *Jag1*^{-/-}) show embryonic lethality due to cardiovascular abnormalities. Expression levels of Notch components are dynamic during development (spatially as well as temporarily). Notch1 is expressed in various tissues, including the heart and vascular endothelial cells. Notch3 is predominantly expressed in vascular SMCs and Notch4 is restricted to vascular endothelial cells. Dll1, Dll4, Jag1, and Jag2 are expressed in vascular endothelium; Jag1 is expressed in addition in SMCs and is involved in SMC maturation (Beckers *et al.*, 1999; Krebs *et al.*, 2000; Shutter *et al.*, 2000; Nijjar *et al.*, 2001; Villa *et al.*, 2001; Iso *et al.*, 2003; Karsan 2005; Hofmann and Iruela-Arispe, 2007; Kume, 2009).

Developmental implications – angiogenic sprouting

Another important mechanism Notch signalling is involved in, is angiogenic sprouting with tip/stalk cell specification. The combined effect of tip cell migration and stalk cell proliferation results in vascular growth (Gerhardt *et al.*, 2003; Hofman and Iruela-Arispe, 2007).

Vascular growth is guided by hypoxia. Hypoxic cells upregulate VEGF-A (a secreted VEGF form), leading to the formation of a gradient. Initially equipotent endothelial cells all express the VEGF-A receptor complex Kdr(VEGFR2)/Nrp1. Via the principle of lateral inhibition, the endothelial cell experiencing the highest VEGF-A concentration gains a competitive advantage and VEGF receptor activation leads to enhanced Dll4 expression (in concert with Foxc1 and Foxc2 transcription factors); this cell attains the tip cell phenotype. In consequence, Dll4 activates Notch signalling in the neighbouring cell, leading to downregulation of *Kdr/Nrp1*, thereby rendering this cell unresponsive to VEGF-A and lowering Dll4 expression. Thus, conversion to a tip cell is prevented and the cell adapts a stalk phenotype (Horowitz and Simons, 2008; Carmeliet *et al.*, 2009; Kume, 2009; Phng and Gerhardt, 2009). By this mechanism VEGF and Dll4 signalling forms a negative-feedback loop, controlling tip cell selection and the frequency of sprouting (Horowitz and Simons, 2008; Carmeliet *et al.*, 2009). Inactivation of Dll4/Notch leads to the formation of a highly branched and dense vascular network, but vessels are nonproductive and inefficient in

oxygen delivery (Hellström *et al.*, 2007; Hofmann and Iruela-Arispe, 2007; Siekmann and Lawson, 2007; Suchting *et al.*, 2007).

Tip cells lack a lumen and extend filopodia to explore growth factor signals and guidance cues in the surrounding tissue. Stalk cells enclose a luminal space, forming a tubule at the stalk of the vascular sprout (Gerhardt *et al.*, 2003; Roca and Adams, 2007). VEGF induces migration of tip cells and proliferation of stalk cells, which is needed to form a new vessel branch (Carmeliet *et al.*, 2009; Phng and Gerhardt, 2009). However, Notch signalling has been shown to promote a quiescent endothelial phenotype. So how could Notch activation in stalk cells promote endothelial cell proliferation during stalk elongation? Phng and co-workers revealed that interaction of Nrarp, Notch and Wnt is required. Nrarp is a downstream target of Notch which counteracts Notch signalling by destabilizing NICD. Wnt signalling and Nrarp expression in stalk cells override Notch activity to induce cell-cycle arrest and at the same time Notch prevents the stalk cells from becoming tip cells (Phng *et al.*, 2009; Carmeliet *et al.*, 2009).

Developmental implications – arterial/venous specification

As already mentioned before, there are significant molecular differences between endothelial cells in arteries (expressing ephrin-B2) and veins (expressing EphB4). These differences are generated by VEGF and Notch interactions in the lateral mesoderm. Analyses revealed that VEGF induces Notch signalling via the ligand Dll4 (Lawson *et al.*, 2002; Duarte *et al.*, 2004; Gale *et al.*, 2004; Roca and Adams, 2007). Angioblasts stimulated by Notch activate the expression of ephrin-B2 and other arterial markers, thereby establishing arterial endothelial identity (Zhong *et al.*, 2000; Zhong *et al.*, 2001; Lawson *et al.*, 2002; Grego-Bessa *et al.*, 2007; Phng and Gerhardt, 2009). Conversely, Notch signalling is suppressed by the venous transcription factor COUP-TFII (You *et al.*, 2005) and accordingly less stimulated angioblasts express EphB4 and endothelial cells gain a venous identity (Adams, 2003; Torres-Vásquez *et al.*, 2003; Gilbert, 2006; Al Haj Zen and Madeddu, 2009; Swift and Weinstein, 2009).

Role in adults – myocardial infarction and heart stress response

Although the engagement of Notch signalling in cardiovascular development has been the focus of a multitude of studies, its role in the postnatal heart and stressed conditions has attained less attention. Only in 2008 first studies attended to this topic.

Gude *et al.* were the first to analyse Notch signalling following myocardial infarction and showed the activation of protective mechanisms in the myocardium, mediated by Notch

(Gude *et al.*, 2008). In the mammalian heart endogenous Notch signalling is low (Gude *et al.*, 2008, Collesi *et al.*, 2008; Kratsios *et al.*, 2010), but expression levels increase in response to acute infarction by permanent coronary occlusion (Gude *et al.*, 2008). 4 days after infarction, NICD and Jag1 were detected in surviving cardiomyocytes of the border zone, whereas Dll4 was predominantly expressed in interstitial areas. Additional Hes1 detection indicated active Notch signalling (Gude *et al.*, 2008). The group treated infarcted hearts with an adenoviral vector expressing NICD and could show improved hemodynamic function, compared to control animals after 4 weeks. Further analyses revealed the relationship of HGF (hepatocyte growth factor), binding to its receptor c-Met (increased in hypertrophic and infarcted cardiac tissue) which in turn induces Delta expression, Notch activation and Hes1 expression. Among others, c-Met activates ERK and Akt/PKB survival signalling in the heart. As Notch1 signalling enhances Akt activity, results suggest Notch signalling as mediator of cell survival (Gude *et al.*, 2008).

Another study analyzed the role of Notch signalling in cardiac hypertrophy and found that the adaptive response of the heart to stress is controlled via Notch1 (Croquelois *et al.*, 2008). Microarray and RT-PCR analyses showed activated genes of *Notch1*, *Jag1*, *RBP-J* and *Hes1* in hypertrophic and dilated adult hearts. Notch1 was detected in cardiomyocytes and mesenchymal cardiac precursors and was stimulated by Jag1 on cardiomyocytes. Using a mouse model of cardiac specific Notch1 deletion, the group showed aggravated hypertrophy, development of fibrosis, impaired cardiac function and increased mortality. The conclusion of the study stated that (a) in cardiomyocytes, Notch represses cardiac gene expression and prevents excessive, detrimental hypertrophy and (b) in cardiac precursors Notch regulates proliferation and differentiation (Croquelois *et al.*, 2008).

Other *in vitro* studies revealed that Notch activation induces cell-cycle re-entry in quiescent cardiomyocytes (Collesi *et al.*, 2008; Campa *et al.*, 2008; Kratsios *et al.*, 2010).

The most recent and second study focusing on Notch involvement after myocardial infarction was performed by Kratsios and co-workers. The group analyzed effects of sustained Notch1 activation after myocardial infarction, using an inducible cardiomyocyte-specific NICD1 mouse model or by intramyocardial delivery of a Notch1 pseudoligand. These approaches resulted in increased survival rates, improved functional performance, and decreased myocardial injury by promoting antiapoptotic mechanisms and cardiomyocyte survival. In addition, minimized fibrosis and enhanced neovascularisation could be observed (Kratsios *et al.*, 2010).

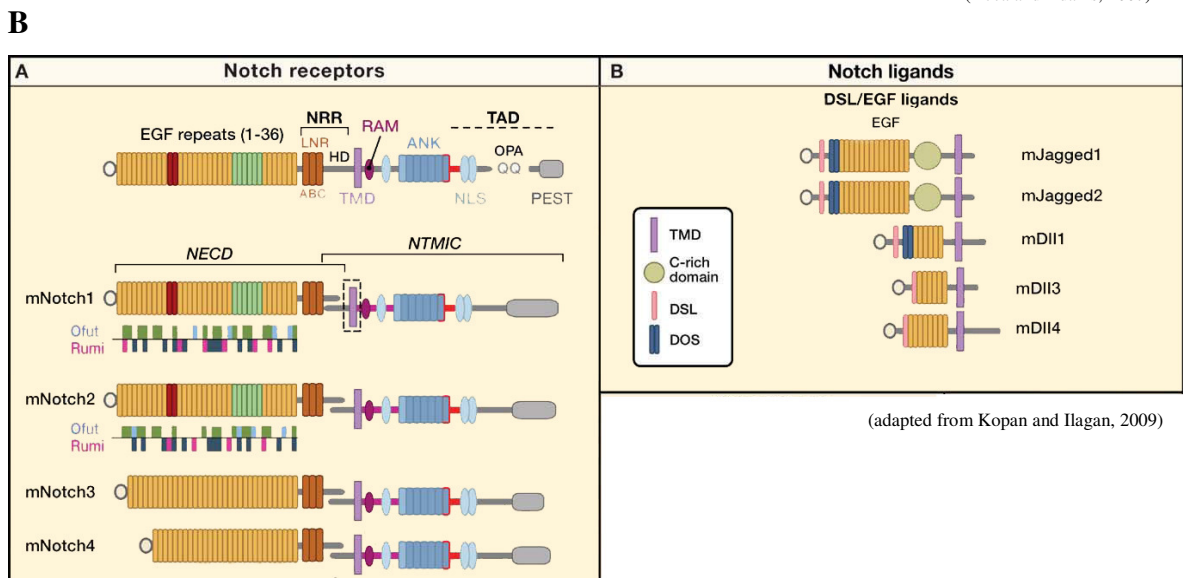
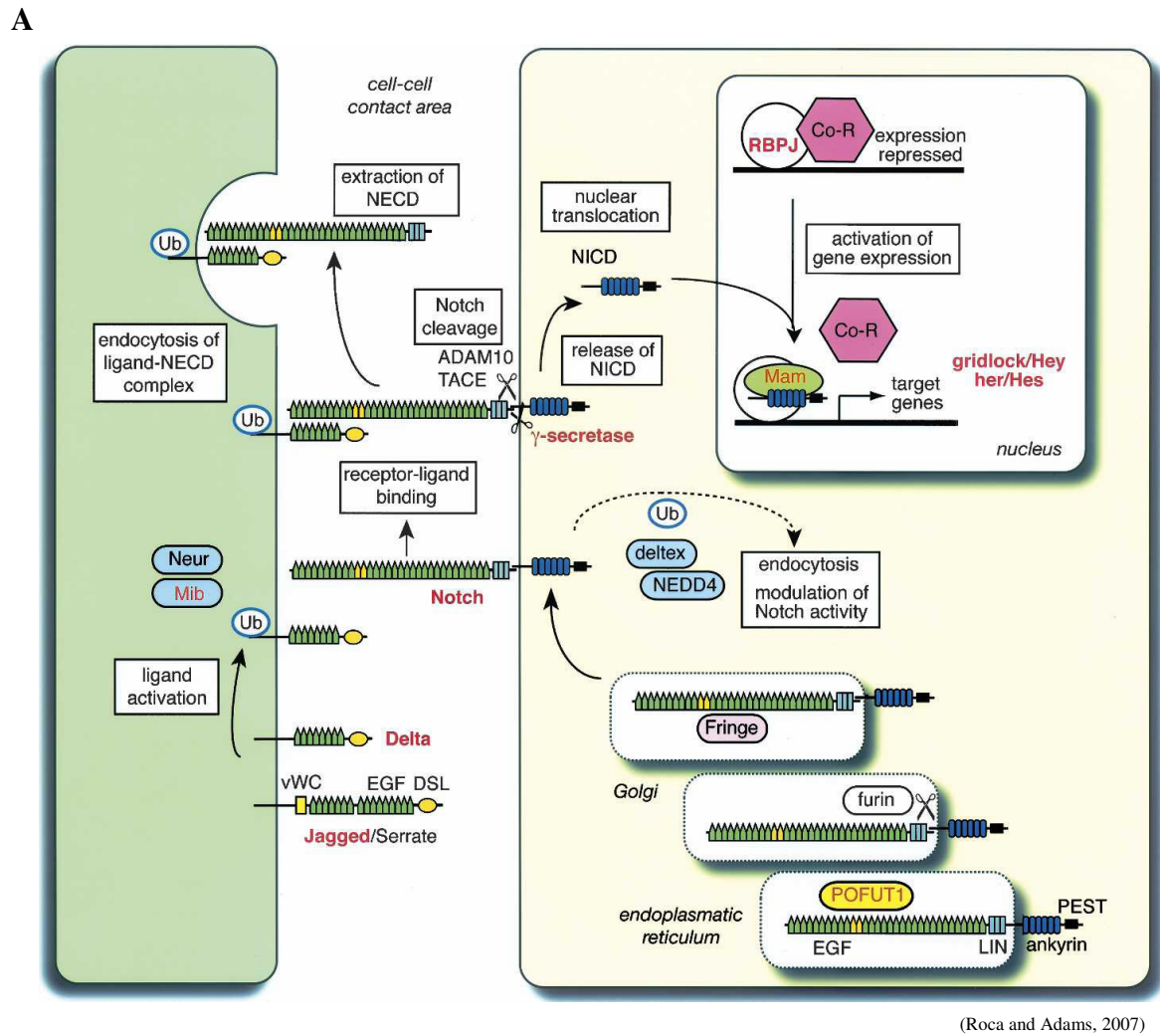


Figure 1.3 Notch signalling. (A) The Notch signalling pathway. Post-translational processing of the Notch preprotein involves glycosylation and fucosylation (POFUT1), as well as cleavage by the protease furin. Fringe-mediated glycosylation modulates Notch responses to ligands. Modification by the E3 ubiquitin ligases Mib and Neur enable DSL proteins to signal through Notch. Notch receptor activity is modulated by ubiquitination involving Nedd4 and deltex proteins. After ligand binding, Notch is processed by ADAM10/TACE and γ -secretase. Nuclear translocation of the NICD and its interaction with RBPJ/CSL and the coactivator Mam trigger the expression of target genes such as Hey and Hes (adapted from Roca and Adams, 2007). **(B) Domain organization of Notch receptors and ligands.** (A) Notch receptor organization – for a

detailed description see text. NRR: negative regulatory region, LNR: Lin12-Notch repeats, HD: heterodimerization domain, TMD: transmembrane domain, NLS: nuclear localization sequence, ANK: ankyrin repeats, TAD: transactivation domain, PEST: proline/glutamic acid/serine/threonine-rich motifs, NECD-NTMIC: Notch extracellular domain-Notch transmembrane and intracellular domain. (B) DSL/EGF ligand organization (adapted from Kopan and Ilagan, 2009).

1.3.3 Involvement of Notch signalling in immunity mediated wound repair

Already described in the chapter dealing with myocardial infarction, the inflammatory response involves the recruitment of two distinct and complementary monocyte subsets (Nahrendorf *et al.*, 2007). Recruited monocytes differentiate to macrophages at the area of inflammation (Gordon and Taylor, 2005). Ly-6C^{hi} monocytes dominate early in the inflammatory phase, whereas Ly-6C^{lo} monocytes dominate rather in the proliferative phase and show enhanced healing properties (Nahrendorf *et al.*, 2007). Polarized macrophages are classified as M1 (classical activated macrophages) with pro-inflammatory function and M2 (alternatively activated macrophages), associated with tissue repair and angiogenesis (Mosser and Edwards, 2008; Limbourg *et al.*, *in review*). Just recently Limbourg and co-workers could provide evidence that Notch signalling is involved in macrophage differentiation. *In vitro* experiments revealed that cultures of PBMC (peripheral blood monocytes)-derived macrophages showed active Notch signalling and an M2 typical phenotype. Inhibition of Notch signalling resulted in macrophages of inflammatory M1 phenotype (Limbourg *et al.*, *in review*). Next, the group tested the hypothesis that by regulating macrophage polarization, Notch signalling regulates the inflammatory and regeneration response after ischemia. In a M2 macrophage-deficient mouse model, effects of cultured M2 macrophages and cultured Notch-deficient M1 macrophages were studied. Cells were injected into ischemic muscles after hindlimb ischemia. Without treatment, mice showed impaired recovery from ischemia. Treatment with M2 macrophages resulted in decreased necrosis and increased angiogenesis, arteriogenesis and arterial branching in the ischemic muscle. Recruitment of CD45+ leukocytes to the ischemic muscle was reduced and tissue necrosis suppressed. In contrast, injection of Notch-deficient M1 macrophages resulted in significantly reduced angiogenesis and arteriogenesis; tissue necrosis was increased. CD45+ leukocyte recruitment, corresponding inflammatory response and fibrosis was enhanced and prolonged, consistent with the development of chronic inflammation. These results were consistent with the role of macrophage subsets in inflammation and tissue recovery, and proved an according involvement of Notch signalling (Limbourg *et al.*, *in review*).

1.4 The Notch ligand Delta-like 1 (Dll1)

1.4.1 Dll1 – further insights

The focus of this thesis is the Notch ligand Dll1. Interaction of Dll1 with Notch in *trans* activates Notch signalling, whereas interaction in *cis* inhibits the pathway (Dyczynska *et al.*, 2007). Apart from its role in the cardiovascular and immune system – which will be discussed in more detail in the following –, Dll1 is involved in a multitude of processes in different stages of development and tissues, including for example cell differentiation in pancreas development (Apelqvist *et al.*, 1999), differentiation and proliferation during inner ear development (Brooker *et al.*, 2006), and specification of vertebral identity (Cordes *et al.*, 2004; Rubio-Aliaga *et al.*, 2007).

In addition to directional signalling through the Notch receptors, further studies have also shown results which indicate that not only NICD interacts with other proteins, but also the intracellular domain (ICD) of some ligands may initiate cascades in the ligand-expressing cell (keyword bi-directional signalling) (LaVoie and Selkoe, 2003; Pfister *et al.*, 2003; Rubio-Aliaga *et al.*, 2007). Evidence shows that – in analogy to Notch receptor processing – Dll1 undergoes an ADAM-mediated ectodomain cleavage, followed by presenilin/ γ -secretase proteolysis of the membrane-tethered C-terminal fragment; the resultant Dll1 ICD can enter the nucleus (LaVoie and Selkoe, 2003; Six *et al.*, 2003, Dyczynska *et al.*, 2007). However, it is unclear whether cleavage is a constitutive event in the absence of a Notch signal, or if it is regulated by a soluble or membrane-associated interacting partner (like Notch) (Six *et al.*, 2003). In addition, the role of the shedded extracellular domain has not been clarified (Six *et al.*, 2003; Mishra-Gorur *et al.*, 2002). Proteolytic ligand processing results in the downregulation of Notch signalling in the neighbouring cell (Qi *et al.*, 1999; Mishra-Gorur *et al.*, 2002; Dyczynska *et al.*, 2007). However, in the condition of receptor and ligand expression on the same cell, effects of ligand processing have not been clarified (Dyczynska *et al.*, 2007).

Analysis of interactions of the Dll1 ICD identified Acvrin1, a MAGUK family member (Pfister *et al.*, 2003). Expression analyses in mouse embryos showed partly overlapping, but also distinct patterns in the central nervous system and the expression of Acvrin1 was altered (i.e. premature expression) in Dll1 null-mutant embryos (Pfister *et al.*, 2003). Another study found Dll1 ICD in the nucleus of neural stem cells in the developing mouse (Hiratochi *et al.*, 2007). In this context, Dll1 ICD bound specifically to the transcription

factors Smad2, Smad3 and Smad4, thereby enhancing Smad-dependent transcription and mediating TGF- β /Activin signalling (Hiratochi *et al.*, 2007).

1.4.2 Dll1 in the cardiovascular system

Dll1 in heart development

Dll1 is expressed in the endocardium at the base of the trabeculae at E9.5 (Grego-Bessa *et al.*, 2007). However, standard targeted Dll1 mutants did not show obvious cardiac defects at this time point, which suggests functional redundancy of this ligand and/or signalling is maintained by Dll4, which shows an identical expression pattern in the trabeculae (Grego-Bessa *et al.*, 2007).

Dll1 in vasculature development

A complete Dll1 knockout is lethal around embryonic day 12 (E12) due to severe bleeding. However, lethality is based rather on defects in surrounding tissues, than on vascular functions (Hrabé de Angelis *et al.*, 1997; Gessler, 2009). Embryos heterozygous for Dll1 are phenotypically normal and survive until adulthood, despite significantly reduced Notch activity (Hrabé de Angelis *et al.*, 1997; Beckers *et al.*, 1999; Schuster-Gessler *et al.*, 2007).

Early vascular patterning in the mouse embryo is mediated by the Notch ligand Dll4. Of all ligands which are expressed in arterial endothelial cells (Dll1, Dll4, Jag1, and Jag2), only Dll4 is expressed at E8.5 and its expression is limited to vascular endothelial cells (Krebs *et al.*, 2000; Kume, 2009). Dll4 acts downstream of VEGF and is the critical ligand in arterial specification (see chapter 1.3.2) (Gessler, 2009).

In contrast, Dll1 is expressed in vascular endothelium of late embryonic stages (Hrabé de Angelis *et al.*, 1997; Beckers *et al.*, 1999; Limbourg *et al.*, 2007). Sørensen *et al.* showed specific expression of Dll1 in fetal arterial endothelial cells beginning at E13.5 (Sørensen *et al.*, 2009). The group analysed embryos with reduced levels of Dll1 or endothelial-specific Dll1 ablation and found lost Notch1 activation, reduced VEGFR2, Nrp1 and ephrinB2 expression, and upregulation of COUP-TFII after E13.5. As Dll4 expression was unchanged in these animals, Dll4 appears to be required for arterial specification, whereas Dll1 mediated Notch activity is required in large arteries to maintain arterial identity in embryonic development (Sørensen *et al.*, 2009). This finding suggests that there is a switch which renders Dll4 incapable to sustain Notch activity, arterial marker expression and vein marker suppression (Gessler, 2009). In normal conditions, COUP-TFII suppresses *Nrp1*

expression and arterial differentiation in venous endothelium (You *et al.*, 2005; Sørensen *et al.*, 2009). Sørensen *et al.* revealed that VEGFR2 and Nrp1 (together forming the VEGF-A receptor complex) downregulation in mutant arteries preceded COUP-TFII expression. This indicates that Dll1-mediated Notch1 activation upregulates VEGFR2 and Nrp1, thereby enhancing VEGF-A responsiveness of arterial endothelial cells (Sørensen *et al.*, 2009; Kume, 2009). Thus, the group showed that Dll1 positively regulates VEGF signalling, which constitutes a contrasting function to Dll4 in growing capillaries where Dll4-mediated Notch signalling occurs downstream of VEGF (Kume, 2009). Summarizing, the study showed that there are functions of Dll1/Notch signalling which cannot be compensated by other ligands, and revealed a novel connection were in arteries Dll1/Notch1 facilitate VEGF sensitivity (Gessler, 2009).

Furthermore, Dll1 has been implicated in smooth muscle differentiation and maturation. Together with Jag1, Dll1 are the primary ligands on arterial endothelial cells, inducing the expression of Notch3 and Jag1 in the neighbouring mural cells. This subsequently promotes and maintains the differentiated mural cell phenotype (High *et al.*, 2008; Liu *et al.*, 2009; Kume, 2009)

Dll1 in adult vasculature

Due to embryonic lethality of Dll1^{-/-} mice, postnatal analyses are reduced to Dll1 heterozygotes (Dll1^{+/-}) which survive to adulthood.

In the adult cardiovascular system Dll1 is selectively expressed in arterial endothelial cells. It is not found in capillaries, venous endothelial cells or other cell types present in the heart (Limbourg *et al.*, 2007). The basal role of Dll1 in the adult vasculature has not been studied so far, but Limbourg and co-workers discovered a critical role of Dll1 in postnatal arteriogenesis (Limbourg *et al.*, 2007). In the mouse model of hindlimb ischemia the expression of Dll1 was induced, Notch signalling activated, ephrin-B2 upregulated, and perivascular cells expressed VEGF and EphB4 while arteries grew. Analogous analyses in ischemia-induced Dll1^{+/-} animals revealed the absence of endothelial Notch activation and ephrin-B2 induction. Perivascular VEGF expression and microvascular angiogenesis were not altered, but arteriogenesis and blood flow recovery were severely impaired (Limbourg *et al.*, 2007). *In vitro* studies showed that VEGF and FGF synergistically induced Dll1 with corresponding Notch activation. This activation was necessary and sufficient to regulate ephrin-B2 expression and induced branching and vascular network formation (Limbourg *et al.*, 2007). The group proposes a model of postnatal arteriogenesis in which the relationship

of Dll1 induction by angiogenic growth factors activates Notch signalling and ephrin-B2 expression; this mediates remodelling and outward growth of the collateral artery towards an EphB4 enriched environment (Limbourg *et al.*, 2007). The observed transient induction of Dll1 in connection with the previous finding of reciprocal Dll1 inhibition by activated Notch receptors might possibly explain the termination of arteriogenesis through Dll1 downregulation after persistent Notch activation (Artavanis-Tsakonas *et al.*, 1999; Limbourg *et al.*, 2007).

In contrast to Dll1, Dll4 is not expressed in larger arteries, but only in capillaries and microvessels; the ligand is not involved in regulating postnatal arteriogenesis (Limbourg *et al.*, 2007). In the adult, Dll4 is rather associated with tumour angiogenesis (tip/stalk cell determination) and is expressed in tumour vasculature (Mailhos *et al.*, 2001; Patel *et al.*, 2005; Hainaud *et al.*, 2006; Kume, 2009).

1.4.3 Dll1 involvement in haematopoiesis

Notch signalling is involved in numerous processes of haematopoietic maturation. Hozumi and co-workers analysed ligand expression and found Dll1 expression in lymphoid tissues: in specific stromal cells of the thymus and in B cells and dendritic cells in the spleen (Hozumi *et al.*, 2004). Based on the Cre/LoxP system the group generated inducible Dll1 knockouts and confirmed deletion in all lymphoid tissues. These animals demonstrated a complete loss of splenic marginal zone B cells, but T cell development was unaffected (Hozumi *et al.*, 2004). Thus, the group concluded that Dll1 was not required for Notch1 activation at the branch point of T cell – B cell development, but Dll1 was essential for the generation of marginal zone B cells. Marginal zone B cells are a particular B cell subset which is derived from already committed B lineage cells, mediated by Notch2. The interaction of Dll1 with Notch2 for marginal zone B cell development was rather based on interaction of precursor with environmental cells, than between equivalent precursors. Consequently, Notch signalling is required for lymphocyte development *in vivo*, but varying receptor/ligand interactions are responsible in different developmental steps (Hozumi *et al.*, 2004).

Another study analysed Dll1 expression on murine peripheral monocytes and macrophages. Moriyama *et al.* found Dll1 expression on a substantial part of Ly-6C^{lo} monocytes (related to healing properties), whereas no Dll1 expression was detected on Ly-6C^{hi} monocytes

(inflammatory properties) (Moriyama *et al.*, 2008). Dll1 was expressed on a considerable fraction of splenic macrophages (CD11b^{hi}/CD68⁺/F4/80⁺/Gr-1⁻). Further characterization of macrophages from the spleen showed higher CD40 expression on Dll1-negative macrophages, compared to Dll1-expressing macrophages. No difference in expression was observed for CD80, CD86, CD14 and MHC class II, comparing Dll1-positive and -negative monocytes/macrophages (Moriyama *et al.*, 2008).

1.5 Objectives and hypotheses

Development and regeneration after injury of the cardiovascular system require a huge array of factors and mechanisms which have to work in a temporal and spatial organized fashion (Darland and D'Amore, 2001). Myocardial infarction is a highly prevalent ischemic disease and multiple studies have demonstrated that only arteriogenesis has considerable ability to fully restore blood flow, which is absolutely critical for the regeneration of all ischemic organs (Deindl and Schaper, 2005; Simons, 2005; Heil *et al.*, 2006). Notch signalling constitutes an evolutionary conserved pathway which plays a pivotal role in the cardiovascular system, and – as activators of the pathway – the Notch ligands play a critical role. The ligand Delta-like 1 (Dll1) has been associated with the maintenance of arterial identity during development (Sørensen *et al.*, 2009) and is a critical regulator of postnatal peripheral limb arteriogenesis (Limbourg *et al.*, 2007). These findings in combination with specific Dll1 expression in arterial endothelium raised the question about its function in coronary arteries and in arteriogenesis after myocardial infarction.

Consequently, the aim of this study was to characterize the involvement of the Notch ligand Dll1 in arterial patterning of coronaries in the adult and its role in ischemic stress responses after myocardial infarction.

Hypotheses

1. A reduced level of Dll1 impairs the development of the coronary arterial system.
2. Arteriogenesis is a critical factor of infarct compensation and positively influences cardiac remodelling.
3. Dll1 is involved in arteriogenesis post MI; its specific arterial endothelial expression suggests that endothelial Dll1 mediates this arteriogenesis.
4. (Partial) loss of Dll1 impairs arteriogenesis and infarct recovery, leading to adverse remodelling.

Questions

1. The findings of Notch involvement in macrophage differentiation and expression of Dll1 on a fraction of monocytes and macrophages give rise to the question of the involvement of Dll1 in inflammatory mediated infarct repair mechanisms.

2. MATERIALS AND METHODS

2.1 Materials

2.1.1 Chemicals, reagents, and buffers

Table 2.1 Chemicals and reagents			
Reagents A-M	Company	Reagents M-Z	Company
1kb DNA ladder	Invitrogen	Miglyol	Caelo
2-mercaptoethanol	Invitrogen	M-MLV RT buffer 5x	Promega
2-methylbutane	Roth	M-MLV Reverse Transcriptase	Promega
Acetone	J.T. Baker	MP	Bio-Rad
Acrylamide mix 30% (Rotiphorese Gel 30)	Roth	NaCl	Roth
Agarose (Seakem LE)	Lonza	NaCl solution 0.9%	B. Braun
ApopTag [®] Plus Fluorescein <i>In Situ</i> Apoptosis Kit	Chemicon	Naphthol-AS-BI-phosphate	Sigma-Aldrich
APS	Roth	Neu-Fuchsin	Fluka
Bradford reagent (Roti-Quant)	Roth	NH ₄ Cl	Sigma
Bromphenol blue	Roth	Nitrocellulose membrane	Roth
BSA	Roth	OCT compound	Sakura
Chloroform	J.T. Baker	PBS	Lonza
Complete Mini, EDTA Protease Inhibitor Tablets	Roche	PBS w/Ca ²⁺ , Mg ²⁺	Lonza
DAPI	Roth	PCR buffer A 10x (10x PCR buffer)	Qiagen
DEPC	AppliChem	PFA	Sigma-Aldrich
Dimethylformamide	Sigma-Aldrich	Phenol/Chloroform	AppliChem
DMSO	AppliChem	Phloxin B	Merck
dNTP mix	Invitrogen	Phosphomolybdic acid	Merck
EDTA	Roth	Picric acid	Sigma-Aldrich
EGTA	Roth	Picrosirius red (Direkt red 80)	Sigma-Aldrich
Eosin G	Merck	PMSF	Sigma-Aldrich
EtOH	J.T. Baker	Propandiol	Merck
Fc Blocking reagent	BD Pharmingen	Proteinase K	Roche

Table 2.1 - continued -			
FCS	Biochrom	Protein ladder	Bio-Rad
Fluorescence mounting medium	Dako	Q-solution 5x	Qiagen
Formaldehyde	Sigma-Aldrich	RNaseOUT™	Invitrogen
Glacial acetic acid	Sigma-Aldrich	Rompun	Bayer
Glutaraldehyde	Sigma-Aldrich	SDS	Roth
Glycerol	Sigma-Aldrich	Serum - Goat	Sigma-Aldrich
Glycine	Sigma-Aldrich	Serum - Donkey	Dianova
HCl	Merck	Sodiumnitrite	Merck
Heparin	Ratiopharm	Sucrose	Roth
Isofluran	Baxter	Tamoxifen (free base)	Sigma-Aldrich
Isopropanol	J.T. Baker	Taq polymerase (genotyping)	made in-house
K-ferricyanide	Sigma-Aldrich	Taq polymerase (PCR)	Qiagen
K-ferrocyanide	Sigma-Aldrich	TEMED	Sigma-Aldrich
Kaiser's glycerol gelatine	Merck	Tris-base	Roth
KCl	Sigma-Aldrich	Tris-HCl	Roth
Ketanest	Pfizer Pharma	TritonX-100	Merck
KHCO ₃	Sigma	Trizol	peqLab
Levamisol	Sigma-Aldrich	Tween-20	Merck
Liquid nitrogen	Linde	Vitro-clud	R. Langenbrinck
Mayer's Hemalum	Sigma-Aldrich	Western Lightning™ Chemiluminescence Reagent	PerkinElmer
Methanol	Roth	X-gal	peqLab
MgCl ₂	AppliChem	Xylol (Roticlear)	Roth

Table 2.2 Buffers and solutions	
Solution	Composition
Anaesthesia cocktail	250 µl 2% Rompun, 4 ml Ketanest (25 mg/ml), ad 10 ml isot. NaCl
Antibody dilution buffer	PBS, 0.3% Triton X-100, 1% BSA
Blocking buffer	PBS, 0.3% Triton X-100, 5% Serum (donkey or goat serum, depending on the species of the secondary antibody)
Evan's blue solution	2% Evan's blue in NaCl 0.9%
Eosin/phloxin solution	86.6 ml 96% EtOH, 1.1 ml 10% Phloxin B, 11.1 ml 2% Eosin G, 1.1 ml Glacial acetic acid
FACS wash buffer	PBS, 4% FCS, 2 mM sodium EDTA
FACS AB mix 1	480 µl FACS wash buffer, 5 µl B220-PE, 5 µl DX5-PE, 5 µl Ly-6G-PE, 5 µl NK1.1-PE, 5 µl F4/80-Biotin, 5 µl CD11c-Biotin, 5 µl I-A ^b -Biotin, 1 µl CD90-PE
FACS AB mix 2	480 µl FACS wash buffer, 2.5µl Ly-6C-FITC, 5µl Strep-PerCP, 5µl CD11b-APC

Table 2.2 - continued -	
IH solution A	44 ml 0.05 M Tris-HCl, 15 ml 0.2M Propandiol, 25 mg Levamisol
IH solution B	13 mg Sodiumnitrite, 312µl ddH ₂ O, 125 µl Neu-Fuchsin solution (5% in 2N HCl)
IH solution C	31 mg Naphthol-AS-BI-phosphate, 375 µl Dimethylformamide
KCl arrest solution	2.5 ml 1M KCl, 2ml Heparin 25000U, ad 50 ml PBS (w/Ca ²⁺ , Mg ²⁺); filtered
LacZ staining solution	1.25 ml X-gal (20 mg/ml), 0.5 ml 0.5M K-ferricyanide, 0.5 ml 0.5 M K-ferrocyanide, 48 ml LacZ wash buffer
LacZ wash buffer	PBS, 2 mM MgCl ₂
Laemmli buffer	50% Glycerol, 160 mM Tris-HCl, 5% 2-mercaptoethanol, 2% SDS, 0.01% Bromphenol blue
PCR buffer B 10x	0.25 M KCl, 0.1 M Tris-HCl pH 8.8, 0.1% TritonX-100
PCR buffer C 10x	0.5 M KCl, 0.1 M Tris-HCl pH 8.5, 20 mM MgCl ₂ , 50% DMSO
Perfusion solution	1.5% PFA, 0.1% Glutaraldehyde, PBS w/Ca ²⁺ , Mg ²⁺ ; filtered
Protein lysis buffer	40 mM Tris-HCl pH 7.4, 150 mM NaCl, 1 mM EDTA, 1 mM EGTA, 1% Triton X-100, 1 mM Na ₃ VO ₄ , 1 mM PMSF, 1x complete mini EDTA-free inhibitor cocktail
Resolving gel (8%)	To prepare 10 ml: 4.6 ml H ₂ O, 2.7 ml 30% Acrylamide mix, 2.5 ml 1.5 M Tris-base pH 8.8, 100 µl 10% SDS, 100 µl 10% APS, 6 µl TEMED
SDS running buffer	25 mM Tris-base, 200 mM Glycine, 0.1% SDS, pH 8.5
Stacking gel (5%)	To prepare 5 ml: 3.4 ml H ₂ O, 0.83 ml 30% Acrylamide mix, 0.63 ml 1.0 M Tris-base pH 6.8, 50 µl 10% SDS, 50 µl 10% APS, 5 µl TEMED
Stripping buffer	62.5 mM Tris-HCl, 2% SDS, 100 mM 2-mercaptoethanol, pH 6.8
TAE	40 mM Tris-base, 1 mM EDTA
Tail lysis buffer	0.1 M Tris-HCl pH 8.5, 5 mM EDTA, 0.2% SDS, 200µg/ml Proteinase K
TAM solution	20mg/ml Tamoxifen in Miglyol; sterile filtered
TBS (IH)	0.05 M Tris-HCl, 0.74 M NaCl, pH 7.4-7.6
TBS 10x (WB)	For 1 liter: 24.2g Tris-base, 80g NaCl, pH 7.6
TBST (WB)	1x TBS with 0.1% Tween-20
TE	10 mM Tris-HCl pH 7.5, 1 mM EDTA
Transfer buffer	25 mM Tris-base, 200 mM Glycine, 20% Methanol
TTC solution	2% TTC in PBS
Whole blood lysis buffer	8.34 g NH ₄ Cl, 1.09 g KHCO ₃ , 10 ml 1% EDTA, ad 1000 ml aqua dest.

2.1.2 Antibodies

Table 2.3 Primary antibodies			
Name	Company; product number	Host	Application, dilution
anti- α -smooth muscle actin – Cy3 (SMA-Cy3)	Sigma; C 6198	Mouse, monoclonal	IF, 1:100

Table 2.3 - continued -			
anti- α -smooth muscle actin – FITC (SMA-FITC)	Sigma; F 3777	Mouse, monoclonal	IF, 1:100
anti-Actin	Sigma; A 2066	Rabbit, polyclonal	WB, 1:5000
anti-mouse CD45	BD Pharmingen; 550539	Rat, monoclonal	IH, 1:100
anti-mouse CD206	AbD Serotec; MCA2235	Rat, monoclonal	IF, 1:100
anti-DII1 (H-265)	Santa Cruz Biotechnology; sc-9102	Rabbit, polyclonal	WB, 1:1000
anti-rat DII1	R&D Systems; AF3970	Sheep, polyclonal	IF, 1:100
anti-mouse F4/80-RPE	AbD Serotec; MCA497PE	Rat, monoclonal	IF, 1:100
Biotinylated <i>Griffonia (Bandeiraea) Simplicifolia</i> Lectin I, Isolectin B4 (IB4-biotin)	Linaris/ Vector Laboratories; B-1205		IF, 1:100
FITC <i>Griffonia (Bandeiraea) Simplicifolia</i> Lectin I, Isolectin B4 (IB4-FITC)	Linaris/ Vector Laboratories; FL-1201		IF, 1:100
Wheat Germ Agglutinin (WGA)-Rhodamine	Linaris/ Vector Laboratories; RL-1022		IF, 1:100

Table 2.4 Secondary antibodies			
Antibody	Company; product number	Host	Application, dilution
Avidin D-Texas Red	Linaris; RAT2006		IF, 1:150
Streptavidin-AP	DakoCytomation; D 0396		IH, 1:100
anti-rabbit HRP	Santa Cruz Biotechnology; sc-2317	Donkey	WB, 1:4000
anti-rat Biotin	DakoCytomation; E0468	Rabbit	IH, 1:100
anti-rat FITC	Dianova/ Jackson ImmunoResearch; 112-095-167	Goat	IF, 1:100
anti-sheep PE	Dianova/ Jackson ImmunoResearch ; 713-116-147	Donkey	IF, 1:100

Table 2.5 FACS antibodies		
Antibody	Company; product number	Reactivity
B220-PE	BD Pharmingen; 553089	Mouse, human
CD11b-APC	BD Pharmingen; 553312	Mouse, human
CD11c-Biotin	BD Pharmingen; 553800	Mouse
CD90-PE	BD Pharmingen; 553005	Mouse
DX5-PE	BD Pharmingen; 553858	Mouse
F4/80-Biotin	Serotec; MCA497	Mouse
I-A ^b -Biotin	BD Pharmingen; 553550	Mouse
Ly-6G-PE	BD Pharmingen; 551461	Mouse

Table 2.5 - continued -		
Ly-6C-FITC	BD Pharmingen; 553104	Mouse
NK1.1-PE	BD Pharmingen; 557391	Mouse
Strep-PerCP	BD Pharmingen; 554064	-

2.1.3 Primers

Primers were synthesized and purchased from Sigma-Aldrich.

Table 2.6 Genotyping primers	
Name	Sequence 5' to 3'
L/F LacZ/Dll1 KO	CAA ATT CAG ACG GCA AAC
R Melta 38	ATC CCT GGG TCT TTG AAG AAG
Cre1	GCC TGC ATT ACC GGT CGA TGC AAC GA
Cre2	GTG GCA GAT GGC GCG GCA ACA CCA TT
R1295	GCG AAG AGT TTG TCC TCA ACC
R523	GGA GCG GGA GAA ATG GAT ATG
R26F2	AAA GTC GCT CTG AGT TGT TAT
Dll1 plox right	GAG AGT ACT GGA TGG AGC AAG
Dll1 plox left	CAC ACC TCC TAC TTA CCT GA

Table 2.7 Semiquantitative RT-PCR primers		
Name	Sequence 5' to 3'	Product size
mDll1 left	TGC AGG AGT TCG TCA ACA AG	458 bp
mDll1 right	GTG CTC GTC ACA CAC AAA CC	
18SrRNA-F	CCT GCG GCT TAA TTT GAC TC	510 bp
18SrRNA-R	GGC CTC ACT AAA CCA TCC AA	

2.1.4 Microscopes and imaging software

Microscopes

- Zeiss Axio Observer.Z1 fluorescence microscope system equipped with bright-field and fluorescent light optics and cameras AxioCamMR3 and AxioCamMR3_2
- Zeiss Stemi 2000-C equipped with a with a AxioCam ICc1 camera

-
- Leica DM4000B microscope equipped with a light polarization system and a DFC 320 camera

Imaging software

- AxioVision Release 4.6 (full version)
- AxioVision LE 4.7 (free download version)
- ImageJ 1.40g
- Leica QWin V3 with Applet Runner “Flächenmessung maskiert von TIF”
- Adobe Photoshop CS3

2.2 Mice handling and animal experiments

2.2.1 Mouse strains, breeding, and handling

In the course of the thesis, 3 mouse strains were used: $Dll1^{+/lacZ}$, $VECad-Cre-ER^{T2}/Dll1^{lox/lox}$, and $VECad-Cre-ER^{T2}/ROSA26R$.

$Dll1^{+/lacZ}$ (Hrabé de Angelis *et al.*, 1997) mice were bred on an isogenic 129S1/SvImJ background. These animals carry a *lacZ*-reporter gene on the second allele, instead of *Dll1*; thereby serving as *Dll1-lacZ* reporter, as well as *Dll1* heterozygous strain. *LacZ* identification mimics endogenous *Dll1* expression (Hrabé de Angelis *et al.*, 1997; Beckers *et al.*, 1999). Mice homozygous for the loss-of-function allele of *Dll1* $Dll1^{lacZ/lacZ}$ die around day 12 of embryonic development (Hrabé de Angelis *et al.*, 1997; Rubio-Aliaga *et al.*, 2007). Heterozygous mutant mice were bred by crossing heterozygous males with non-transgenic females. Non-transgenic littermates (WT) served as controls.

To answer the question if *Dll1* acts from the endothelium, an inducible endothelial *Dll1* knockout mouse strain: $VECad-Cre-ER^{T2}/Dll1^{lox/lox}$ was generated on a mixed C57Bl/J background; the strain was termed e*Dll1* KO after induction.

The $VECad-Cre-ER^{T2}$ mouse line expressed a tamoxifen-inducible Cre-recombinase ($Cre-ER^{T2}$) under control of the vascular endothelial cadherin promoter (*VECad*) (Monvoisin *et al.*, 2006). The *VECad* promoter has been shown to be active in the endothelium during embryonic development and in adult organs (Gory *et al.*, 1999; Alva *et al.*, 2006). The inducible activity of the $Cre-ER^{T2}$ is based on the principle that ER^{T2} (a mutant form of the estrogen receptor ligand-binding domain) is a specific receptor for tamoxifen (the

biologically active form 4-hydroxytamoxifen is a metabolic product) and is unresponsive to natural estrogens. In the absence of tamoxifen, Cre-ER^{T2} protein remains in the cytoplasm, thereby preventing Cre-mediated recombination in the nucleus (Monvoisin *et al.*, 2006).

The homozygous floxed Dll1 (Dll1^{lox/lox}) mouse strain (Hozumi *et al.*, 2004) carried *loxP* sequences flanking *Dll1* exons 3 and 4; exon 4 encodes the DSL region which is essential for binding to the Notch receptor. Cre-mediated recombination removed the floxed region and generated a termination codon by frameshift.

VECad-Cre-ER^{T2}/Dll1^{lox/lox} animals were generated by mating over 2 generations. First VECad-Cre-ER^{T2} transgene-positive animals were mated with Dll1^{lox/lox} animals. VECad-Cre-ER^{T2}/Dll1^{+/lox} F1 animals were again mated with Dll1^{lox/lox} mice, generating amongst others VECad-Cre-ER^{T2}/Dll1^{lox/lox}. The strain was maintained by continuous crossing of VECad-Cre-ER^{T2}/Dll1^{lox/lox} with Dll1^{lox/lox} mice. Dll1 knockout was induced by tamoxifen injection as described in chapter 2.2.3. Non-transgenic littermates, i.e. VECad-Cre-ER^{T2} negative animals (-/Dll1^{lox/lox}) which had also been treated with tamoxifen served as controls (CTRL).

To verify the specificity and efficiency of induction of the VECad-Cre-ER^{T2} strain, mice were crossed with ROSA26R reporter mice (Soriano, 1999; Monvoisin *et al.*, 2006). These mice contain at the ROSA locus a *lacZ* gene and upstream of the gene a floxed stop cassette. Upon Cre recombinase activity, the stop cassette is excised and *lacZ* expression is driven and β -galactosidase activity can be detected by X-gal staining.

Homozygous floxed VECad-Cre-ER^{T2}/ROSA26R animals were generated and maintained using the same scheme as described for the VECad-Cre-ER^{T2}/Dll1^{lox/lox} mouse strain.

Cre activity and reporter gene expression was induced by tamoxifen injection as described. Non-transgenic littermates, i.e. VECad-Cre-ER^{T2} negative animals (-/ROSA26R) which had also been treated with tamoxifen served as controls (CTRL).

After separation from the mother, pups were fitted with an ear tag displaying a unique 4-digit number for identification and a tail biopsy was taken for determination of the genotype.

All animal studies were performed with permission of the State of Niedersachsen, and in compliance with the German Law for the Protection of Animals and the NIH Guide for the Care and Use of Laboratory Animals.

2.2.2 Genotyping

DNA isolation from mouse tail biopsies

Tail clips were obtained from 4 week old mice (weaning age) and incubated in 300µl tail lysis buffer on a shaker at 450 rpm and 56°C overnight. After vortexing, 300 µl phenol/chloroform was added, briefly suspended by vortex and centrifuged for 10 min at 13000 rpm. 200 µl of the supernatant was carefully transferred to a new tube and the containing genomic DNA precipitated by addition of 600 µl 100% ethanol (EtOH), thorough shaking and incubation for 10 min at room temperature. The DNA was pelleted by centrifugation for 3 min at 9000 rpm, the supernatant removed and the pellet washed with 500 µl 70% EtOH. After another centrifugation for 3 min at 9000 rpm and removal of the supernatant, the DNA pellet was air dried and reconstituted in 100 µl TE buffer. To inactivate DNases and dissolve the pellet completely, the DNA was incubated for 2 h at 56°C. The genomic DNA solution was stored at 4°C, or for long-term storage at -20°C.

PCR

Dll1-lacZ PCR	
Reaction composition	PCR program
30.5 µl ddH ₂ O 5 µl 10x PCR buffer B 5 µl 15 mM MgCl ₂ 1 µl 10 mM dNTP-mix 1 µl Primer L/F LacZ/Dll1 KO 1 µl Primer R Melta 38 2.5 µl DMSO 2 µl Taq polymerase 2 µl genomic DNA	1. 94°C 3 min 2. 94°C 30 sec 3. 53°C 30 sec 4. 72°C 45 sec 5. repeat step 2-4 39x 6. 72°C 7 min
The PCR product was run on a 1% agarose gel. A band of 580 bp indicated the Dll1-lacZ allele; no band indicated the wildtype allele. The PCR was always performed with appropriate controls, i.e. wildtype, Dll1-lacZ, and H ₂ O.	

VE-Cadherin -Cre^{ERT2} PCR	
Reaction composition	PCR program
18 µl ddH ₂ O 2.5 µl 10x PCR buffer C 0.5 µl 10 mM dNTP-mix 1 µl Primer Cre1 1 µl Primer Cre2 1 µl Taq polymerase 1 µl genomic DNA	1. 94°C 3 min 2. 94°C 45 sec 3. 61°C 45 sec 4. 72°C 1 min 5. repeat step 2-4 33x 6. 72°C 7 min
The PCR product was run on a 1% agarose gel. A band indicated the presence of the VE-Cadherin-Cre ^{ERT2} transgene. The PCR was always performed with appropriate controls, i.e. wildtype, VE-Cadherin-Cre ^{ERT2} transgene positive, and H ₂ O.	

Rosa26R PCR	
Reaction composition	PCR program
9.5 μ l ddH ₂ O 2.5 μ l 10x PCR buffer A 5 μ l Q-solution 1.5 μ l 25mM MgCl ₂ 0.5 μ l 10 mM dNTP-mix 1 μ l Primer R1295 1 μ l Primer R523 1 μ l Primer R26F2 1 μ l Taq polymerase 2 μ l genomic DNA	1. 93°C 3 min 2. 93°C 30 sec 3. 58°C 30 sec 4. 72°C 1 min 5. repeat step 2-4 37x 6. 72°C 7 min
The PCR product was run on a 1% agarose gel. A band at 500 bp showed the wildtype allele; a band at 250 bp showed the ROSA26R floxed allele. The PCR was always performed with appropriate controls, i.e. wildtype, ROSA26R heterozygous floxed, ROSA26R homozygous floxed, and H ₂ O.	

Dll1 flox/flox PCR	
Reaction composition	PCR program
40 μ l ddH ₂ O 5 μ l 10x PCR buffer C 1 μ l 10 mM dNTP-mix 1 μ l Primer Dll1 plox left 1 μ l Primer Dll1 plox right 1 μ l Taq polymerase 1 μ l genomic DNA	1. 94°C 3 min 2. 94°C 30 sec 3. 54°C 30 sec 4. 72°C 30 sec 5. repeat step 2-4 29x 6. 72°C 10 min
The PCR product was run on a 2% agarose gel. A band at 204 bp showed a wildtype allele; a band at 238 bp showed a Dll1 floxed allele. The PCR was always performed with appropriate controls, i.e. wildtype, Dll1 flox heterozygous, Dll1 flox homozygous, and H ₂ O.	

2.2.3 Knockout induction

For induction of Cre recombinase activity in VECad-Cre-ER^{T2}/Dll1^{lox/lox} and VECad-Cre-ER^{T2}/ROSA26R mice, animals 8 weeks of age were treated. Therefore, 100 μ l TAM solution was applied by intraperitoneal injection on 5 consecutive days, which is equivalent to a treatment of 10 mg tamoxifen per animal in total (Monvoisin *et al.*, 2006). After completion of treatment, animals were left for 9 days before analysis or infarction by LAD occlusion surgery.

2.2.4 Echocardiography

Functional heart analysis was performed by means of echocardiography. Mice were analysed under continuous sedation by isofluran inhalation (1-3%), after fur removal at the chest using hair removal cream. Left ventricular, two-dimensional long-axis images were

obtained in B- and M-mode by transthoracic echocardiography using a VisualSonics Vevo 770 High-Resolution Imaging System equipped with a 30MHz RMV-707B scanning head. Calculation basics are summarized in the following tables; calculations were automatically performed by the software based on the measured parameters.

Parameter	Description	Measurement type	Units
Endo Area; d (LVED area)	LV endocardial area; diastole	Polygon area	mm ²
Endo Area; s	LV endocardial area; systole	Polygon area	mm ²
Endo Major; d	LV endocardial major axis; diastole	Linear distance	mm
Endo Major; s	LV endocardial major axis; systole	Linear distance	mm
Heart Rate	Heart rate		BPM
LVEDV	Left ventricular end-diastolic volume	(Calculation)	μl
LVESV	Left ventricular end-systolic volume	(Calculation)	μl
SV	Stroke volume	(Calculation)	μl
EF	Ejection fraction	(Calculation)	%
CO	Cardiac output	(Calculation)	μl/min

LV parameter	Formula
LVEDV	$\frac{4\pi}{3} \times \frac{End\ Major; d}{2} \times \left(\frac{End\ Area; d}{\pi \left(\frac{End\ Major; d}{2} \right)} \right)^2$
LVESV	$\frac{4\pi}{3} \times \frac{End\ Major; s}{2} \times \left(\frac{End\ Area; s}{\pi \left(\frac{End\ Major; s}{2} \right)} \right)^2$
SV	$LVEDV - LVESV$
EF	$\frac{LVEDV - LVESV}{LVEDV} \times 100$
CO	$SV \times Heart\ Rate$

2.2.5 Permanent LAD ligation surgery

Ten- to twelve-week-old mice were subjected to permanent left anterior descending coronary artery (LAD) ligation. Therefore, mice were anaesthetized by isoflurane inhalation, intubated and ventilated with oxygen supplemented with isoflurane (1.5%) using a rodent ventilator. The chest wall was shaved and the mouse placed on a heating pad to maintain body temperature at 37°C. A thoracotomy was performed in the second left intercostal space and the left coronary artery was permanently ligated with a simple interrupted suture (Prolene monofil 6-0) at the site approximately 1 mm below the edge of the left cardiac auricle. The chest wall was closed in two layers: the ribs were adapted with a line of 3 simple interrupted sutures (Polyester braided 5-0). Muscles were placed back into position with a simple interrupted suture (Silk braided 6-0). The skin was closed with 3 horizontal mattress sutures (Polyester braided 5-0). Mice were extubated as they started to breathe spontaneously and allowed to recover. Antibiotic prophylaxis was not given, but no apparent infection was observed in any animal during the course of study.

Sham operation involved thoracotomy and suturing, without LAD occlusion.

2.2.6 Perfusion fixation, tissue embedding, and cryosectioning

For various baseline and infarcted heart analyses, *in situ* fixation and processing of diastolic arrested hearts was performed. (Perfusion fixation was not done if protein or RNA was isolated or for FACS analysis of spleen tissue) Therefore, mice were narcotised with approximately 0.4 ml anaesthesia cocktail, the chest cavity opened and the heart and aorta exposed. After opening of the right atrium, all solutions were perfused through the heart retrograde through the aorta with a pressure of 80 mm Hg. The heart was arrested in diastole by perfusion of KCl arrest solution until beating of the heart stopped, followed by 10 ml ice-cold perfusion solution.

The heart was taken out, placed in 15% sucrose solution (in PBS w/ Ca^{2+} Mg^{2+}) for 2-4 h in ice, followed by 30% sucrose solution (in PBS w/ Ca^{2+} Mg^{2+}) overnight at 4°C. Tissue was embedded in OCT-compound, snap frozen in 2-methylbutane cooled in liquid nitrogen and stored at -20°C until further processing.

Frozen tissue (complete hearts, collection of sections starting below level of the atria) was cut into 10 μm sections with a cryotome. Two times 3 sections were placed on one microscope slide, dried at room temperature for 2 h and stored at -20°C.

2.3 Basic methodology

2.3.1 Staining protocols

Evan's blue and TTC staining

For Evan's blue and TTC staining, mice were narcotised with approximately 0.4 ml anaesthesia cocktail, the chest cavity opened and the heart exposed. The heart was perfused with 0.3 ml Evan's blue solution by injection through the right ventricle. The stained heart was excised, washed gently in PBS on ice, placed in a mould of aluminium foil, and a solution of 3% agarose in PBS added. After cooling and solidifying, the fixed heart was cut cross-sectional into 6 equal pieces using a razorblade device and the agarose removed again. The pieces were incubated in pre-warmed TTC solution at 37°C for 10 minutes, transferred to 3% formaldehyde solution and analysed.

H&E staining

For H&E staining, cryosections were immediately used from -20°C.

1. Fix in 70% EtOH for 1 min, followed by rinsing with ddH₂O
2. Stain with Mayer's Hemalum for 3 min
3. Rinse with tap water and fix by dipping in 0.5% HCl in EtOH
4. Remove unspecific staining with warm running tap water for 10 min
5. Immerse for 15 sec in 80% EtOH, then for 15 sec in 96% EtOH
6. Stain with eosin/phloxin solution for 3 sec
7. Dehydrate in ascending alcohol series 2 min each: 90% EtOH , 96% EtOH, 100% EtOH and 100% EtOH
8. Clear with Xylol for 10 min and mount with coverslips and Vitro-clud

Immunofluorescence staining

For immunofluorescence staining, frozen cryosections were fixed in 4% PFA for 15 min at room temperature. After 3 washes in PBS for 5 min each, sections were incubated with blocking buffer (containing serum of the same species as the secondary antibody) for 1 h in a humidified chamber. After removal of the blocking solution, primary antibody diluted in antibody dilution buffer was added and incubated in a humidified chamber at 4°C overnight. Next, the slides were washed three times with PBS for 5 min each, followed by incubation with the appropriate secondary antibody diluted in antibody dilution buffer for 2 h in a dark humidified chamber. For co-staining, slides were washed three times for 5 min with PBS and incubated with the second primary antibody in antibody dilution buffer for 2 h in a

humidified chamber. The sections were washed again three times in PBS for 5 min, the second secondary antibody added and incubated for 2 h in a humidified chamber, in case the primary antibody was not directly coupled. After another 3 washes with PBS, nuclei were stained using DAPI solution (0.5 $\mu\text{g}/\text{ml}$ in ddH_2O) for 2 min, sections washed with PBS, dipped shortly in ddH_2O and mounted with fluorescence mounting medium.

Immunohistochemistry

For immunohistochemistry staining based on an alkaline phosphatase (AP)-coupled avidin-biotin system, frozen cryosections were dried for 5 min and fixed in acetone for 10 min at room temperature. The sections were left for 1 min to let the acetone evaporate and incubated with primary antibody (diluted in TBS/1% BSA) for 1 h at room temperature in a humidified chamber. After three 5 min washes with TBS, a biotin-coupled secondary antibody (diluted in TBS/1% BSA) was added and incubated for 1 h in a humidified chamber. Sections were washed three times with TBS for 5 min each and incubated with streptavidin-AP conjugate (diluted in TBS) for 1 h. During another three washes with TBS for 5 min, developing solution was prepared by giving IH solution B to IH solution A and then adding IH solution C. Sections were incubated in filtered developing solution for 10 min and washed shortly with tap water three times. For counterstaining, Mayer's Hemalum was used for 2 min and washing performed with tap water for 10 min. Slides were mounted using liquefied Kaiser's glycerol gelatine.

LacZ staining

For LacZ staining, cryosections were transferred from -20°C to precooled PBS/0.2% glutaraldehyde and fixed for 10 min at 4°C . After 3 washing steps with LacZ wash buffer for 5 minutes each, staining was done with LacZ staining solution at 37°C overnight with protection from light. For tissue counterstaining with eosin, sections were washed in PBS and rinsed in 70% EtOH, followed by steps 6 to 8 of the H&E staining protocol.

Picrosirius red staining

For picrosirius red staining, cryosections were washed in tap water for 10 min and ddH_2O for 5 min. To prevent background staining, sections were immersed in 0.2% phosphomolybdic acid for 5 min, followed by staining in filtered 0.1% picrosirius red in saturated picric acid overnight. Excess staining was removed by dipping in 0.01N HCl, and dehydrated and fixed by dipping in 70% EtOH and rinsing in 100% EtOH for 3 min twice. Sections were cleared with Xylol for 10 min and mounted with coverslips and Vitro-clud.

TUNEL staining

TUNEL staining of cryosections was performed using the ApopTag[®] Plus Fluorescein *In Situ* Apoptosis Detection Kit according to the manufacturer's instructions. Therefore, cryosections (immediately used from -20°C) were fixed in 1% paraformaldehyde in PBS for 10 min at room temperature, washed in PBS for 5 min twice, post-fixed in precooled ethanol:acetic acid 2:1 for 5 min at -20°C and washed again in PBS for 5 min twice. Excess liquid was removed and the sections circled with a delimiting pen. Equilibration buffer was applied on the sections and incubated for 5 min. The liquid was removed and working strength TdT enzyme added and incubated in a humidified chamber at 37°C for 1 h. The reaction was stopped by washing of the slides in working strength stop/wash buffer for 10 min at room temperature, followed by 3 washes in PBS for 1 min each. Next, anti-digoxigenin conjugate was added and incubated in a dark humidified chamber for 30 min at room temperature. After 4 washing steps in PBS for 2 min each, nuclei were counterstained in DAPI solution (0.5 µg/ml in ddH₂O) for 2 min, washed with PBS, dipped shortly in ddH₂O and mounted with fluorescence mounting medium.

2.3.2 RNA isolation and RT-PCR

Total RNA isolation

For Dll1 expression analysis after myocardial infarction, total RNA was isolated from the apex part of the heart (i.e. lower half; infarcted or sham control) of wildtype animals. For verification of endothelial Dll1 knockout after tamoxifen treatment, whole hearts and aorta samples were used.

Heart tissue sample was homogenized in the presence of 1 ml Trizol reagent and incubated for 5 min at room temperature to permit complete dissociation of nucleoprotein complexes. (Aorta samples were homogenized in 0.4 ml Trizol and the following reagent volumes downscaled accordingly.) After addition of 0.2 ml chloroform the solution was shaken vigorously for 15 sec and incubated for 3 min. The sample was centrifuged at 13000 rpm for 15 min at 4°C, the upper aqueous phase transferred to a fresh tube and 0.5 ml isopropanol added and left for 10 min in order to precipitate RNA. Following another centrifugation at 13000 rpm and 4°C, the supernatant was removed and the RNA pellet washed with 1 ml 75% EtOH by vortexing and centrifugation at 7500 rpm and 4°C for 5min. After supernatant removal, the pellet was air-dried briefly and reconstituted in 20 µl TE buffer. Integrity of

isolated total RNA was verified on an agarose gel; quality and concentration were measured on a NanoDrop[®] ND-1000. RNA samples were stored at -20°C.

Reverse transcription-PCR (RT-PCR) and PCR

RT-PCR	
Procedure	Master mix per sample
<ol style="list-style-type: none"> 1. 1 µg total RNA was used and the volume adjusted to 12 µl with DEPC-H₂O 2. 2 µl 10 µM oligo(dT)₁₈ primer was added and incubated at 70°C for 5 min, followed by immediate cooling on ice for 5 min 3. 11 µl of the master mix was added, incubated at 42°C for 60 min and the enzyme reaction stopped at 70°C for 15 min 	2.75 µl DEPC-H ₂ O 5 µl 5x M-MLV RT reaction buffer 1.25 µl 10 mM dNTP-mix 1 µl RNaseOUT [™] 1 µl M-MLV Reverse Transcriptase

PCR	
mD11 PCR	18S rRNA PCR
<u>Reaction composition</u> 15.90 µl ddH ₂ O 2.5 µl 10x PCR buffer C 2 µl 5x Q-solution 0.5 µl 10 mM dNTP-mix 1 µl Primer mD11 left 1 µl Primer mD11 right 0.1 µl Taq polymerase 2 µl cDNA <u>Program</u> <ol style="list-style-type: none"> 1. 95°C 3 min 2. 95°C 45 sec 3. 60°C 45 sec 4. 72°C 90 sec 5. repeat step 2-4 37x 6. 72°C 7 min 	<u>Reaction composition</u> 11.40 µl ddH ₂ O 2.5 µl 10x PCR buffer A 5 µl 5x Q-solution 1.5 µl 25 mM MgCl ₂ 0.5 µl 10 mM dNTP-mix 1 µl Primer 18SrRNA-F 1 µl Primer 18SrRNA-R 0.1 µl Taq polymerase 2 µl cDNA <u>Program</u> <ol style="list-style-type: none"> 1. 95°C 5 min 2. 95°C 10 sec 3. 57°C 30 sec 4. 72°C 30 sec 5. repeat step 2-4 24x 6. 72°C 7 min
PCR products were detected by electrophoresis through a 1% agarose gel in TAE buffer.	

2.3.3 Protein isolation and Western blotting

Protein isolation

Protein was isolated from the apex part of the heart (i.e. lower half; infarcted or sham control) of wildtype animals. Tissue samples were washed in PBS once, homogenized with 0.5 ml ice-cold 1x protein lysis buffer and incubated for 30 min on ice. Next, the protein lysate was cleared by centrifugation at 13000 rpm and 4°C for 10 min, the supernatant

transferred to a fresh tube and the protein sample stored at -80°C . Protein concentration was measured based on Bradford.

SDS-PAGE

Samples were prepared by dilution in Laemmli buffer, boiled at 95°C for 5 min, cooled on ice for 1 min and centrifuged for 5 min at 13000 and 4°C to eliminate any protein aggregates and thereby reduce background staining.

A SDS-polyacrylamide gel (5% stacking gel, 8% resolving gel) was loaded with 20 μg protein per sample. Proteins were separated in a vertical electrophoresis chamber unit with SDS running buffer at 115V for about 1 h 45 min.

Western blot

The separated proteins were transferred from the SDS-PAGE gel to a nitrocellulose membrane by wet tank electroblotting in transfer buffer for 2 hours at 360 mA.

For specific protein detection, the membrane was washed with TBST for 5 min at room temperature and unspecific antibody binding blocked by incubation in 5% MP/TBST for 1 h. The primary antibody was diluted in 5% MP/TBST and incubated with the membrane at 4°C overnight. After three 5 min washes with TBST, HRP-conjugated secondary antibody diluted in 5% MP/TBST was added and incubated for 1 h at room temperature. The blot was washed three times with TBST for 5 min each and the protein-HRP system detected using Western LightningTM Chemiluminescence Reagent according to the manufacturer's instructions.

Western blot stripping

For removal of primary and secondary antibody after detection, blots were stripped for re-use. Therefore, the membrane was incubated in stripping buffer at 60°C for 1 h and washed thoroughly in TBST at least three times for 10 min. Afterwards, blots could be blocked and incubated with antibody again.

2.3.4 FACS analysis

Spleen tissue to be analysed by FACS was squeezed with the rough surface of two microscope slides and carefully collected adding FACS wash buffer. The solution was centrifuged for 7 min at 300g, the supernatant discarded and the pellet resuspended using 1 ml FACS wash buffer. Afterwards, 10 ml whole blood lysis buffer was added and the

mixture incubated for 10 min at room temperature with occasional vortexing. The solution was washed once by centrifugation for 7 min at 300g and the pellet resuspended by FACS wash buffer. To remove debris, the mixture was sieved through a 30 μm cell strainer. Following, the solution was centrifuged for 7 min at 300g, counted and resuspended with FACS wash buffer to obtain a concentration of 5 million cells per 300 μl solution. The resultant cell solution was divided into FACS tubes with 300 μl cell solution per sample. 5 μl Fc Blocking reagent was added per sample and incubated for 10 min at 4°C. Afterwards, 50 μl FACS antibody mix 1 was added, vortexed and incubated for 30 min at 4°C. After 2 washing steps for 7 min at 300g, 250 μl washing buffer was added and 50 μl FACS antibody mix 2. The solution was vortexed, incubated for 30 min at 4°C, washed twice by centrifugation for 7 min at 300g, FACS wash buffer added and FACS analysis performed on a BD FACSCalibur.

2.4 Data analyses

2.4.1 Dll1 positive vessel threshold size

To determine the minimal size of Dll1 positive vessels, cryosections from the middle portion of Dll1^{+lacZ} baseline hearts stained with lacZ were analyzed; 1 section per animal and 8 animals in total were used. From each section the inner circumference of all lacZ positive vessels was measured and the corresponding diameter calculated. The smallest diameter determined was defined as Dll1 positive minimal vessel size.

2.4.2 SMA positive vessel quantification

In a baseline setting, SMA positive vessels were evaluated in SMA immunofluorescent stained sections counterstained with DAPI. 4 animals per group were used and from each animal 3 parallel sections from the basis and 3 sections from the apex of the heart were analyzed. From each complete section the inner circumference of all SMA positive vessels was measured and the according inner diameter calculated. Vessels were organized according to their diameter in groups of <20 μm (resistance vessels), 20-50 μm , 50-100 μm and >100 μm (conductance vessels). The final mean data were normalized to the section area to account for the difference in heart size of WT versus Dll1^{+lacZ} animals and expressed as the number of SMA positive vessels per 1 mm^2 .

For quantification of arteriogenesis, SMA positive vessels were measured in immunofluorescence stained sections from the middle portion of the heart, 7 days after infarction and compared with values from the same middle portion of the heart in baseline conditions. Arteriogenesis was evaluated on one section per animal analyzing both border zones present. To account for the variance in shape of infarction and wall thickness in the border zone, a grid was used for the analysis. The grid with a square size of 0.25 mm² (500x500 μm) was placed so that 1/3 of the square area was located in the infarcted and 2/3 located in the non-infarcted area of the border zone (refer to Figure 2.1), as more arteriogenesis was expected to take place in the viable myocardium. The number of squares was variable, depending on the shape and wall thickness. The grid was placed using images with a 50x magnification; actual vessel measurement was performed on 100x images. The inner circumference of all SMA positive vessels within the grid was measured and the according diameter calculated accordingly. Only structures showing a clear circular structure were scored as vessels, as especially the infarcted area showed at times strong staining but without clear visible vascular structures (see Figure 2.1) (myofibroblasts expressing SMA). The vessel number per group (<20 μm, 20-50μm, and >50 μm) was normalized according to the number of squares analyzed; therefore arteriogenesis was expressed as the number of SMA positive vessels per 0.25 mm². 4 and 8 animals per group were analyzed under baseline and 7 day infarction conditions, respectively.

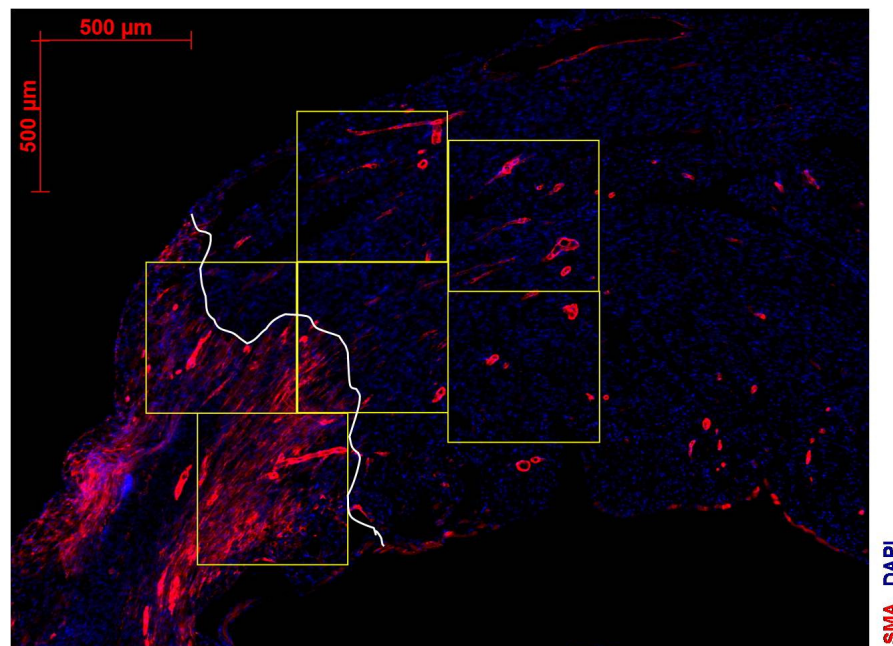


Figure 2.1 Example of grid placement for quantification of arteriogenesis. SMA (red) and DAPI (blue) immunofluorescent image with 50x magnification, showing grid placement so that 1/3 of the grid area is

located in the infarcted area and 2/3 in the non-infarcted myocardium. The white line demarks the border between the infarcted and non-infarcted areas. Actual measurement of vessels within the grid was performed using images with 100x magnification. Only structures showing a clear circular structure were scored as vessel.

2.4.3 LAD domain measurement

For quantification of the LAD domain, mice underwent LAD ligation surgery (without closing of the chest wall), immediately followed by Evan's blue staining and processing of the heart. The area of the myocardium not stained in blue represented the area supplied by the LAD. Images were taken from both sides of all 6 heart pieces and the LAD domain calculated as the mean of all 12 measured values. The LAD domain was expressed as percent of the total section area and corresponds to the area-at-risk after in the myocardial infarction experiment setting. Six animals per group were analyzed.

2.4.4 Infarct size and other LV parameters

Infarct size

1 day after induction of myocardial infarction, infarct size was determined by Evan's blue and TTC staining. The area of the myocardium not stained with Evan's blue represents the area-at-risk (AAR), where infarcted areas (MI) appear pallid, and viable myocardium red (example shown in Figure 2.2 A). Images were taken from both sides of all 6 heart pieces. Areas were traced manually in the digital images and automatically measured by the computer. AAR was expressed as percent of the total section area and the mean of all 12 measured values from each heart was calculated. MI area was expressed as percent of the total section area and the mean of all 12 measured values from each heart determined. For calculation of the ratio MI/AAR, individual area values (pallid area over red area) were calculated and the mean determined from each heart.

Analysis of the infarct size (Pfeffer *et al.*, 1979, Pfeffer *et al.*, 1984; Takagawa *et al.*, 2007) of animals 7 and 28 days after permanent LAD ligation was performed on H&E stained sections. Per heart, 5 equally distributed sections were stained, digital images taken and parameters measured by computer-aided planimetry. Omitting the right ventricle in all measurements, from each section the length of the scar and noninfarcted myocardium of the endocardial and epicardial surfaces was determined (example shown in Figure 2.2 B). For each slide the infarct size was calculated using the formula:

$$\text{Infarct Size (\%)} = \frac{(b + d)}{(a + c)} \times 100$$

a = epicardial circumference (mm)

b = epicardial infarct length (mm)

c = endocardial circumference (mm)

d = endocardial infarct length (mm)

The total infarct size (MI) from each heart was calculated as average of all sections:

$$\text{MI (\%)} = \frac{\sum (\text{Infarct Size (\%)})}{\text{Number of sections}}$$

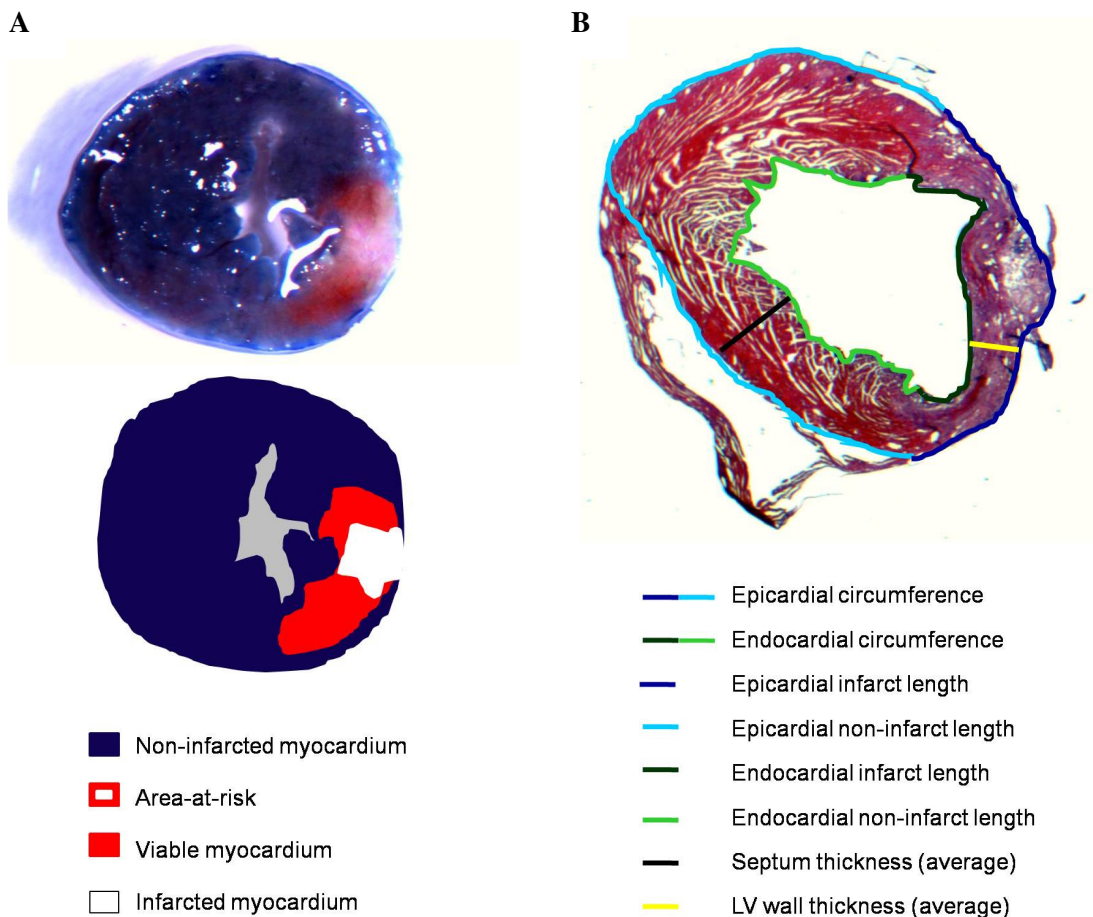


Figure 2.2 Example staining and parameter measurement for infarct size determination. (A) Evan's blue and TTC staining for MI 1d infarct analysis. (B) LV parameter assessment for MI 7d and MI 28d infarct size determination on H&E stained sections.

Epicardial parameters

Epicardial parameters were measured as described above. From each heart, average values from all 5 sections were used for epicardial circumference, as well as epicardial infarct length and epicardial remote length.

Septum and left-ventricular wall thickness

Septum and wall thickness were measured on the same H&E stained sections as used for the determination of infarct size. However, only the middle 3 sections were used for quantification. Parameters were measured by computer-aided planimetry (manual tracing and automatic measurement by the computer) and for each heart the average value from all 3 sections taken.

2.4.5 CSA, myocyte density, and capillary density

Mean cross-sectional area (CSA), myocyte density, and capillary density were measured on WGA, isolectin B4, and DAPI immunofluorescent co-stained cryosections, delineating cell membranes, capillaries and nuclei, respectively. Staining was performed on sections from the central portion of the heart.

For CSA, randomly picked fields within the remote area were selected and the myocyte cross-sectional area measured of at least 100 cells in which the nucleus and a clear staining of the cell borders was visible. Myocyte outlines were traced manually in digital images and automatically measured by the software. CSA was expressed as the mean cell area from 3 animals with 3-4 random fields per animal, for each group.

Myocyte and capillary density were measured by manually counting total cardiomyocyte and capillary numbers in a defined field located in the remote area with a size of 0.08 mm². 3 fields per animal and 3 animals per group were analyzed. Myocyte density was expressed as myocyte number per field and capillary density as number of capillaries per myocyte.

2.4.6 Apoptosis

Apoptosis was evaluated on TUNEL stained cryosections from the middle portion of the infarction. The total number of TUNEL positive cells was manually counted in digital images with a 200x magnification and the tissue area measured in each image to account for wall thinning after infarction. For each image the number of TUNEL positive cells was corrected for the actual area and taken as number of apoptotic cells per 0.5 mm². 3 images

each were counted from the remote, border zone and infarct area. 3, 6, and 5 animals per genotype were analyzed in the groups 3, 7, and 28 days after infarction, respectively.

2.4.7 Fibrosis

Quantification of collagen density was performed on picrosirius red stained sections (staining collagen in red on a yellow tissue background) from the middle portion of the infarcted area. Collagen was assessed in digital images of 400x magnification taken with bright-field and polarized light. Collagen quantification was performed by computer-based planimetry (the colour space was defined by the user and the area measured by the software) on bright-field images and collagen density expressed as collagen positive area in percent of the total tissue area. 3 images per area were evaluated from baseline myocardium and remote, border zone and infarcted areas 28 days post infarction; 4 animals per group were used. The quality of the newly formed collagen was evaluated on polarized light images showing thick, closely packed mature collagen fibres by orange-red birefringency and loosely packed, less cross-linked and immature collagen fibres by yellow-green birefringency (Whittaker *et al.*, 1994; Whittaker, 1998).

2.4.8 CD45 positive area

The area of CD45 positive cells was measured on CD45 immunohistochemically stained sections. Two images per area were taken with a 100x magnification from the baseline myocardium and remote, border zone and infarct area in MI settings. By computer-based planimetry (the colour space was defined by the user and the area measured by the software), CD45 positive area (red stained cells on a blue stained tissue background) was measured and expressed as CD45+ cell area in percent of the total tissue area from each image. 3 to 9 animals per group were analysed baseline and 3, 7, and 28 days after infarction.

2.4.9 Statistics

Data were collected in a blinded fashion. Results were expressed as mean \pm SEM. Differences between two groups were analyzed by Student's *t* test. The survival curve after MI was determined according to Kaplan-Meier and data compared by Log-rank test (Cox-Mantel). A two-sided P value of 0.05 or less was considered statistically significant.

3. RESULTS

3.1 Baseline phenotype of Dll1^{+lacZ} mice

3.1.1 Selective endocardial and coronary endothelial expression of Dll1 in coronary arteries >20 µm

Analysis of Dll1 expression by lacZ staining of whole hearts and heart sections of adult Dll1^{+lacZ} animals revealed a distinctive expression in the endocardium and endothelium of coronary arteries (Figure 3.1 A), but no expression was detected in veins or capillaries. As expected, wildtype (WT) control animals did not show any staining (data not shown). The observed expression pattern was in accordance with Dll1 expression in the adult vasculature described by Limbourg *et al.* (2007).

As not all arteries showed lacZ staining in the heart sections, a Dll1 positive vessel threshold size was determined. Evaluation of lacZ positive vessels showed that 95.8% had a diameter above or equal to 20 µm, whereas only a minor number (4.2%) revealed a diameter lower than 20 µm (Figure 3.1 C). Consequently, allowing for biological variance, a threshold size of selective Dll1 expression can be set to coronary arteries with a minimal inner diameter of 20 µm. All arteries above 20 µm showed Dll1 expression.

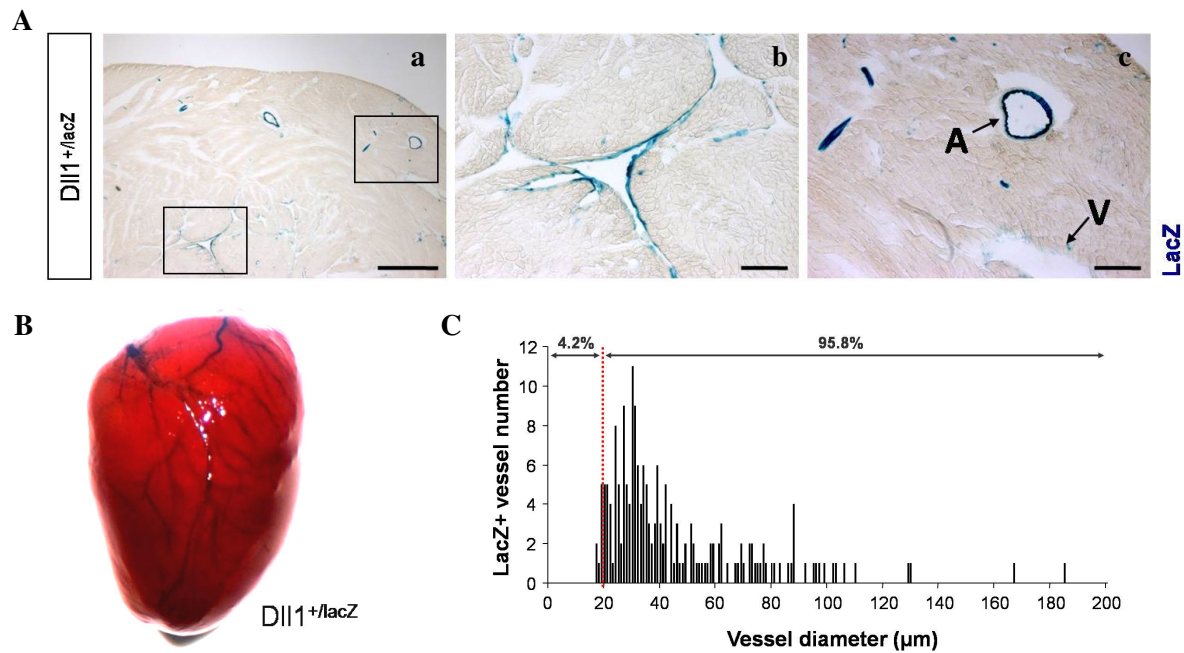


Figure 3.1 Specific endocardial and coronary endothelial expression of *Dll1* in arterial vessels >20 μm . (A-B) *Dll1* expression depicted by lacZ staining of (A) heart sections and (B) whole-mount heart of *Dll1^{+lacZ}* mice. (b) and (c) depict close-ups of the marked sections in (a). Figures showing expression in the endocardium and endothelium of coronary arteries, but not veins or capillaries. Scale bar (a) 500 μm , (b-c) 100 μm ; A: artery, V: vein. (C) Diameter determination of lacZ positive vessels showing 95.8% of positive arteries having a diameter above 20 μm . Allowing for biological variance, a threshold size of selective *Dll1* expression can be set to coronary arteries with a minimal inner diameter of 20 μm . (Vessel numbers depict the entire analysis of n=8 animals.)

3.1.2 *Dll1* regulates heart size, but does not impair cardiac function

To analyse long-term effects of *Dll1* heterozygosity, a 18 months follow up was carried out using *Dll1^{+lacZ}* animals. Animals were viable, fertile and healthy. Survival data showed no difference in life expectancy in comparison to WT animals (Figure 3.2 A), indicating that *Dll1* heterozygosity did not cause major congenital malformations. Mice revealed no gross morphological abnormalities of the heart.

Body weight and body size - as determined by femur length measurement - was comparable in animals 18 months of age (Figure 3.2 B) (Body weight, WT: 37.5 ± 3.1 g vs. *Dll1^{+lacZ}*: 34.8 ± 2.8 g, n = 10/7, P = n.s.; Femur length (FL), WT: 1.71 ± 0.07 cm vs. *Dll1^{+lacZ}*: 1.70 ± 0.07 cm, n = 10/7, P = n.s.). Interestingly however, hearts from *Dll1* heterozygous mice were smaller (Heart weight (HW), WT: 0.221 ± 0.041 g vs. *Dll1^{+lacZ}*: 0.156 ± 0.054 g, n = 10/7, P = 0.037; Ratio HW/FL (g/cm), WT: 0.128 ± 0.020 vs. *Dll1^{+lacZ}*: 0.092 ± 0.032 , n = 10/7, P = 0.026).

This finding was confirmed by echocardiographic analysis of left-ventricular mass (LV mass) and left-ventricular end-diastolic area (LVED area) on mice 10 weeks of age. Calculated LV mass and directly measured LVED area were significantly reduced in $Dll1^{+/lacZ}$ animals (Figure 3.3) (LV mass, WT: 108.2 ± 6.2 mg vs. $Dll1^{+/lacZ}$: 73.3 ± 11.9 mg, $n = 7/7$, $P = 0.0002$; LVED area, WT: 12.04 ± 1.58 mm² vs. $Dll1^{+/lacZ}$: 9.72 ± 1.67 mm², $n = 12/11$, $P = 0.028$). Further functional heart analyses revealed normal heart rates, but interestingly the calculated ejection fraction (EF) was significantly increased in $Dll1$ heterozygotes (Heart rate, WT: 423 ± 44 BPM vs. $Dll1^{+/lacZ}$: 435 ± 37 BPM, $n = 12/11$, $P = \text{n.s.}$; EF, WT: $65.9 \pm 8.5\%$ vs. $Dll1^{+/lacZ}$: $74.3 \pm 6.1\%$, $n = 12/11$, $P = 0.044$). Calculated stroke volume (SV) and cardiac output (CO), however, were comparable with WT animals (SV, WT: 25.21 ± 5.06 μl vs. $Dll1^{+/lacZ}$: 25.09 ± 7.12 μl , $n = 12/11$, $P = \text{n.s.}$; CO, WT: 10.65 ± 2.51 ml/min vs. $Dll1^{+/lacZ}$: 11.16 ± 3.72 ml/min, $n = 12/11$, $P = \text{n.s.}$).

These data imply, that the smaller heart size in $Dll1$ heterozygous mice (with normal body weight) is compensated by a higher ejection fraction, resulting in a normal stroke volume and – as the heart rate is equal – comparable cardiac output. This finding elucidates the normal survival of $Dll1$ heterozygous mice.

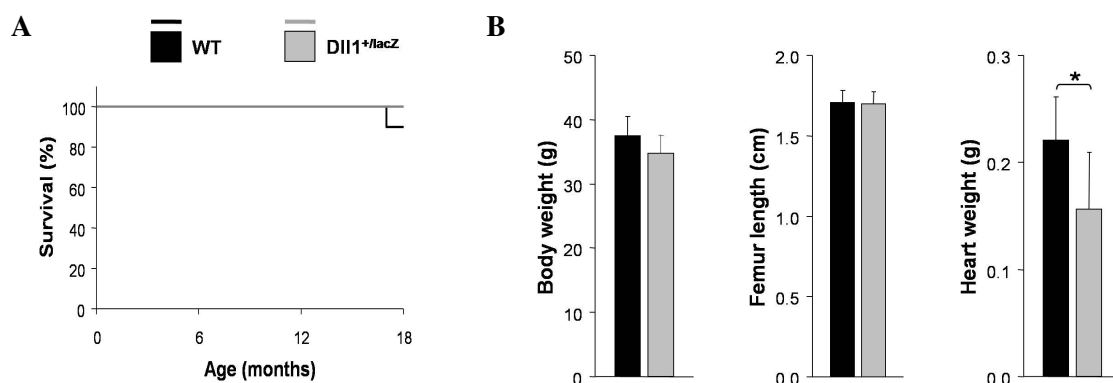


Figure 3.2 Normal survival, but smaller heart size in heterozygous $Dll1$ mice. (A) Kaplan-Meier curve showing unvaried long-term survival comparing WT and $Dll1^{+/lacZ}$ mice. (B) Morphometric analyses of mice at an age of 18 months revealing unchanged body weight and body size (femur length measurement), but smaller heart size in $Dll1$ heterozygotes, compared to WT. (A-B) $n=10/7$; $*P<0.05$.

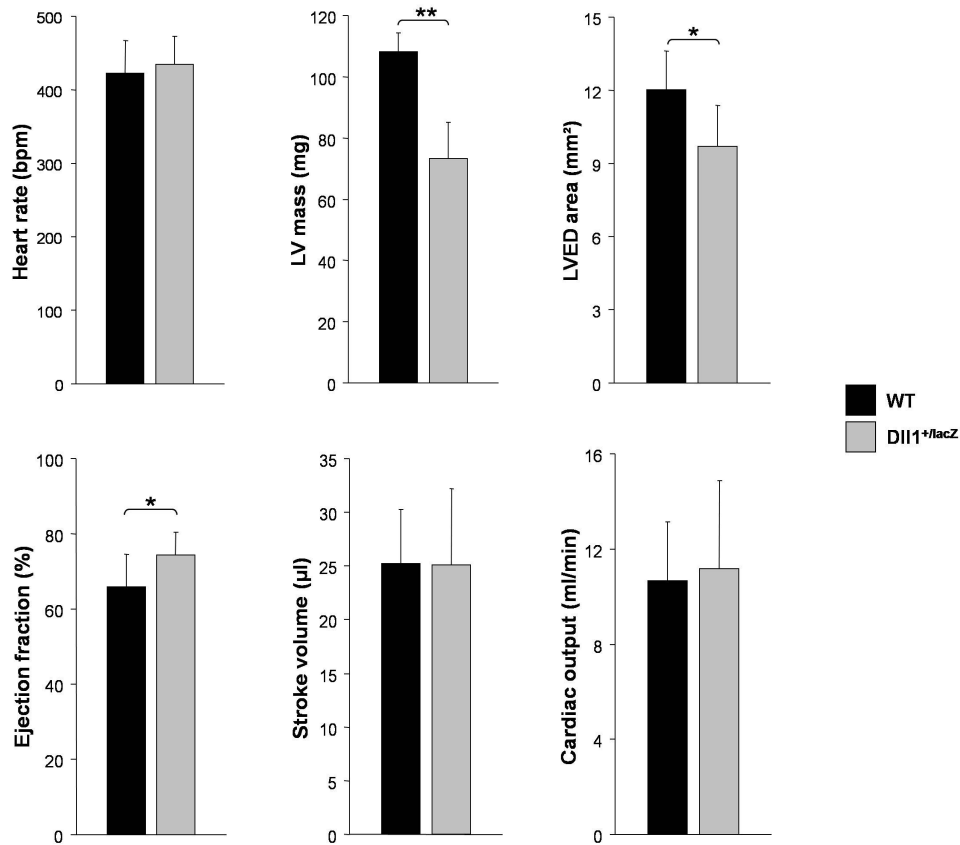


Figure 3.3 Unimpaired cardiac function of Dll1^{+/-lacZ} mice. Echocardiographic study (mice 10 weeks old) confirming a smaller heart size in Dll1^{+/-lacZ} animals by measurement of LVED area and LV mass determination. Measured heart rates were comparable, but the calculated ejection fraction was increased in Dll1 heterozygotes. Calculated stroke volume and cardiac output were comparable with WT data. n=12/11 (LV mass n=7/7); * $P < 0.05$, ** $P < 0.01$.

3.1.3 Dll1 regulates the coronary artery phenotype

As Notch signalling has been shown to play an essential role in vascular development, we analysed effects of Dll1 heterozygosity on adult coronary vasculature. 10 weeks old animals were evaluated and SMA positive vessels - identifying arteries - quantified in heart sections. Analyses in the basis part of the heart (directly below the atria) (Figure 3.4 A) showed a significantly reduced number of medium and large conductance vessels ($>20 \mu\text{m}$) in Dll1^{+/-lacZ} animals (Number of vessels 20-50 μm per mm^2 , WT: 2.92 ± 0.43 vs. Dll1^{+/-lacZ}: 1.14 ± 0.35 , $P = 0.002$; Number of vessels 50-100 μm per mm^2 , WT: 0.44 ± 0.02 vs. Dll1^{+/-lacZ}: 0.25 ± 0.06 , $P = 0.004$; Number of vessels $>100 \mu\text{m}$ per mm^2 , WT: 0.30 ± 0.06 vs. Dll1^{+/-lacZ}: 0.12 ± 0.03 , $P = 0.006$). On the other hand, the number of resistance vessels smaller $20 \mu\text{m}$, i.e. vessels not showing Dll1 expression, was significantly elevated (Number

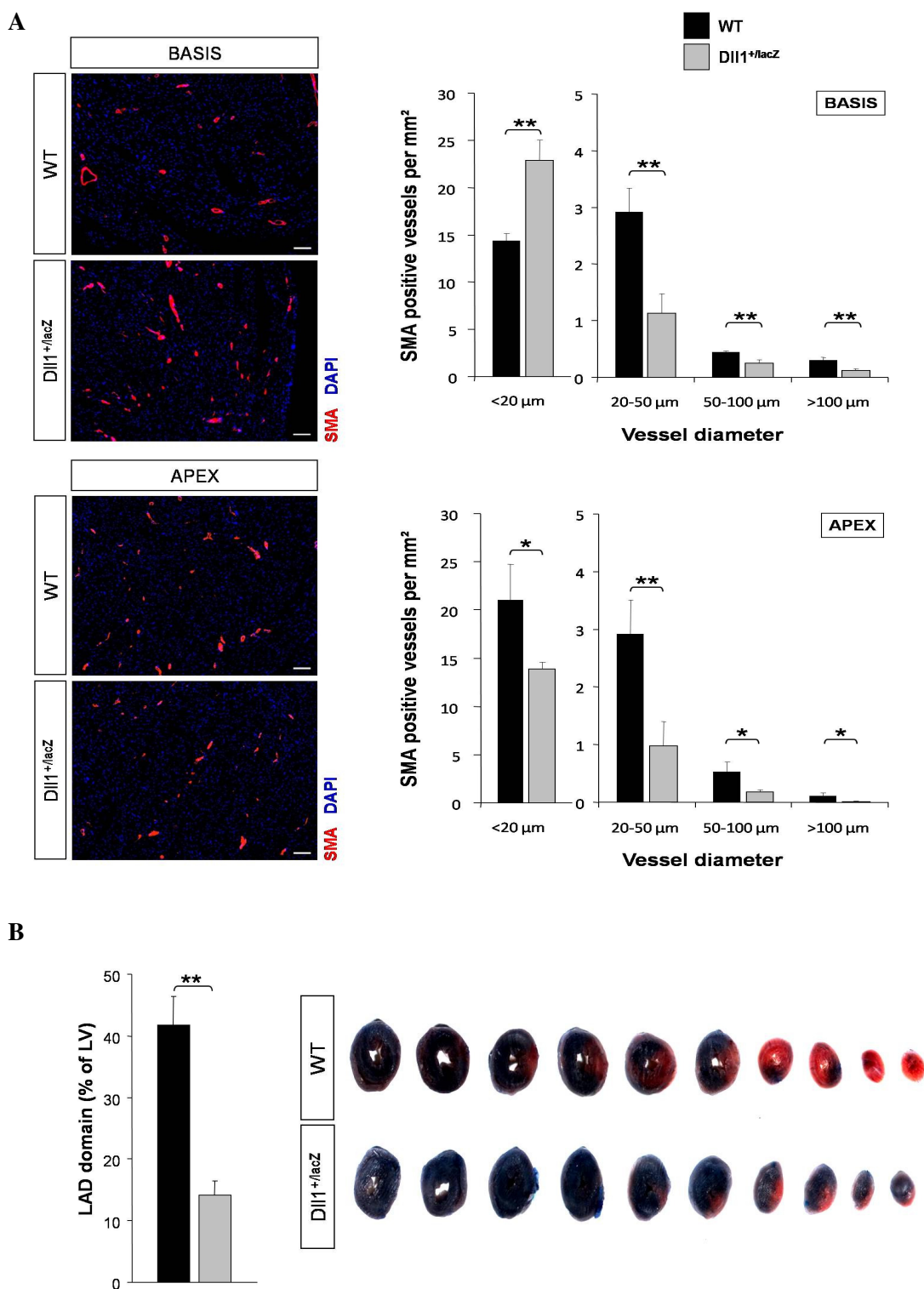
of vessels $<20\ \mu\text{m}$ per mm^2 , WT: 14.40 ± 0.79 vs. $\text{Dll1}^{+/lacZ}$: 22.88 ± 2.15 , $P = 0.002$). Quantification of vessel numbers in the apex heart region revealed again a reduced number of conductance vessels bigger than $20\ \mu\text{m}$, yet the number of resistance vessels smaller $20\ \mu\text{m}$ was also significantly reduced in this part, in contrast to the basis analysis (Number of vessels $<20\ \mu\text{m}$ per mm^2 , WT: 21.04 ± 3.71 vs. $\text{Dll1}^{+/lacZ}$: 13.88 ± 0.71 , $P = 0.033$; Number of vessels $20\text{-}50\ \mu\text{m}$ per mm^2 , WT: 2.91 ± 0.60 vs. $\text{Dll1}^{+/lacZ}$: 0.98 ± 0.42 , $P = 0.008$; Number of vessels $50\text{-}100\ \mu\text{m}$ per mm^2 , WT: 0.53 ± 0.17 vs. $\text{Dll1}^{+/lacZ}$: 0.18 ± 0.04 , $P = 0.028$; Number of vessels $>100\ \mu\text{m}$ per mm^2 , WT: 0.11 ± 0.06 vs. $\text{Dll1}^{+/lacZ}$: 0.01 ± 0.01 , $P = 0.027$).

This finding is reasonable as it shows that in Dll1 heterozygous mice coronary vessel size is smaller from the start and therefore a reduced number of vessels will reach more distant regions – apex – of the heart.

The finding of a decreased number of conductance vessels in Dll1 heterozygous hearts raised the question if there is a difference in area that is supplied by the left anterior descending artery (LAD). To answer this question, Evan's blue staining was performed immediately after LAD occlusion, leaving the area supplied by the LAD unstained (red) and staining the rest of the heart in blue. Area quantification (Figure 3.4 B) demonstrated a significantly smaller LAD domain in $\text{Dll1}^{+/lacZ}$ animals, in comparison to WT (LAD domain in % of LV area, WT: 41.75 ± 4.71 vs. $\text{Dll1}^{+/lacZ}$: 14.11 ± 2.38 , $n = 6/6$, $P = 3\text{E-}6$).

These data describe an adult coronary artery phenotype in Dll1 heterozygous animals which is based on developmental mechanisms. During heart development, arteriogenesis propagates after onset of perfusion and continues after birth to satisfy the increasing needs of a growing heart. It is evident, that reduced Dll1 level impair developmental/neonatal coronary arteriogenesis (the number of large conductance vessels is already decreased in neonates; data not shown), resulting in an adult phenotype.

In addition, data indicate a correlation between heart size and coronary vasculature. Impaired development of the coronary vasculature due to reduced levels of Dll1 presumably caused reduced heart weight and size.



3.1.4 Decreased number of total monocytes and Ly-6C^{lo} monocytes in Dll1^{+lacZ} spleen tissue, but not in blood

Notch signalling has been shown to be associated with monocyte/macrophage differentiation. Thus, FACS analyses were performed (Figure 3.5) from blood and spleen tissue and monocyte subsets characterized under basal conditions. Subsets were determined as described by Nahrendorf *et al.* (2007): monocytes and their lineage descendants were defined as CD11b^{hi} (CD90/B220/CD49/NK1.1/Ly-6G)^{lo} mononuclear cells; these were further divided into Ly-6C^{hi} (F4/80/CD11c)^{lo} monocytes and Ly-6C^{lo} (F4/80/CD11c)^{lo} monocytes (Ly-6C^{lo} (F4/80/CD11c)^{hi} defines macrophages/dendritic cells) (Nahrendorf *et al.*, 2007).

Quantification of FACS data revealed a comparable total cell number in spleen tissue of WT and Dll1 heterozygous animals (Spleen-total cell number, WT: 73,988,462 ± 7,247,438 vs. Dll1^{+lacZ}: 57,218,182 ± 5,341,709, n = 12/11, P = n.s.). However, monocyte cell numbers were significantly reduced in Dll1^{+lacZ} animals (Spleen-monocytes (by gating), WT: 13,643,913 ± 1,189,418 vs. Dll1^{+lacZ}: 8,858,182 ± 1,025,864, n = 12/11, P = 0.005; Spleen-monocytes (gating and CD11b+), WT: 1,061,198 ± 107,283 vs. Dll1^{+lacZ}: 717,733 ± 121,529, n = 12/11, P = 0.041). Monocyte subset analyses of Ly-6C^{hi} cells showed decreased numbers in Dll1 heterozygotes, but lower levels didn't show significance (Spleen-Ly-6C^{hi} monocytes, WT: 508,790 ± 53,747 vs. Dll1^{+lacZ}: 346,543 ± 73,293, n = 12/11, P = n.s.(0.068)). The number of Ly-6C^{lo} monocytes in Dll1 heterozygous spleen tissue was significantly lower compared to WT (Spleen-Ly-6C^{lo} monocytes, WT: 153,634 ± 15,963 vs. Dll1^{+lacZ}: 104,005 ± 14,077, n = 12/11, P = 0.027).

In contrast to spleen analyses, circulating monocytes and monocyte subsets from the blood did not show significant changes in Dll1 heterozygotes, compared to WT (Blood-total cell number per ml, WT: 2,678,072 ± 213,781 vs. Dll1^{+lacZ}: 2,865,559 ± 279,792, n = 16/12, P = n.s.; Blood-monocytes per ml (by gating), WT: 213,045 ± 26,433 vs. Dll1^{+lacZ}: 228,592 ± 24,761, n = 16/12, P = n.s.; Blood-monocytes per ml (gating and CD11b+), WT: 108,466 ± 11,234 vs. Dll1^{+lacZ}: 98,779 ± 12,131, n = 16/12, P = n.s.; Blood-Ly-6C^{hi} monocytes per ml, WT: 78,190 ± 8,076 vs. Dll1^{+lacZ}: 66,126 ± 9,925, n = 16/12, P = n.s.; Blood-Ly-6C^{lo} monocytes per ml, WT: 24,325 ± 2,870 vs. Dll1^{+lacZ}: 24,141 ± 2,138, n = 16/12, P = n.s.).

These data suggest that in the adult Dll1 is involved in monocyte and monocyte subset generation in the spleen and not in the generation of circulating monocytes in the blood, although another study proposes that the spleen does not likely produce monocytes, but rather serves as site for monocyte storage (Swirski *et al.*, 2009).

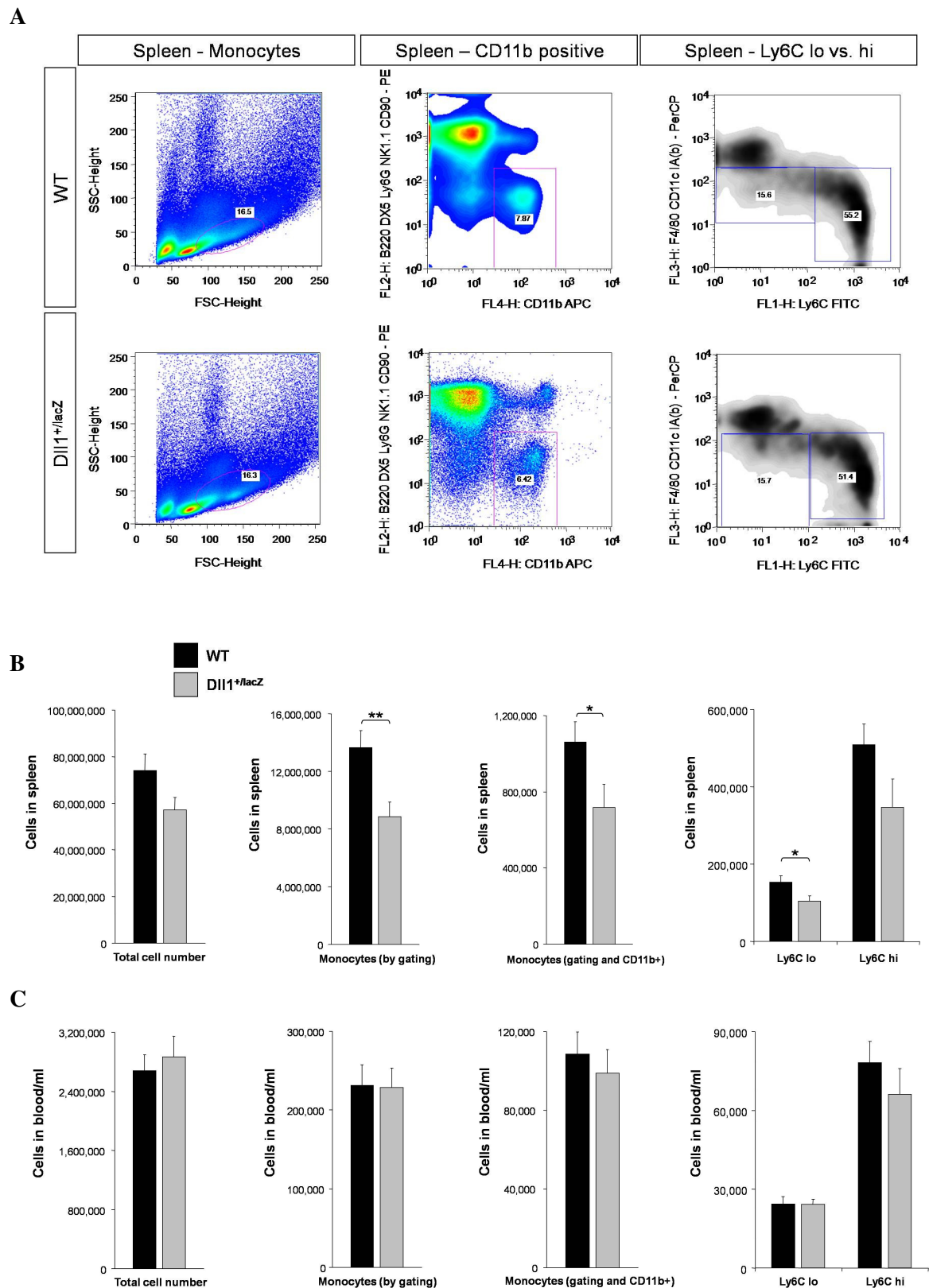


Figure 3.5 Decreased number of total monocytes and Ly-6C^{lo} monocytes in Dll1^{+/-lacZ} spleen tissue, but not in blood. (A) Graphic representation of FACS analysis of mouse spleen tissue. (B) Quantification of FACS analyses showing a comparable total cell number in the spleen of WT and Dll1^{+/-lacZ} mice. Analysis of monocytes revealed significantly reduced monocyte numbers in Dll1^{+/-lacZ} spleen. The number of Ly-6C^{hi} monocytes was not altered, but Ly-6C^{lo} monocyte numbers were significantly decreased in Dll1 heterozygotes, compared to WT. n=12/11; **P*<0.05, ***P*<0.01. (C) FACS analysis of circulating monocytes from the blood showing no significant changes in Dll1 heterozygotes, compared to WT. n=16/12; **P*<0.05.

3.2 Healing after myocardial infarction in $Dll1^{+/lacZ}$ animals

3.2.1 Reduced expression of $Dll1$ increases infarct size and impairs cardiac function 4 weeks post MI

The second part of the study dealt with the ischemic stress response in $Dll1$ heterozygous animals after myocardial infarction (MI), employing a permanent LAD ligation model. Constant ligation of the LAD immediately below the left auricular level has been shown to result in a statistically significant reproducible infarct size (Salto-Tellez *et al.*, 2004).

One important parameter for the assessment of the initial myocardial infarction is the area-at-risk (AAR). This area describes the extent of the infarct-affected myocardial tissue (i.e. tissue within the distal perfusion bed of the ligated coronary artery). The AAR consists of true infarcted areas and viable myocardium. The viable myocardium within the AAR can be rescued by healing mechanisms and reperfusion, which is important to prevent infarct enlargement. The AAR is determined by Evan's blue staining: the area of the myocardium not stained in blue represents the AAR. Within the AAR, infarcted areas (MI) appear pallid, and viable myocardium red.

Analysis of infarcted hearts 1 day after operation (Figure 3.6 A) revealed a significantly smaller AAR in $Dll1$ heterozygous animals, as expected with respect to LAD domain data (AAR (% of LV), WT: 40.0 ± 2.8 vs. $Dll1^{+/lacZ}$: 12.8 ± 2.1 , $n = 3/3$, $P = 0.0007$). However, the relative fraction of the infarct area of the AAR was not significantly altered (Ratio MI/AAR, WT: 0.475 ± 0.040 vs. $Dll1^{+/lacZ}$: 0.417 ± 0.050 , $n = 3/3$, $P = n.s.$).

In accordance, $Dll1^{+/lacZ}$ animals exhibit an initial smaller infarct size, compared to WT 1 day post MI (Figure 3.6 B). The high initial infarct size in WT animals increased slightly, but not significantly 7 days after infarction and stayed constant in the following 3 weeks. In contrast and although infarcts were initially smaller in $Dll1$ heterozygous animals, infarct size continued to increase over time, resulting finally in significantly larger infarcts in $Dll1^{+/lacZ}$ mice 4 weeks after infarction, compared to WT animals (Infarct size MI 1d, WT: 24.5 ± 1.6 % vs. $Dll1^{+/lacZ}$: 8.0 ± 0.6 %, $n = 3/3$, $P = 0.0003$; Infarct size MI 7d, WT: 35.4 ± 10.8 % vs. $Dll1^{+/lacZ}$: 27.5 ± 8.0 %, $n = 12/12$, $P = n.s.$; Infarct size MI 28d, WT: 36.9 ± 13.3 % vs. $Dll1^{+/lacZ}$: 49.4 ± 9.3 %, $n = 12/14$, $P = 0.049$; WT - MI 1d vs. MI 7d $P = n.s.$; WT - MI 7d vs. MI 28d $P = n.s.$; WT - MI 1d vs. MI 28d $P = n.s.$; $Dll1^{+/lacZ}$ - MI 1d vs. MI 7d $P = 0.010$; $Dll1^{+/lacZ}$ - MI 7d vs. MI 28d $P = 3E-5$; $Dll1^{+/lacZ}$ - MI 1d vs. MI 7d $P = 1E-5$).

One important aspect after infarction is cardiac function. Echocardiographic analyses of ejection fraction and stroke volume were consistent with infarct size data. After a higher baseline ejection fraction in Dll1 heterozygotes (described earlier in chapter 3.1.2), EF was significantly reduced in both groups 7 days after infarction (Figure 3.7 A). In the following 3 weeks EF was stable in WT animals, whereas a further decrease was apparent in Dll1^{+/*lacZ*} mice (EF Baseline, WT: 65.9 ± 8.5 % vs. Dll1^{+/*lacZ*}: 74.3 ± 6.0 %, n = 12/11, P = 0.045; EF MI 7d, WT: 38.2 ± 3.6 % vs. Dll1^{+/*lacZ*}: 46.4 ± 7.4 %, n = 7/8, P = n.s.; EF MI 28d, WT: 36.0 ± 11.3 % vs. Dll1^{+/*lacZ*}: 21.5 ± 7.3 %, n = 12/13, P = 0.024; WT - BL vs. MI 7d P = 1E-5; WT - MI 7d vs. MI 28d P = n.s.; WT - BL vs. MI 28d P = 4E-5; Dll1^{+/*lacZ*} - BL vs. MI 7d P = 1E-6; Dll1^{+/*lacZ*} - MI 7d vs. MI 28d P = 8E-5; Dll1^{+/*lacZ*} - BL vs. MI 28d P = 2E-11).

In accordance, WT mice showed a decreased stroke volume 7 days post infarction, but constant values 28 days after ligation (Figure 3.7 B). In infarcted Dll1 heterozygous animals stroke volume decreased slightly, but not significantly after 7 days. 28 days after MI, the stroke volume was strongly deteriorated and significantly lower than in WT animals (SV Baseline, WT: 25.2 ± 5.1 µl vs. Dll1^{+/*lacZ*}: 25.1 ± 7.1 µl, n = 12/11, P = n.s.; SV MI 7d, WT: 19.3 ± 3.3 µl vs. Dll1^{+/*lacZ*}: 23.1 ± 6.4 µl, n = 7/8, P = n.s.; SV MI 28d, WT: 17.9 ± 4.7 µl vs. Dll1^{+/*lacZ*}: 10.7 ± 2.3 µl, n = 12/13, P = 0.022; WT - BL vs. MI 7d P = 0.042; WT - MI 7d vs. MI 28d P = n.s.; WT - BL vs. MI 28d P = 0.025; Dll1^{+/*lacZ*} - BL vs. MI 7d P = n.s.; Dll1^{+/*lacZ*} - MI 7d vs. MI 28d P = 0.003; Dll1^{+/*lacZ*} - BL vs. MI 28d P = 0.0009).

In addition, assessment of LV dilation was performed by echocardiographic measurement of LVED area (Figure 3.7 C). Although in WT no significant change of LVED area was determined when comparing baseline to MI 7d or MI 7d to MI 28d, some degree of dilation was still observed, as the LVED area significantly increased when comparing baseline to MI 28d data. In Dll1^{+/*lacZ*} mice, however, strong dilation was observed by a significant increase in LVED area from baseline via day 7 to day 28 post infarction (LVED area Baseline, WT: 12.04 ± 1.58 mm² vs. Dll1^{+/*lacZ*}: 9.72 ± 1.67 mm², n = 12/11, P = 0.028; LVED area MI 7d, WT: 14.24 ± 2.59 mm² vs. Dll1^{+/*lacZ*}: 13.47 ± 3.02 mm², n = 7/8, P = n.s.; LVED area MI 28d, WT: 15.45 ± 2.51 mm² vs. Dll1^{+/*lacZ*}: 20.41 ± 4.11 mm², n = 12/13, P = 0.041; WT - BL vs. MI 7d P = n.s.; WT - MI 7d vs. MI 28d P = n.s.; WT - BL vs. MI 28d P = 0.025; Dll1^{+/*lacZ*} - BL vs. MI 7d P = 0.024; Dll1^{+/*lacZ*} - MI 7d vs. MI 28d P = 0.009; Dll1^{+/*lacZ*} - BL vs. MI 28d P = 7E-6).

These data point to functional remodelling (infarct size stabilization, compensation of cardiac function and moderate dilation (as expected based on the Frank-Starling

mechanism)) in WT animals post infarction, whereas in Dll1 heterozygous mice increase of infarct size, functional deterioration and strong left-ventricular dilation provide first evidence for adverse remodelling.

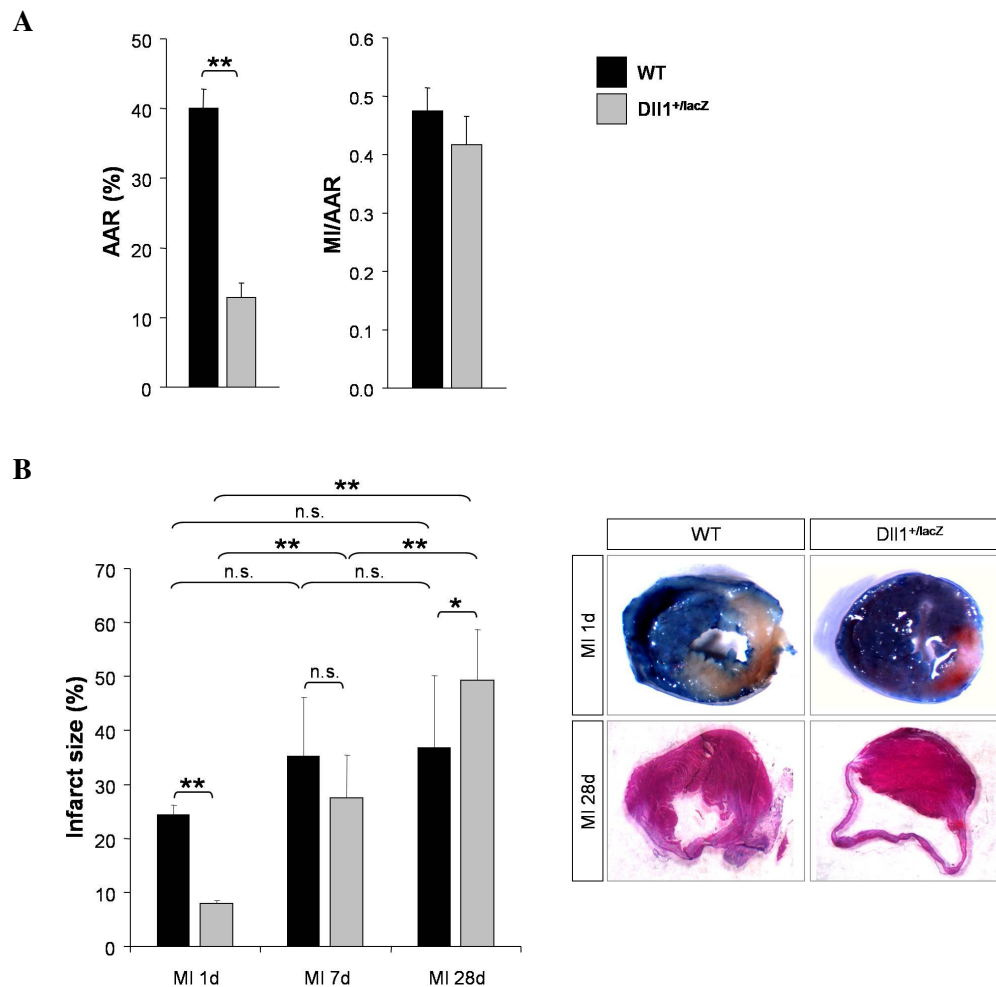


Figure 3.6 Increased infarct size in Dll1 heterozygous mice 4 weeks post infarction. (A) 1 day infarction analysis of area-at-risk (AAR) and infarct area by Evan's blue and TTC staining, showing a decreased AAR, but comparable ratio of infarct area to AAR. $n=3/3$; $**P<0.01$. (B) Quantification and graphic representation of infarct size 1 day (Evan's blue and TTC staining), 7 days and 28 days (H&E staining) after infarction. The initial infarct size is smaller in Dll1 heterozygotes, but increases significantly in the analyzed course of 4 weeks after MI, whereas the initial larger infarct size in WT mice is compensated and stays constant over time. MI 1d $n=3/3$, MI 7d $n=12/12$, MI 28d $n=12/14$; $*P<0.05$, $**P<0.01$; n.s.: not significant.

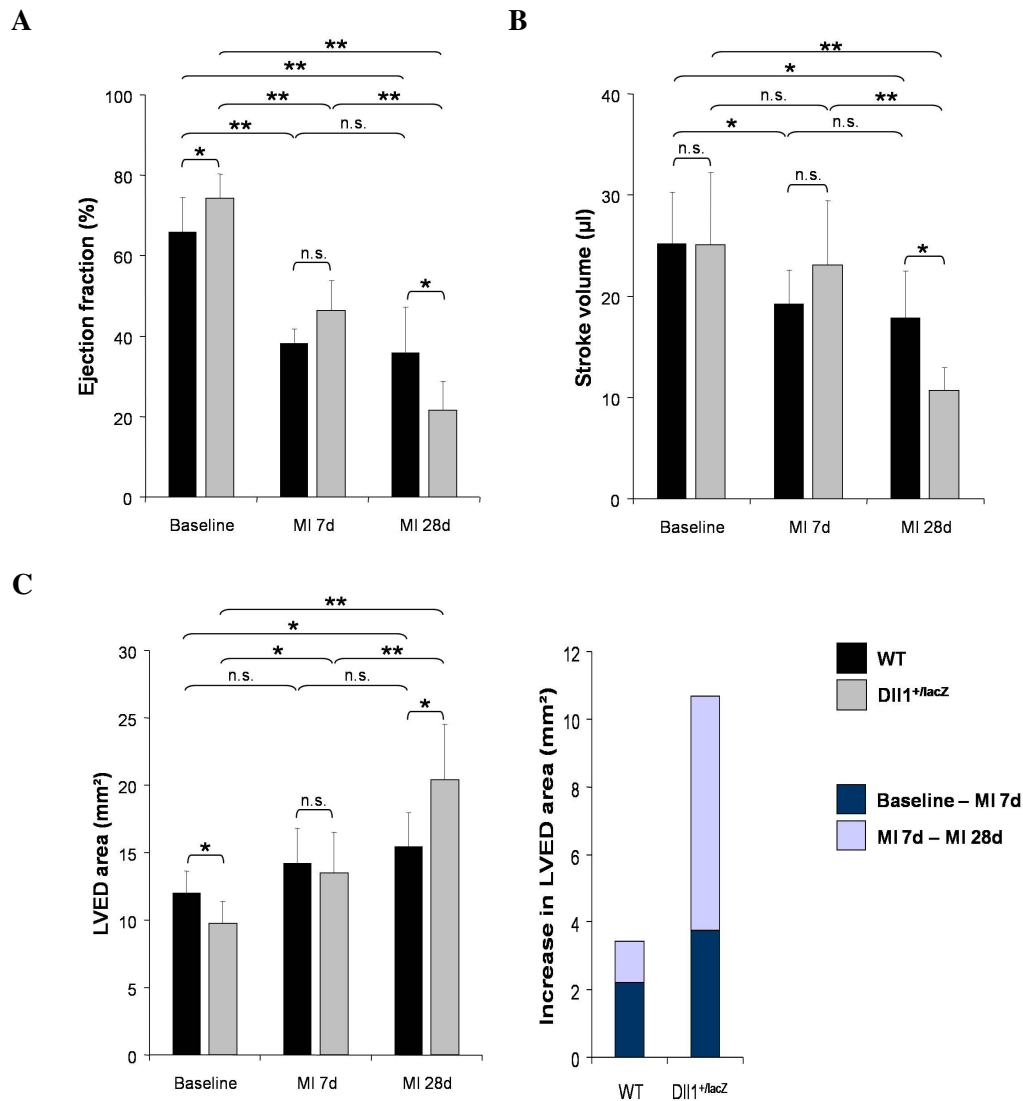


Figure 3.7 Diminished levels of Dll1 cause impaired cardiac function and strong LV dilation 4 weeks after MI. (A-C) Echocardiographic analyses of ejection fraction, stroke volume and LVED area after infarction. (A) Decreased ejection fraction in both, WT and Dll1^{+/-lacZ} hearts 7 days after infarction. In the following course of time EF is stable in WT, but decreases further in Dll1 heterozygotes. (B) In accordance, the stroke volume is constant in WT animals 4 weeks after infarction, after an initial decrease. Dll1^{+/-lacZ} animals show no significant change of SV 7 days after infarction, but a strong deterioration in the following. (C) Analysis of LVED area showing a small, but significant increase after MI in WT animals, comparing baseline to MI 28d. Dll1 heterozygous animals, however, revealing a significant increase in LVED area after infarction, indicating strong left ventricular dilation. (A-C) Baseline n=12/11, MI 7d n=7/8, MI 28d n=12/13; * $P < 0.05$, ** $P < 0.01$; n.s.: not significant.

3.2.2 Impaired LV remodelling after infarction in Dll1 heterozygous mice

Increased dilation and infarct expansion in Dll1^{+/-lacZ} animals

To quantify left-ventricular geometry in relation to infarct area, heart sections were measured and epicardial circumference data collected – including the distinction of remote

(non-infarcted) and infarct fraction in MI conditions (Figure 3.8 A, B). Baseline analysis confirmed a smaller heart size of $Dll1^{+/lacZ}$ animals. WT animals displayed a small, but not significant increase in epicardial circumference, whereas hearts of $Dll1$ heterozygous animals showed massive dilation by a significant increase in epicardial circumference from baseline via day 7 to day 28 after LAD ligation (Epic. circ. Baseline, WT: 13.29 ± 0.53 mm vs. $Dll1^{+/lacZ}$: 11.93 ± 0.66 mm, $n = 7/6$, $P = 0.037$; Epic. circ. MI 7d, WT: 13.50 ± 1.19 mm vs. $Dll1^{+/lacZ}$: 12.99 ± 0.68 mm, $n = 12/12$, $P = \text{n.s.}$; Epic. circ. MI 28d, WT: 13.92 ± 1.18 mm vs. $Dll1^{+/lacZ}$: 15.14 ± 1.89 mm, $n = 12/14$, $P = \text{n.s.}$; WT - BL vs. MI 7d $P = \text{n.s.}$; WT - MI 7d vs. MI 28d $P = \text{n.s.}$; WT - BL vs. MI 28d $P = \text{n.s.}$; $Dll1^{+/lacZ}$ - BL vs. MI 7d $P = 0.036$; $Dll1^{+/lacZ}$ - MI 7d vs. MI 28d $P = 0.006$; $Dll1^{+/lacZ}$ - BL vs. MI 28d $P = 0.010$). After infarction, the fraction of infarct and remote length of the epicardial circumference was unchanged in WT animals, comparing day 7 and day 28 after infarction, which is reasonable as infarct size was constant during this period as well (WT, Remote length MI 7d: 9.22 ± 1.77 mm vs. Remote length MI 28d: 9.67 ± 1.34 mm, $P = \text{n.s.}$; WT, Infarct length MI 7d: 4.28 ± 1.67 mm vs. Infarct length MI 28d: 3.91 ± 1.87 mm, $P = \text{n.s.}$). With respect to fractions in infarcted $Dll1^{+/lacZ}$ mice, infarct length increased significantly from day 7 to day 28 post infarction and remote length decreased ($Dll1^{+/lacZ}$, Remote length MI 7d: 9.28 ± 0.95 mm vs. Remote length MI 28d: 7.65 ± 1.40 mm, $P = 0.019$; $Dll1^{+/lacZ}$, Infarct length MI 7d: 3.71 ± 0.94 mm vs. Infarct length MI 28d: 7.49 ± 1.73 mm, $P = 3E-5$). The decrease in remote length directly reflects the increase in infarct size, whereas the increase in infarct length also is an indicator for heart dilation, as the infarct scar appears to wear out and explains the increase in total epicardial circumference.

The assumption that the infarct scar wears out in the course of time was also observed based on wall thickness data (equivalent to infarct thickness and a measure of infarct scar thinning) (Figure 3.8 C). WT animals showed a significant reduction of wall thickness directly after infarction, i.e. in 7 day analyses, but no further decrease during the following 3 weeks. $Dll1^{+/lacZ}$ animals did not show a thinner wall after infarction – which might be reasoned by the smaller infarct size –, but a significant decrease was apparent from day 7 to day 28 after operation, resulting in significantly thinner LV walls in comparison to WT animals after 28 days (Wall thickness Baseline, WT: 0.97 ± 0.07 mm vs. $Dll1^{+/lacZ}$: 0.83 ± 0.07 mm, $n = 7/6$, $P = 0.017$; Wall thickness MI 7d, WT: 0.62 ± 0.13 mm vs. $Dll1^{+/lacZ}$: 0.78 ± 0.14 mm, $n = 12/12$, $P = 0.030$; Wall thickness MI 28d, WT: 0.51 ± 0.08 mm vs. $Dll1^{+/lacZ}$: 0.32 ± 0.07 mm, $n = 12/14$, $P = 0.0004$; WT - BL vs. MI 7d $P = 0.0001$; WT - MI

7d vs. MI 28d P = n.s.; WT - BL vs. MI 28d P = 1E-7; Dll1^{+lacZ} - BL vs. MI 7d P = n.s.; Dll1^{+lacZ} - MI 7d vs. MI 28d P = 0.0000001; Dll1^{+lacZ} - BL vs. MI 28d P = 2E-8).

Infarct expansion (thinning and elongation of the infarcted area) after myocardial infarction is an indicator of adverse remodelling. The strong increase of infarct portion of the epicardial circumference and the strong decrease of left-ventricular wall thickness show that in Dll1 heterozygous animals infarct expansion takes place after MI.

More pronounced ventricular and myocyte hypertrophy in Dll1 heterozygotes

Another aspect of infarct response is hypertrophy. Moderate cardiomyocyte hypertrophy in the remote myocardium is a part of compensatory remodelling, to counteract intensified wall stress. In adverse remodelling, however, increasing loading conditions lead to progressive hypertrophy.

Characterization of ventricular hypertrophy was performed on septum thickness data (equivalent to the remote myocardium) (Figure 3.8 D). Data illustrated a slight increase in WT animals which was only apparent, comparing baseline and MI 28d time points. Dll1 heterozygous mice did not show shifted data at first. 4 weeks after infarction, however, animals demonstrated a strong and highly significant increase in septum thickness (Septum thickness Baseline, WT: 1.31 ± 0.11 mm vs. Dll1^{+lacZ}: 1.09 ± 0.16 mm, n = 7/6, P = 0.039; Septum thickness MI 7d, WT: 1.45 ± 0.29 mm vs. Dll1^{+lacZ}: 1.21 ± 0.22 m, n = 12/12, P = n.s.; Septum thickness MI 28d, WT: 1.63 ± 0.19 mm vs. Dll1^{+lacZ}: 1.60 ± 0.26 mm, n = 12/14, P = n.s.; WT - BL vs. MI 7d P = n.s.; WT - MI 7d vs. MI 28d P = n.s.; WT - BL vs. MI 28d P = 0.017; Dll1^{+lacZ} - BL vs. MI 7d P = n.s.; Dll1^{+lacZ} - MI 7d vs. MI 28d P = 0.003; Dll1^{+lacZ} - BL vs. MI 28d P = 0.002).

As second measure, myocyte hypertrophy was determined by analysis of cardiomyocyte cross-sectional area (CSA) (Figure 3.9 A). CSA analysis showed smaller myocytes under baseline conditions in Dll1 heterozygous animals. After infarction, both WT and Dll1^{+lacZ} mice revealed a highly significant increase in CSA (CSA Baseline, WT: 273 ± 46 μm^2 vs. Dll1^{+lacZ}: 214 ± 42 μm^2 , n = 3/3, P = 7E-32; CSA MI 7d, WT: 291 ± 65 μm^2 vs. Dll1^{+lacZ}: 237 ± 46 μm^2 , n = 3/3, P = 6E-21; CSA MI 28d, WT: 320 ± 84 μm^2 vs. Dll1^{+lacZ}: 389 ± 95 μm^2 , n = 3/3, P = 6E-12; WT - BL vs. MI 7d P = 0.004; WT - MI 7d vs. MI 28d P = 0.0003; WT - BL vs. MI 28d P = 1E-9; Dll1^{+lacZ} - BL vs. MI 7d P = 5E-7; Dll1^{+lacZ} - MI 7d vs. MI 28d P = 1E-69; Dll1^{+lacZ} - BL vs. MI 28d P = 1E-74). Yet, Dll1 heterozygous conditions showed a more pronounced enlargement of myocyte size, giving final CSA values

significantly larger than final myocyte size in WT animals and a respective stronger myocyte hypertrophy after MI.

In correspondence with CSA data, the number of myocytes per field (Figure 3.9 B) was higher in Dll1 heterozygotes under baseline conditions. After infarction myocyte numbers decreased slightly, but not significantly in WT animals. Dll1^{+/*lacZ*} mice revealed a significant reduction of myocyte numbers comparing 7 and 28 days post infarction (Myocytes per field Baseline, WT: 210 ± 18 vs. Dll1^{+/*lacZ*}: 236 ± 22, n = 3/3, P = 0.042; Myocytes per field MI 7d, WT: 201 ± 21 vs. Dll1^{+/*lacZ*}: 213 ± 26, n = 3E-5; WT - BL vs. MI 7d P = n.s.; WT - MI 7d vs. MI 28d P = n.s.; WT - BL vs. MI 28d P = 0.002; Dll1^{+/*lacZ*} - BL vs. MI 7d P = n.s.; Dll1^{+/*lacZ*} - MI 7d vs. MI 28d P = 6E-6; Dll1^{+/*lacZ*} - BL vs. MI 28d P = 6E-8).

These results show that in WT animals hypertrophy takes place, as expected in compensatory remodelling. However, in Dll1 heterozygous animals absolute differences of myocyte size and septum thickness are higher (although hearts are smaller), indicating that hypertrophy is more pronounced in Dll1 heterozygous than in WT animals, adding another aspect of adverse remodelling.

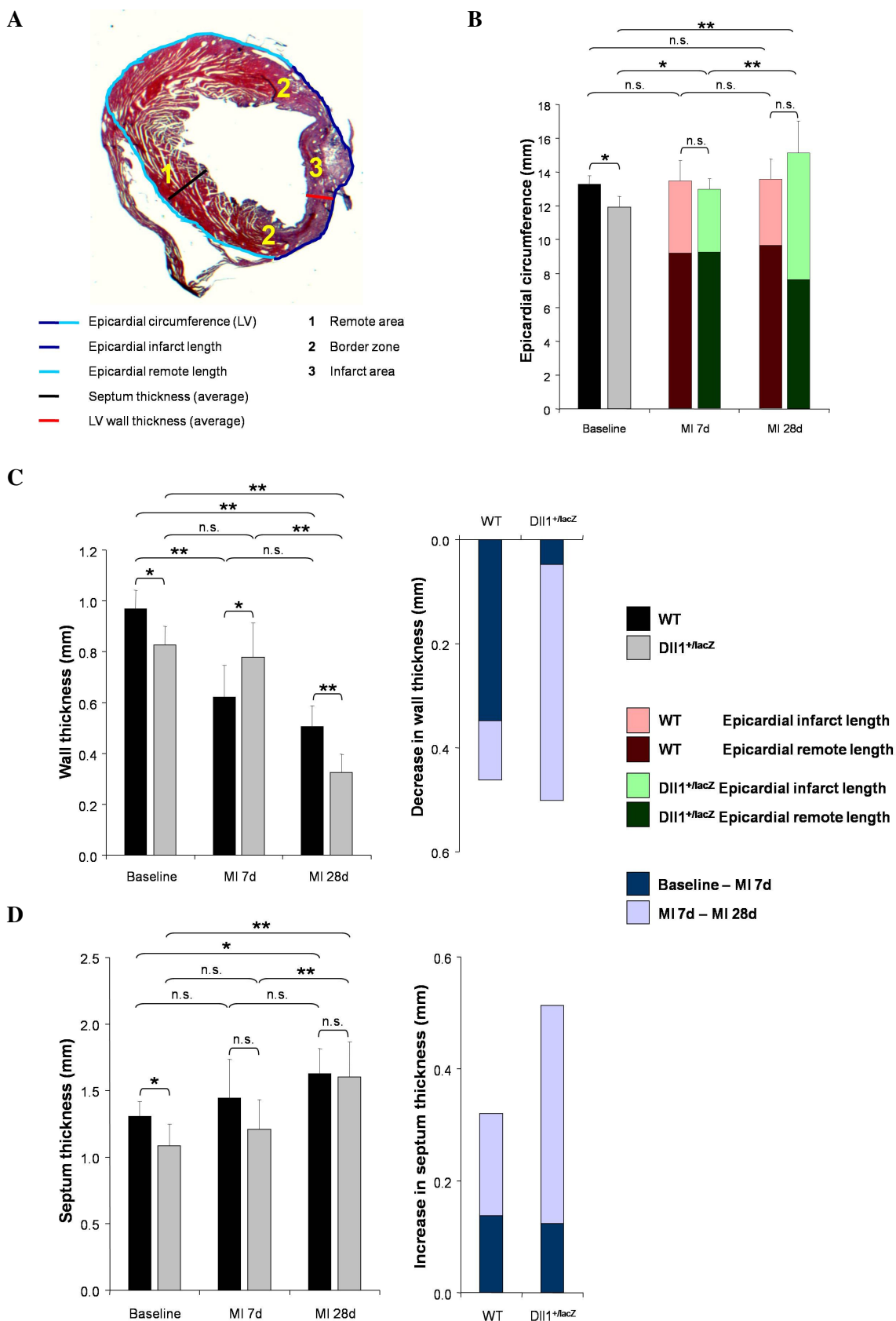


Figure 3.8 Infarct expansion and increased ventricular dilation and hypertrophy in *DII1* heterozygous animals. (A) Graphic representation and (B) quantification of epicardial circumference measurement including remote and infarct fraction after MI. Analysis showing increased infarct length and increased total epicardial circumference 28 days after infarction under *DII1*^{+/*lacZ*} conditions, in compliance with infarct size and LVED area analyses. (C) Examination of left ventricular wall thickness showing strong thinning in both WT and *DII1*^{+/*lacZ*} after MI, but stronger first in WT animals 7 days post infarction and later in

Dll1^{+lacZ} (over the following 3 weeks of analysis). (D) Septum thickness showing weak hypertrophy in WT animals after infarction. Strong hypertrophy is apparent by an increase in septum thickness in Dll1 heterozygous conditions 4 weeks after infarction. (B-D) Baseline n=7/6, MI 7d n=12/12, MI 28d n=12/14. * $P < 0.05$, ** $P < 0.01$; n.s.: not significant.

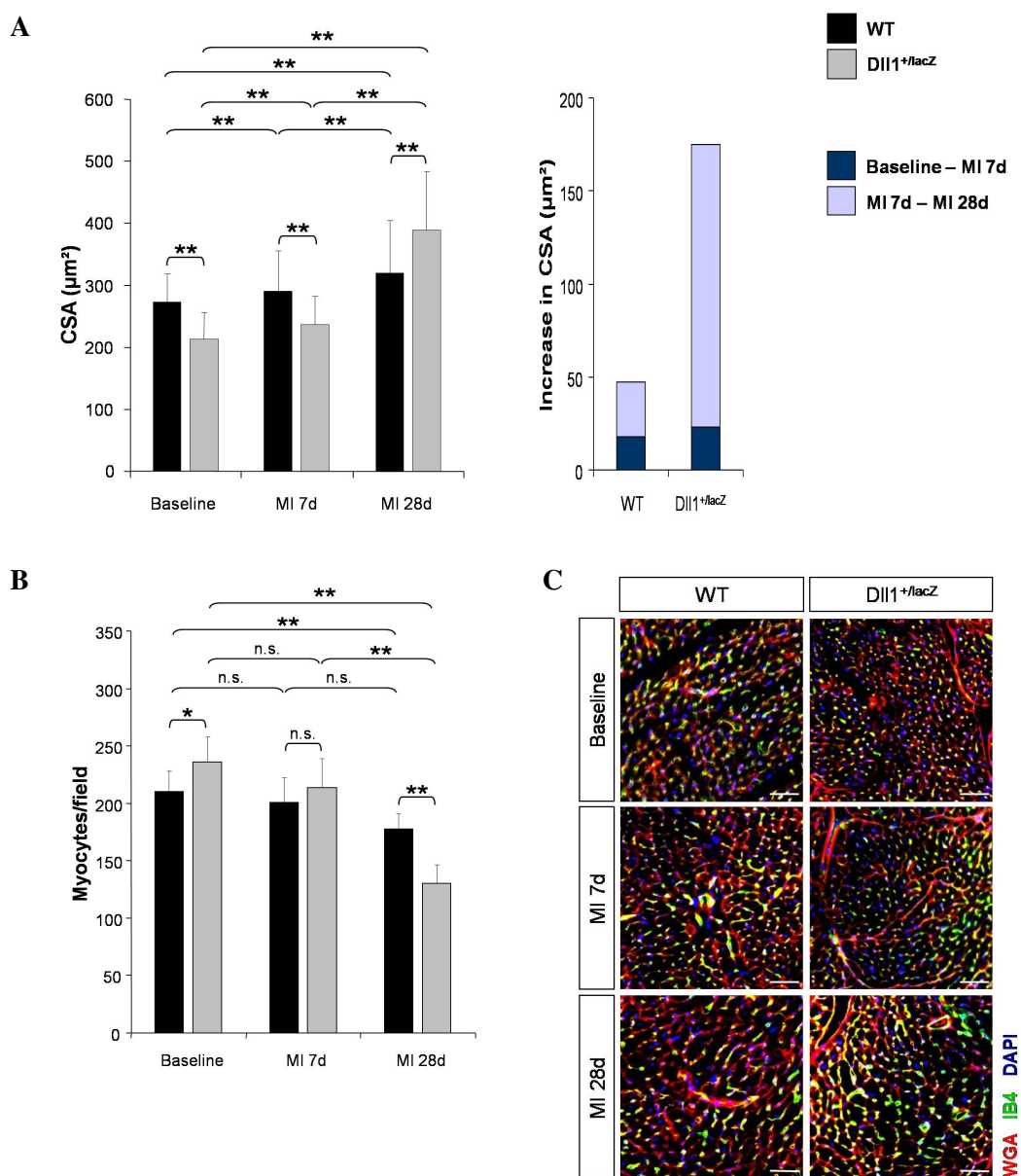


Figure 3.9 Myocyte hypertrophy in Dll1^{+lacZ} mice. (A) Analysis of cross-sectional area (CSA) revealing smaller myocytes under baseline conditions in diminished Dll1 conditions, but a stronger increase in CSA and respective stronger myocyte hypertrophy after MI, in comparison to infarcted WT conditions. (B) In correspondence with CSA, the number of myocytes per field is higher under baseline conditions, but decreases stronger after infarction in Dll1^{+lacZ} animals. (A-B) n=3/3 (3-4 fields each); * $P < 0.05$, ** $P < 0.01$; n.s.: not significant. (C) Representative immunofluorescence images used for quantification of CSA, myocyte density and capillary density in WT and Dll1^{+lacZ} heart sections. Staining shows WGA (red) to mark cell membranes, capillaries by isolectin B4 (green), and nuclei by DAPI (blue). Scale bar 50μm.

Lower apoptotic response to MI in Dll1 heterozygous mice

Myocardial infarction triggers an ischemic stress response and induces cell death. To assess the involvement of cell death by apoptosis, TUNEL staining was performed. Evaluation (Figure 3.10) demonstrated low, comparable baseline values in WT and Dll1^{+lacZ} animals (Apoptotic cells per 0.5 mm² - Baseline, WT: 0.09 ± 0.17 vs. Dll1^{+lacZ}: 0.18 ± 0.31, n = 5/5, P = n.s.). 3 days after infarction the number of apoptotic cells was significantly elevated in WT animals in all areas – remote, border zone and infarct –, compared to Dll1^{+lacZ}; WT values MI 3d were significantly higher than baseline data (MI 3d , Apoptotic cells per 0.5 mm² - Remote, WT: 4.21 ± 3.77 vs. Dll1^{+lacZ}: 0.22 ± 0.37, n = 3/3, P = 0.049; Apoptotic cells per 0.5 mm² - Border zone, WT: 67.16 ± 43.18 vs. Dll1^{+lacZ}: 6.97 ± 3.46, n = 3/3, P = 0.022; Apoptotic cells per 0.5 mm² - Infarct, WT: 89.25 ± 65.77 vs. Dll1^{+lacZ}: 11.62 ± 1.32, n = 3/3, P = 0.029). 7 days after infarction, WT animals showed an increase in apoptotic cells in the remote area, but a decreased number of apoptotic cells in the border zone and the infarct area. Dll1 heterozygous mice showed elevated levels of apoptotic cells in all three areas when compared to MI 3d, but data were still below WT level (MI 7d , Apoptotic cells per 0.5 mm² - Remote, WT: 11.04 ± 14.06 vs. Dll1^{+lacZ}: 3.66 ± 6.09, n = 6/6, P = n.s.; Apoptotic cells per 0.5 mm² - Border zone, WT: 33.47 ± 18.82 vs. Dll1^{+lacZ}: 18.12 ± 7.65, n = 6/6, P = n.s.; Apoptotic cells per 0.5 mm² - Infarct, WT: 75.78 ± 43.08 vs. Dll1^{+lacZ}: 33.72 ± 10.47, n = 6/6, P = 0.033). 4 weeks after infarction the apoptotic response has completely ceased in WT and Dll1^{+lacZ} hearts in all areas (MI 28d , Apoptotic cells per 0.5 mm² - Remote, WT: 0.27 ± 0.43 vs. Dll1^{+lacZ}: 0.00 ± 0.00, n = 4/5, P = n.s.; Apoptotic cells per 0.5 mm² - Border zone, WT: 0.80 ± 0.64 vs. Dll1^{+lacZ}: 1.84 ± 1.57, n = 4/5, P = n.s.; Apoptotic cells per 0.5 mm² - Infarct, WT: 0.00 ± 0.00 vs. Dll1^{+lacZ}: 4.88 ± 4.88, n = 4/5, P = n.s.). Consequently - on the basis of the time points analysed -, Dll1^{+lacZ} animals reveal a lower extent of apoptosis after myocardial infarction. However, to answer if reduced apoptotic cell numbers are based on the initial smaller infarct size or as direct effect of Dll1 heterozygosity, more time points would have to be analyzed. Only with more time points a statement could be made if apoptotic response is rather time-shifted and increases later than in WT. Though, even if apoptosis is in fact decreased in Dll1 heterozygous mice, obviously massive cell death does occur as apparent on the increase in infarct size. In principle, necrosis and autophagy can contribute to cell death. Although necrosis is rather connected with acute cell death in the infarcted area immediately after MI, it is possible that due to impaired arteriogenesis in Dll1 heterozygotes, ischemia is prolonged and necrosis persists. This is especially important for the cardiomyocytes at risk in the border zone and could explain the

increase in infarct size. However, persistent ischemia due to impaired arteriogenesis could also cause increased autophagy and corresponding effects on infarct size. Therefore, additional quantification of necrosis and autophagy would be needed to answer which type of cell death is altered in Dll1 heterozygous animals. In addition, not only cardiomyocytes undergo cell death after MI. Also other cell types associated with infarct response like inflammatory cells or myofibroblasts undergo apoptosis in a time-dependent manner. It is possible that altered cell infiltration might account for the observed difference in apoptotic cells.

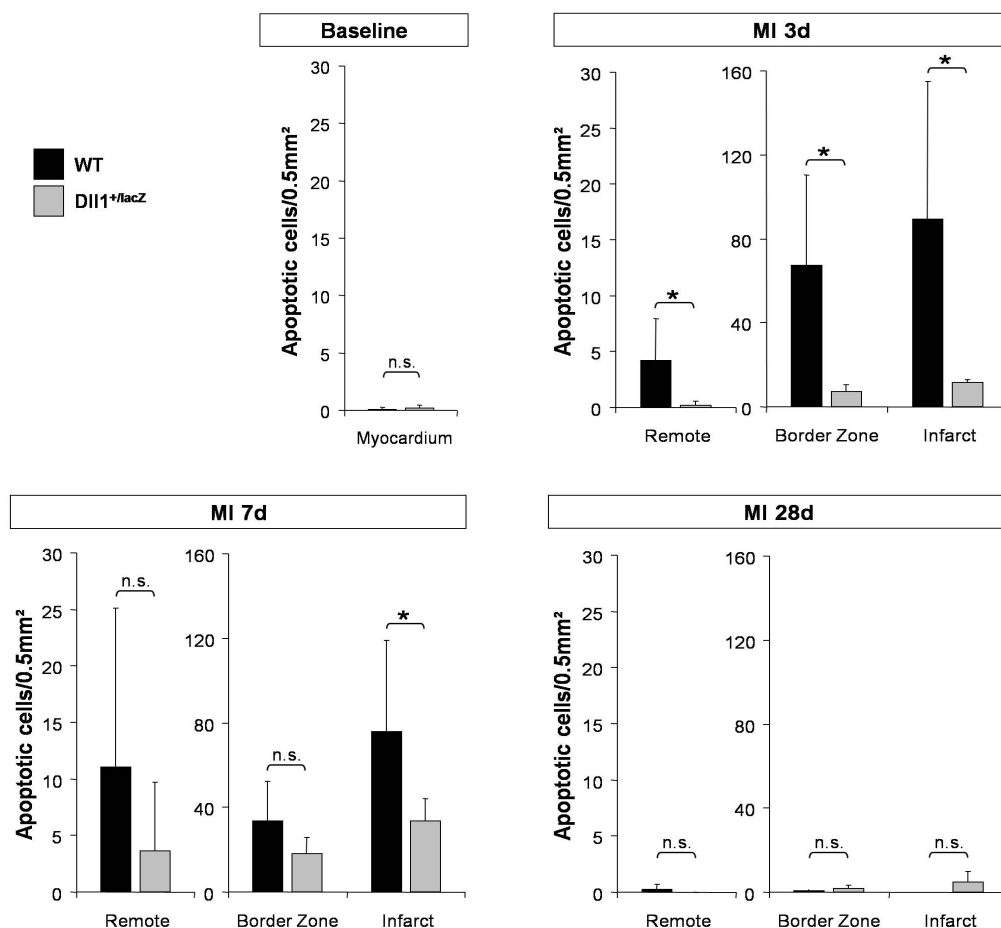


Figure 3.10 Lower apoptotic response after myocardial infarction in Dll1^{+/lacZ} mice, compared to WT. Quantification of apoptosis (TUNEL staining) showing increased numbers of apoptotic cells per area in WT heart sections 3 days after infarction, but not in Dll1 heterozygotes. 7 days after infarction the number of apoptotic cells has decreased in WT. Numbers slightly increased in all areas under Dll1 heterozygous conditions, but were still below WT levels. 4 weeks after infarction the apoptotic response has completely ceased in both conditions and all areas. MI 3d n=3/3 (3 fields per zone), MI 7d n=6/6 (3 fields per zone), MI 28d n=4/5 (3 fields per zone); * $P < 0.05$, ** $P < 0.01$; n.s.: not significant.

Increased fibrotic response in the infarct zone of Dll1^{+lacZ} animals

As the wound matures, collagen is deposited and cross-linked to stabilize the scar. Collagen maturation and organized alignment increases the strength of the wound. A disorganized, immature collagen matrix cannot withstand the cardiac load, leading to dilation and a higher probability of rupture. Deposition of interstitial collagen in the noninfarcted myocardium has a negative influence as it is associated with ventricular stiffness in the remote area.

Sirius red polarization microscopy of collagen fibres (Figure 3.11 A) demonstrated in both groups – WT and Dll1 heterozygous – thick, tightly packed mature fibres (orange-red) in the border zone and the infarct zone, 28 days after infarction. No loosely assembled, immature fibres (yellow-green) could be observed. Quantification of collagen fractional areas (Figure 3.11 B) showed comparable and low baseline values. 4 weeks after infarction, no changes in collagen density were observed in the remote area of WT and Dll1^{+lacZ} animals compared to baseline, indicating that interstitial myocardial fibrosis did not occur in both genotypes. Analysing border zone and infarct areas 4 weeks after infarction, increased collagen density was apparent, resulting in comparable values in the border zone and higher collagen density in the infarct zone of Dll1 heterozygous mice, compared to WT (Collagen density - Baseline, WT: 0.60 ± 0.37 % vs. Dll1^{+lacZ}: 0.53 ± 0.35 %, $n = 4/4$, $P = \text{n.s.}$; Collagen density - Remote MI 28d, WT: 0.68 ± 0.33 % vs. Dll1^{+lacZ}: 0.45 ± 0.14 %, $n = 4/4$, $P = \text{n.s.}$; Collagen density - Border zone MI 28d, WT: 37.50 ± 5.40 % vs. Dll1^{+lacZ}: 42.50 ± 9.20 %, $n = 4/4$, $P = \text{n.s.}$; Collagen density - Infarct MI 28d, WT: 67.10 ± 9.30 % vs. Dll1^{+lacZ}: 85.40 ± 4.40 %, $n = 4/4$, $P = 0.0003$).

Thus, fibrosis analysis revealed mature collagen fibres with increased collagen deposition in Dll1 heterozygotes. Increased collagen deposition after infarction is actually associated with LV stiffness and dysfunction, whereas decreased collagen deposition (below normal) can lead to LV dilation (Jugdutt, 2003). However, although increased collagen is observed in Dll1 heterozygous animals after myocardial infarction, it is not possible to conclude that this is directly related to increased stiffness and dysfunction, as in Dll1 heterozygous mice the final infarct size is bigger than in WT animals. Based on the experiments performed it is not possible to tell if collagen deposition is adequate for the corresponding infarct size, or if it is above or below adequate collagen levels. Collagen fibre maturation and organization in the scar seemed not be impaired.

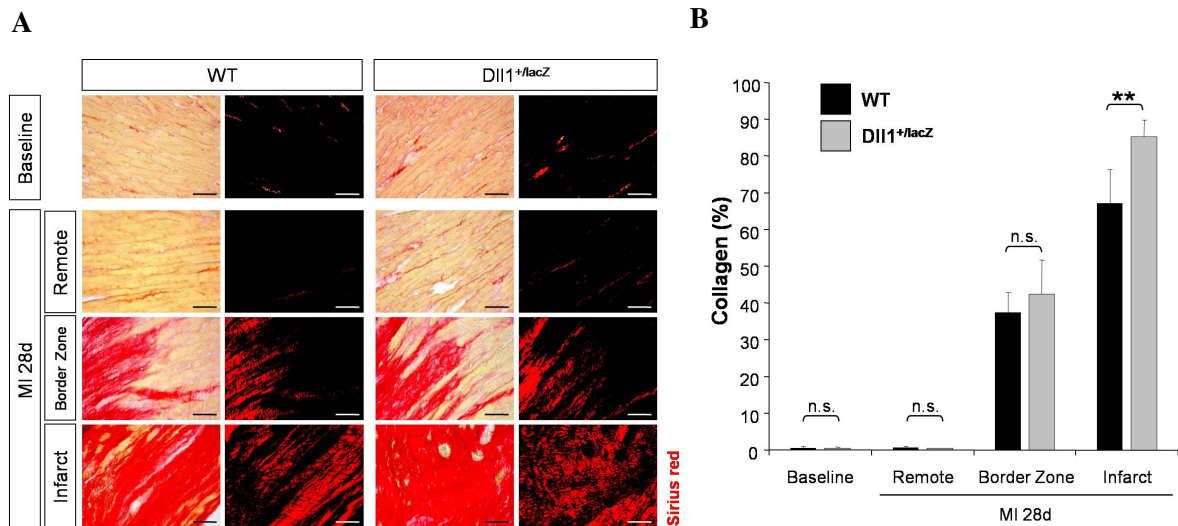


Figure 3.11 Increased fibrotic response in the infarct zone of Dll1^{+lacZ} hearts 4 weeks post MI. (A) Representative bright field (left panel) and polarized light (corresponding right panel) images of collagen deposition visualized by Sirius red staining. Scale bar 50 μ m. (B) Fibrosis analysis by collagen quantification showing comparable collagen content under baseline conditions in WT and Dll1 heterozygous heart sections. 4 weeks post infarction, collagen density is not increased in remote areas of both genotypes. Border zone areas show increased, but comparable levels of collagen deposition in WT and Dll1^{+lacZ} hearts, whereas infarct areas show higher collagen levels with increased fibrosis in Dll1 heterozygous mice. Baseline n=4/4 (3 fields per zone), MI 28d n=4/4 (3 fields per zone); ** P <0.01; n.s.: not significant.

3.2.3 Increased inflammatory response to MI in Dll1 heterozygous mice

Enhanced leukocyte infiltration in Dll1^{+lacZ} animals

To assess inflammatory processes after infarction, in a first analyses leukocytes were identified by CD45 immunohistochemistry staining (Figure 3.12). Quantification of the area occupied by CD45⁺ cells showed significantly higher leukocyte infiltration in the border zone and infarct area of Dll1^{+lacZ} mice, compared to WT, 3 days after myocardial infarction. At the same time point of analysis leukocyte infiltration in the remote area was low and comparable in both genotypes (MI 3d n=3/3, CD45⁺ cell area - Remote, WT: 2.1 ± 0.4 % vs. Dll1^{+lacZ}: 3.0 ± 1.0 %, $P = \text{n.s.}$; CD45⁺ cell area - Border zone, WT: 26.5 ± 3.8 % vs. Dll1^{+lacZ}: 44.3 ± 8.2 %, $P = 0.021$; CD45⁺ cell area - Infarct, WT: 41.2 ± 5.0 % vs. Dll1^{+lacZ}: 81.8 ± 7.7 %, $P = 0.002$). 7 days post MI, levels of CD45⁺ cells significantly increased in the remote area of both genotypes, with a stronger progress in Dll1 heterozygotes. CD45⁺ cell area in the border zone and the infarct zone of WT animals stayed constant, but decreased significantly in both areas of Dll1^{+lacZ} mice, giving comparable final values at this time point (MI 7d n=6/9, CD45⁺ cell area - Remote, WT:

4.8 ± 1.0 % vs. Dll1^{+lacZ}: 6.1 ± 1.6 %, P = 0.034; CD45+ cell area - Border zone, WT: 33.4 ± 6.0 % vs. Dll1^{+lacZ}: 27.2 ± 11.0 %, P = n.s.; CD45+ cell area - Infarct, WT: 51.9 ± 20.3 % vs. Dll1^{+lacZ}: 48.7 ± 19.1 %, P = n.s.; WT Remote - MI 3d vs. MI 7d P = 0.002; WT Border zone - MI 3d vs. MI 7d P = n.s.; WT Infarct - MI 3d vs. MI 7d P = n.s.; Dll1^{+lacZ} Remote - MI 3d vs. MI 7d P = 0.004; Dll1^{+lacZ} Border zone - MI 3d vs. MI 7d P = 0.020; Dll1^{+lacZ} Infarct - MI 3d vs. MI 7d P = 0.014). 4 weeks after myocardial infarction, leukocyte infiltration has ceased in all areas of both, WT and Dll1^{+lacZ} animals (MI 28d n=5/7 , CD45+ cell area - Remote, WT: 0.1 ± 0.1 % vs. Dll1^{+lacZ}: 0.2 ± 0.1 %, P = n.s.; CD45+ cell area - Border zone, WT: 2.1 ± 1.2 % vs. Dll1^{+lacZ}: 1.3 ± 1.2 %, P = n.s.; CD45+ cell area - Infarct, WT: 5.9 ± 3.6 % vs. Dll1^{+lacZ}: 6.2 ± 5.0 %, P = n.s.).

These data show initially enhanced leukocyte infiltration in Dll1 heterozygotes, but total leukocyte numbers also decline earlier than in WT conditions. Increased leukocyte infiltration 3 days after infarction was especially intriguing with regard to the initial smaller infarct size in Dll1 heterozygotes, indicating a misbalance of inflammation to the corresponding infarct size.

Time shifted, increased macrophage infiltration in Dll1 heterozygotes

Identification of mature macrophages was performed by F4/80 immunofluorescence staining (Figure 3.13). 3 days post MI, microscopy showed high macrophage infiltration in the infarct zone, as well as in the border zone (infarct side) of WT animals, but not in the remote. Dll1 heterozygous mice did not show macrophage infiltration in the remote and border zone; the infarct area revealed only sporadic F4/80 positive cells. However, 7 days after infarction Dll1^{+lacZ} animals exhibited a massive increase of macrophages in all three zones: remote, border zone and infarct. At this time point macrophages in the infarct zone of WT mice were still apparent, but numbers subsided.

These observations indicate an increased, but time shifted infiltration of macrophages in Dll1 heterozygotes after myocardial infarction. This poses the question which cell types account for the early increased leukocyte infiltration and requires further investigation. In addition, cardiac repair requires the containment of inflammation into the infarct area; extension into the remote can cause matrix degradation in this area and contribute to adverse remodelling (Frangogiannis, 2008). With this regard, the observed infiltration of F4/80 macrophages in the remote of Dll1 heterozygous infarcted hearts is of special importance .

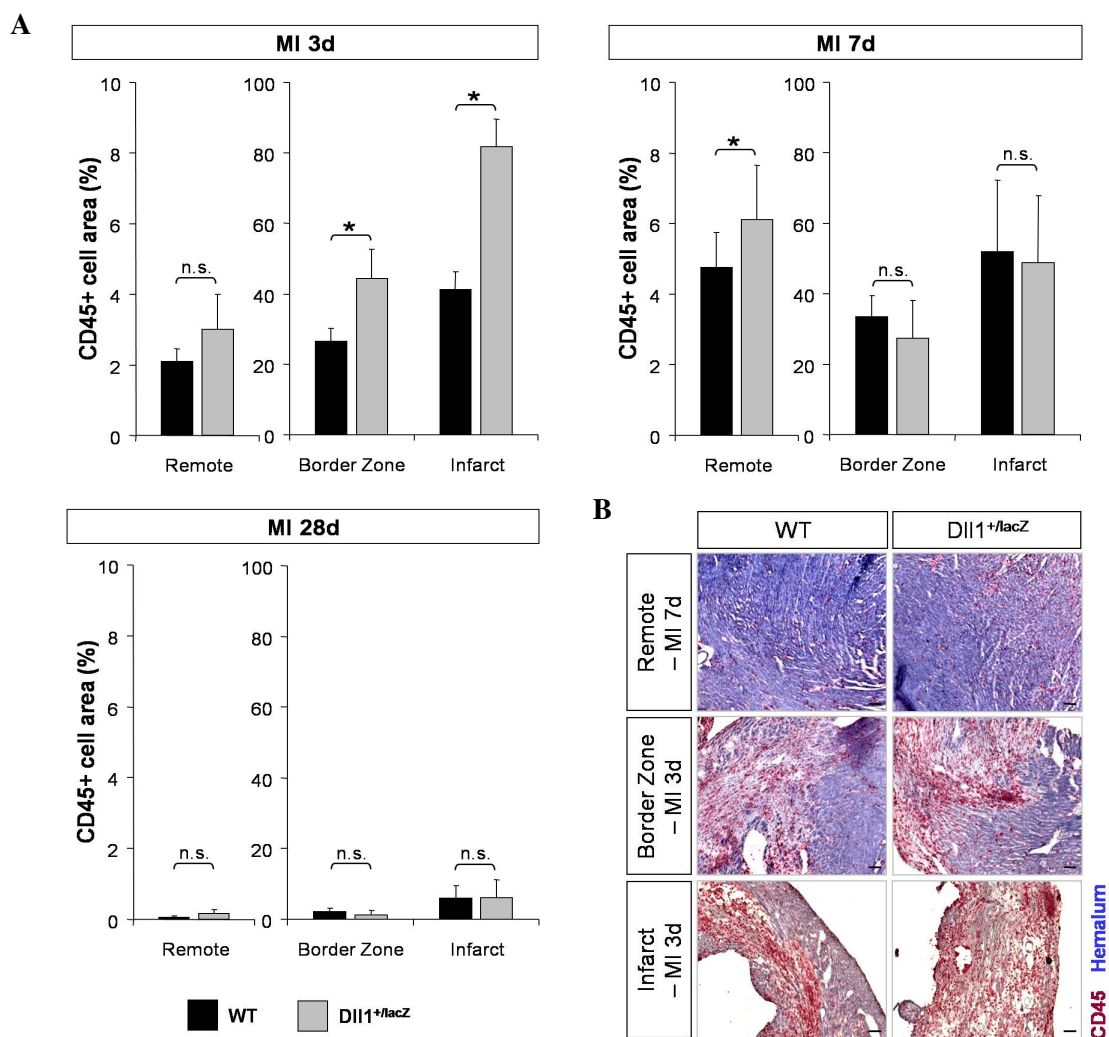


Figure 3.12 Enhanced leukocyte infiltration after MI in Dll1^{+/lacZ} mice. (A) Quantification of leukocyte infiltration by CD45 staining showing elevated levels at first in the border zone and infarcted area of Dll1 heterozygous mice 3 days after infarction in comparison to WT. 7 days post MI, increased CD45+ cell area is more prominent in the remote of Dll1^{+/lacZ} than in WT animals. 4 weeks after infarction leukocyte infiltration has ceased in all areas of WT and Dll1^{+/lacZ} heart sections. MI 3d n=3/3 (2 fields per area), MI 7d n=6/9 (2 fields per area), MI 28d n=5/7 (2 fields per area); * $P < 0.05$, ** $P < 0.01$; n.s.: not significant. (B) Representative immunohistochemical staining of CD45 (red) counterstained with hemalum (blue). Scale bar 100 μ m.

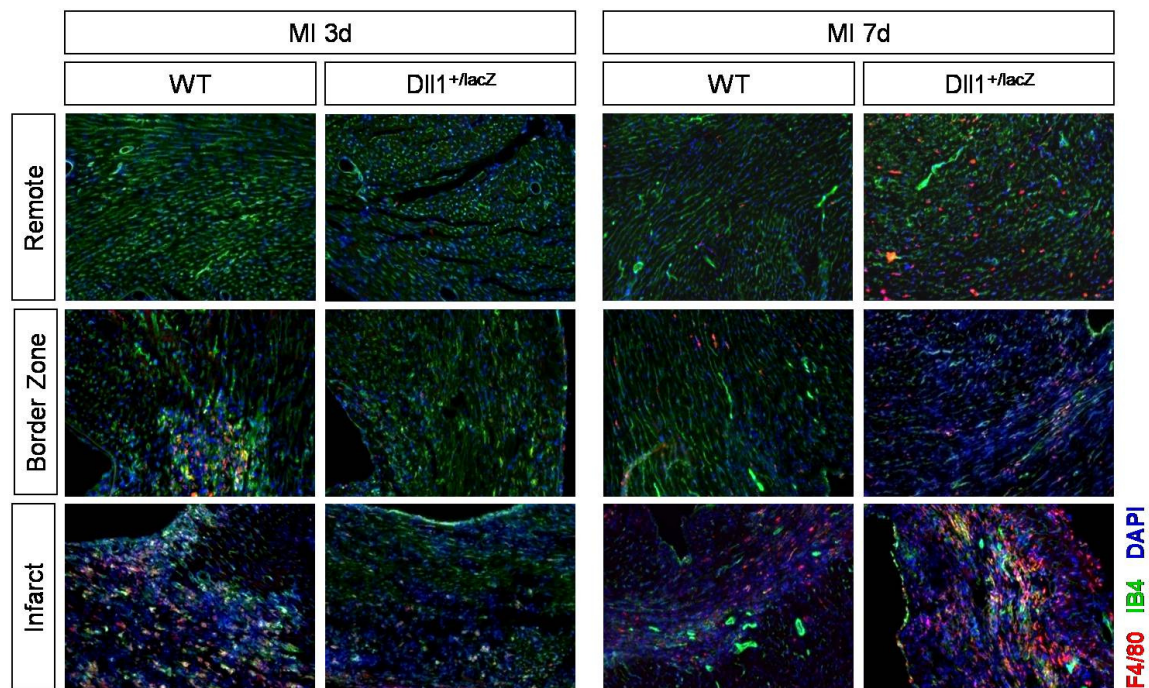


Figure 3.13 Time shifted, increased macrophage infiltration in Dll1 heterozygotes. Immunofluorescence staining of WT and Dll1^{+/-lacZ} heart sections showing macrophages by F4/80 (red), capillaries and vessel endothelium by isolectin B4 (green) and nuclei using DAPI (blue). Fluorescence microscopy revealing macrophage infiltration in infarcted area of WT animals 3 days after infarction, but not in Dll1 heterozygous mice. 7 days after infarction, Dll1 heterozygotes show a massive increase of macrophages in all three zones – remote, border zone and infarct –, whereas in WT animals macrophage infiltration has subsided.

Lower M2 macrophage infiltration in Dll1^{+/-lacZ} infarcted hearts

To identify alternative activated macrophages (M2) associated with repair mechanisms, CD206 immunofluorescence staining was performed (Figure 3.14). Microscopy of heart sections 3 days after infarction demonstrated relatively high levels of CD206 positive cells in the infarct and border zone of WT animals, as well as single M2 macrophages in the remote. In comparison, Dll1 heterozygous animals showed significantly reduced M2 macrophage infiltration in all three areas: remote, border zone and infarct. Analyses 7 days post MI exhibited in WT animals even increased CD206 positive cell numbers in the infarct zone and relatively constant values (comparing to MI 3d) in the border zone and the remote. In Dll1^{+/-lacZ} animals the already low number of CD206 positive cells even declined and only sporadic M2 macrophages were visible in the remote and the infarct area.

These analyses show that M2 macrophage infiltration is lower and subsides even earlier than in WT animals, indicating reduced initiation of healing and repair in Dll1 heterozygotes.

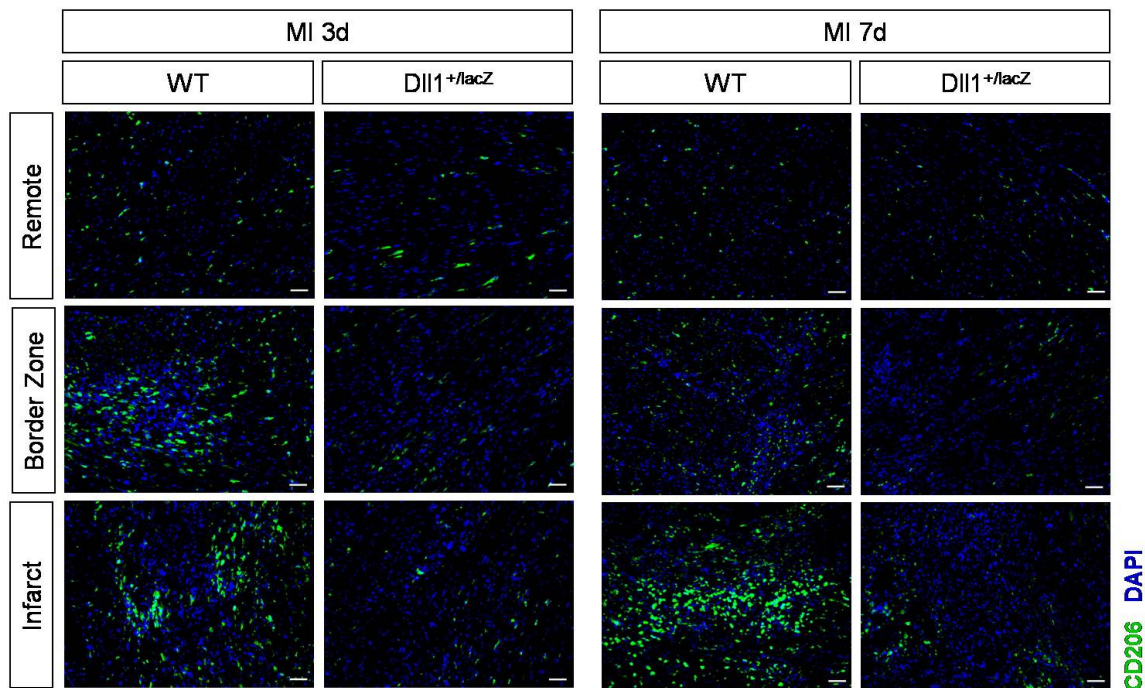


Figure 3.14 Lower M2 macrophage infiltration in $Dll1^{+/-lacZ}$ infarcted hearts. Immunofluorescence microscopy showing M2 macrophages by CD206 (green) and nuclei using DAPI (blue). Staining reveals CD206 positive cells in the remote, border zone and infarct in WT sections 3 days and 7 days after MI. $Dll1^{+/-lacZ}$ animals show lower CD206 positive cell numbers in all areas 3 days after infarction, which are even reduced 7 days post MI. Scale bar 50 μ m.

3.2.4 $Dll1$ expression is upregulated after myocardial infarction

To determine where $Dll1$ exerts its function (leading to adverse remodelling in $Dll1$ heterozygous mice), $Dll1$ expression was analysed after LAD ligation by lacZ staining in $Dll1^{+/-lacZ}$ animals, and RNA and protein analyses in WT heart tissue.

Molecular expression analyses of WT left-ventricular heart tissue showed an upregulation of $Dll1$ on RNA and protein level after infarction, compared to sham operated controls (Figure 3.15 A, B). Both, RNA and protein pattern, demonstrated an increase in expression level from baseline via day 1 to day 3 post infarction, followed by reduced levels – but still above sham conditions – at day 7 after MI again.

Determination of $Dll1$ expression pattern by lacZ staining of infarcted heart sections of $Dll1^{+/-lacZ}$ animals (Figure 3.15 C), illustrated that 7 days post MI endothelial $Dll1$ is still present in arterial vessels of the remote area. In the border zone, as well as in the infarct zone $Dll1$ expression is increased and can be detected in vascular structures. Based on this

simple staining a further classification of Dll1 positive vessels to arteries or veins was not possible. In addition, in all three areas – remote, border zone and infarct – other Dll1 positive structures could be detected which looked rather like single cells than vascular structures. Further analyses 28 days post MI revealed a strong decrease of Dll1 expression in the border and infarct zone; only sporadic vessels and single cells stained lacZ positive. In the remote, however, Dll1 expression retained similar to remote staining 7 days post MI and to baseline staining in unstressed myocardium.

To further characterize and classify Dll1 positive structures, immunofluorescence co-staining was performed (Figure 3.15. D) comparing WT and Dll1^{+lacZ}, baseline and infarcted heart sections. By immunofluorescence, no Dll1 expression could be detected in baseline myocardium of WT and Dll1^{+lacZ} tissue, which likely reflects the different sensitivities of the detection techniques. Likewise, no vessels in the remote, border zone and infarct of WT and Dll1^{+lacZ} conditions 3 and 7 days post MI showed Dll1 expression by fluorescence. The only exception were sporadic Dll1 positive arteries (Figure 3.15 D - arrow) and single cells (Figure 3.15 D - arrow heads) in the border zone of WT animals 3 days after infarction. This finding implies that low Dll1 expression levels and therefore low fluorescence levels could not be detected by fluorescence microscopy with the antibodies applied. Only structures expressing Dll1 above a certain threshold level – as sporadic arteries and cells in the border zone of WT animals 3 days after infarction – exhibited enough fluorescence intensity to be detectable.

These findings show induction of Dll1 in vessels in the border zone after MI, which is of special importance, as the border zone is the area that responds with arteriogenesis.

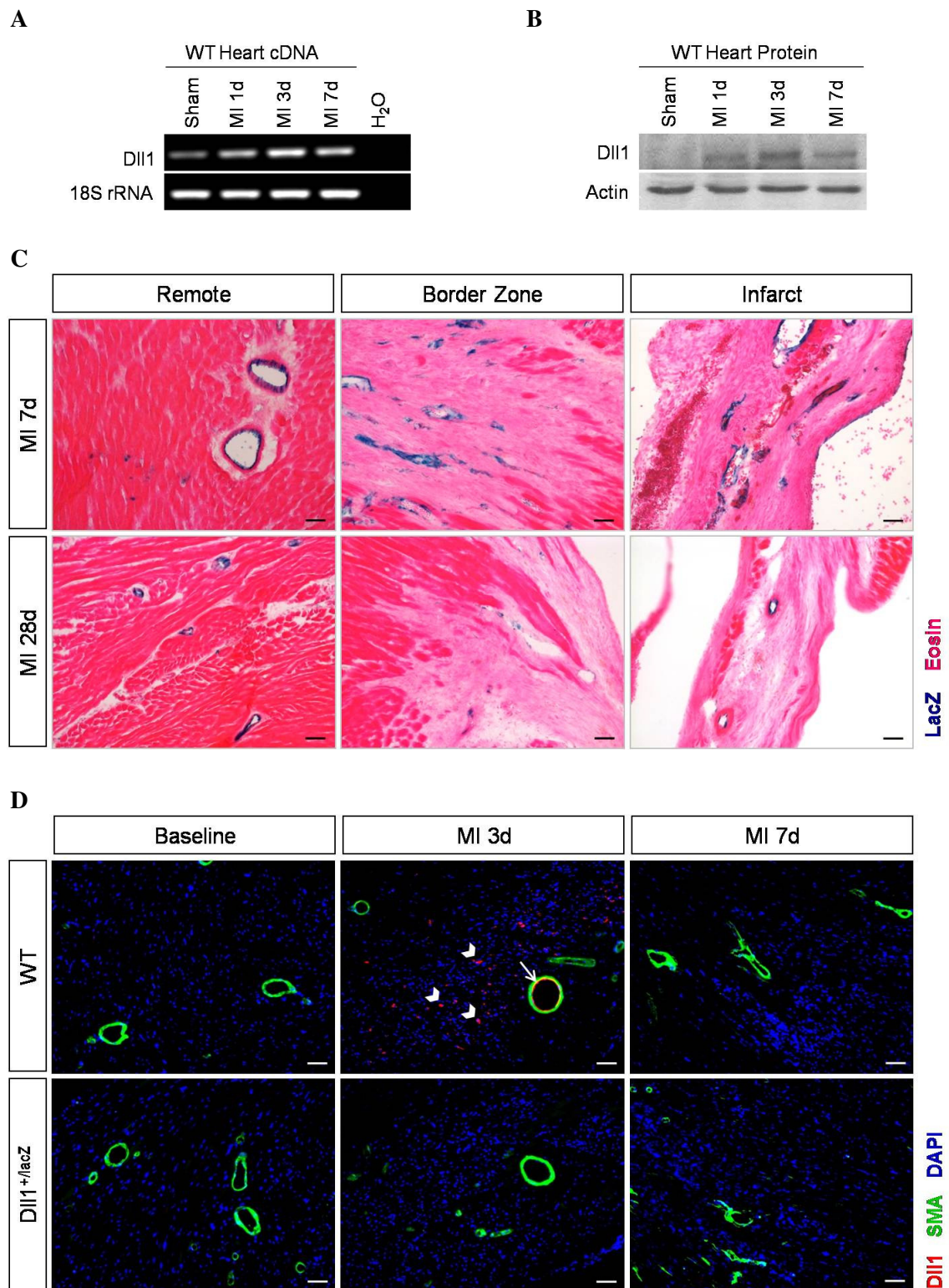


Figure 3.15 Dll1 expression is induced after MI. (A) Dll1 RNA and (B) protein levels are increased directly after MI in infarcted LV samples of WT mice hearts. (C) LacZ (blue) and eosin (red) counterstaining in infarcted heart sections of Dll1^{+lacZ} mice showing increased Dll1 expression in the border and infarct zone 7 days post MI, in vascular structures, as well as in single cells. 28 days after MI Dll1 expression is decreased again, but retains normal in the remote area. Scale bar 50µm. (D) Immunofluorescence staining of WT and Dll1^{+lacZ} heart sections showing Dll1 (red), SMA (green) and nuclei (blue). Fluorescence microscopy revealing Dll1 expression only in sporadic vessels (arrow) and single cells (arrow heads) in the border zone of WT sections, 3 days post MI. Scale bar 50µm.

3.2.5 Reduced expression of Dll1 impairs arteriogenesis, but not angiogenesis after myocardial infarction

Formation of new blood vessels is critical for supplying the healing myocardium with oxygen and nutrients. Therefore, angiogenesis and arteriogenesis are an essential component of wound healing. Although angiogenesis provides the capillary network for efficient nutrient distribution, only arteriogenesis can provide adequate perfusion necessary for the regeneration after myocardial infarction. Within this regard, of special importance is the border zone, as this area contains the cardiomyocytes at risk which can be rescued by reperfusion.

Analyzing angiogenesis after infarction by quantification of capillaries per cardiomyocyte (Figure 3.16 A), WT animals illustrated an increase in capillaries comparing baseline to MI 7d. 28 days after infarction, no further changes in capillary density were observed. In relation, Dll1^{+lacZ} mice also showed an increase in capillary density, but only comparing MI 7d and MI 28d conditions, not directly after infarction comparing baseline to MI 7d (Capillaries per cardiomyocyte - Baseline, WT: 1.14 ± 0.14 vs. Dll1^{+lacZ}: 1.18 ± 0.08 , n = 3/3, P = n.s.; Capillaries per cardiomyocyte – MI 7d, WT: 1.32 ± 0.06 vs. Dll1^{+lacZ}: 1.15 ± 0.05 , n = 3/3, P = 0.0001; Capillaries per cardiomyocyte – MI 28d, WT: 1.34 ± 0.05 vs. Dll1^{+lacZ}: 1.31 ± 0.20 , n = 3/3, P = n.s.; WT - BL vs. MI 7d P = 0.009; WT - MI 7d vs. MI 28d P = n.s.; Dll1^{+lacZ} - BL vs. MI 7d P = n.s.; Dll1^{+lacZ} - MI 7d vs. MI 28d P = 0.048).

To analyze arteriogenesis 7 days after infarction, SMA positive vessels in the border zone were quantified (Figure 3.16 B). Examining WT data, a highly significant increase of vessel numbers was observed in resistance vessels smaller 20 μm and in conductance vessels from 20-50 μm , comparing baseline and MI 7d time points. Vessel numbers above 50 μm were not significantly different (Number of vessels <20 μm per 0.25 mm², WT BL: 4.18 ± 0.85 vs. WT MI 7d: 9.10 ± 1.19 , n = 4/9, P = 2E-6; Number of vessels 20-50 μm per 0.25 mm², WT BL: 0.73 ± 0.13 vs. WT MI 7d: 1.01 ± 0.15 , n = 4/9, P = 0.009; Number of vessels >50 μm per 0.25 mm², WT BL: 0.17 ± 0.03 vs. WT MI 7d: 0.14 ± 0.12 , n = 4/9, P = n.s.). This response to infarction was completely missing in Dll1 heterozygous mice, where no change of vessel number could be observed in any vessel size (Number of vessels <20 μm per 0.25 mm², Dll1^{+lacZ} BL: 4.72 ± 1.02 vs. Dll1^{+lacZ} MI 7d: 4.23 ± 0.41 , n = 4/8, P = n.s.; Number of vessels 20-50 μm per 0.25 mm², Dll1^{+lacZ} BL: 0.27 ± 0.10 vs. Dll1^{+lacZ} MI 7d: 0.21 ± 0.12 , n = 4/8, P = n.s.; Number of vessels >50 μm per 0.25 mm², Dll1^{+lacZ} BL: 0.07 ± 0.02 vs. Dll1^{+lacZ} MI 7d: 0.06 ± 0.06 , n = 4/8, P = n.s.).

Therefore, the level of angiogenic response is similar in both experimental groups, but delayed in Dll1 heterozygous animals. This is probably a direct effect of the smaller initial infarct size. However, diminished levels of Dll1 cause a complete lack of arteriogenic response, as illustrated by a complete absence of vessel growth. This impaired arteriogenesis after MI in Dll1 heterozygotes adds yet another aspect to the obvious adverse remodelling that is taking place in these animals.

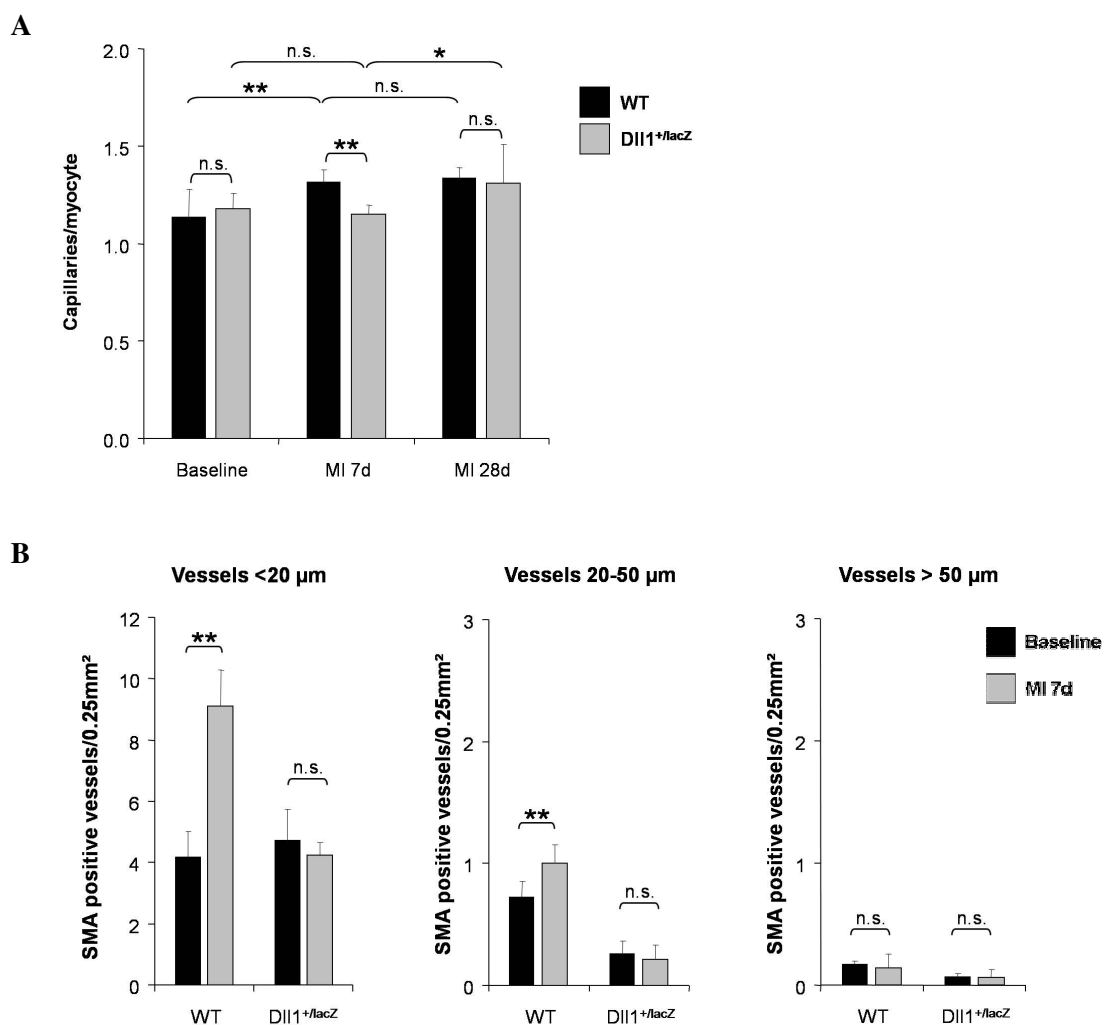


Figure 3.16 Impaired arteriogenesis, but not angiogenesis in Dll1 heterozygous mice. (A) Comparable, but delayed angiogenesis 4 weeks post infarction in WT and Dll1^{+/lacZ} animals shown by an increase of capillaries per cardiomyocyte. In WT the increase is prominent 7 days after MI, whereas in Dll1^{+/lacZ} the increase is only visible 28 days post infarction. (Representative immunofluorescence images Figure 3.10 C.) n=3/3 (3-4 fields each). (B) Quantification of arteriogenesis in the border zone 7 days post MI categorized by vessel size. WT animals showing a strong increase of vessels <50μm, in comparison to baseline WT conditions, whereas in Dll1^{+/lacZ} hearts this infarct response is missing. Baseline n=4/4 (3 sections each), MI 7d n=9/8 (2 border zones each); *P<0.05, **P<0.01; n.s.: not significant.

3.2.6 Altered mortality of Dll1 heterozygous mice after myocardial infarction

Data clearly indicated adverse remodelling taking place in Dll1 heterozygous animals. As adverse remodelling is associated with chronic heart failure and death, a survival analysis was performed after LAD ligation.

Examination of survival after permanent LAD occlusion operation resulted in a high mortality of WT animals within the first 7 days after infarction (Figure 3.17 A). Dll1 heterozygous mice displayed a significantly lower incidence of death during the first 7 days after LAD ligation, as determined by Log-rank test (WT: 22 of 68 animals died, equivalent to a survival of 69%; Dll1^{+/*lacZ*}: 8 of 61 animals died, equivalent to a survival of 87%; $P = 0.0085$). Within the following 3 weeks mortality in WT animals decelerated and reached a constant level of survival, whereas mortality in Dll1^{+/*lacZ*} animals accelerated. Final survival 4 weeks after infarction was comparable in both groups (Figure 3.17 B) (WT: 5 of 68 animals died, equivalent to a final survival of 60%; Dll1^{+/*lacZ*}: 21 of 61 animals died, equivalent to a 28 day survival of 52%; $P = \text{n.s.}$).

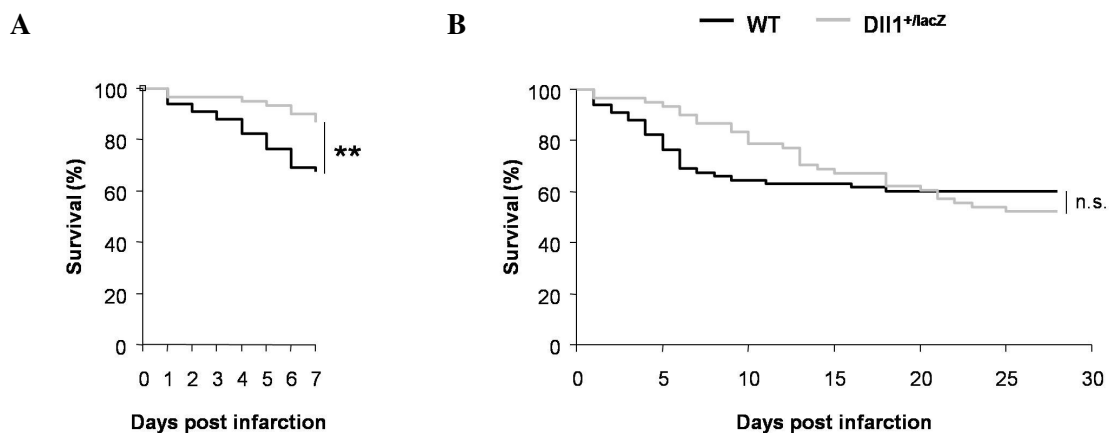


Figure 3.17 Altered mortality of Dll1 heterozygous mice post infarction. Kaplan-Meier curves showing (A) decreased mortality within 7 days after MI and (B) subsequent increased mortality within the following 3 weeks in Dll1 heterozygotes, compared to WT. Final survival 4 weeks post MI was comparable in both groups. $n=68/61$; $**P<0.01$; n.s.: not significant..

These data demonstrate the initially beneficial effect of the developmental/neonatal coronary artery phenotype in Dll1 heterozygous animals, evident on the initial smaller infarct size and improved 1 week survival after myocardial infarction. However, whereas

functional remodelling is apparent in constant survival in WT animals over time, adverse remodelling is again implicated by an increased long-term mortality in Dll1 heterozygotes. Although final survival 4 weeks after infarction did not show significant differences, additional follow-up analyses beyond 4 weeks would be of major interest. A further mortality would be expected in Dll1 heterozygotes in support of adverse remodelling associated with proceeding dysfunction and progressive heart failure.

3.3 Not endothelial Dll1 is the major determinant in infarct healing

As Dll1 was selectively expressed in the arterial endothelium and upregulated and detected mainly in vascular structures in the heart after myocardial infarction, we hypothesized that endothelial Dll1 contributes to the infarct phenotype in Dll1 heterozygous animals described in the previous chapter 3.2. To investigate this hypothesis, an inducible endothelial Dll1 knockout mouse strain VECad-Cre-ER^{T2}/Dll1^{lox/lox} (termed eDll1 KO after induction) was generated and analyzed. Due to the inducibility of the system, animals did not possess the confounding developmental/neonatal coronary artery phenotype of Dll1^{+lacZ} animals.

To verify the specificity and efficiency of induction of the VECad-Cre-ER^{T2} strain, a homozygous floxed VECad-Cre-ER^{T2}/ROSA26R strain was used (for detailed description and according references on mouse strains see methodology chapter 2.2.1). Vascular endothelial cadherin (VECad) promoter specific Cre expression was characterized by lacZ staining in induced VECad-Cre-ER^{T2}/ROSA26R animals and revealed specific, panendothelial activity in major arteries and veins, as well as in capillaries of various mouse tissues (Figure 3.18 A).

Verification of Dll1 downregulation in eDll1 KO animals was performed on RNA level by RT-PCR (Figure 3.18 C). 7 days after knockout induction, analysis revealed decreased Dll1 RNA levels in the heart and aorta, in comparison to appropriate controls (CTRL - Cre negative animals (-/Dll1^{lox/lox}) which had also been treated with the inducing agent tamoxifen).

Survival analyses demonstrated unchanged survival of eDll1 KO mice after induction, in comparison to CTRL (Figure 3.18 D), indicating no impairment of life expectancy due to tamoxifen treatment or endothelial Dll1 knockout.

Investigation of infarct size 4 weeks after myocardial infarction (Figure 3.18 E) revealed comparable values in CTRL and eDll1 KO conditions (Infarct size, CTRL: 39.41 ± 10.92 % vs. eDll1 KO: 33.74 ± 10.62 %, n = 10/12, P = n.s.).

This result was in contrast to the expected outcome and disproves the formulated hypothesis. Obviously, endothelial Dll1 is not the major determinant causing the adverse remodelling phenotype observed in Dll1 heterozygous animals. However, further analyses especially of Dll1 expression and arteriogenesis, but also of inflammation, dilation, hypertrophy and cardiac function would be needed to elucidate exact differences of MI response in Dll1^{+lacZ} and eDll1 KO animals.

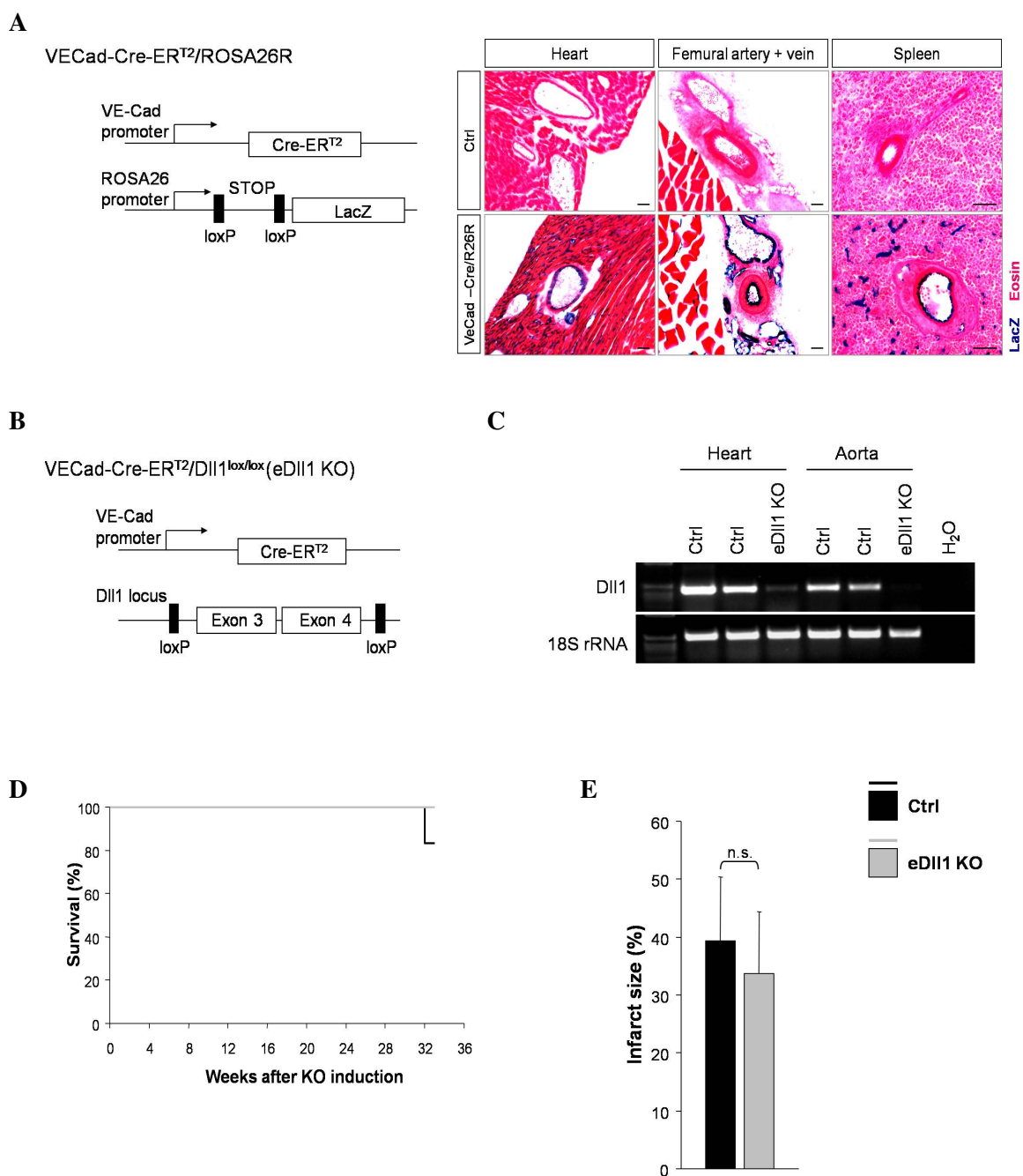


Figure 3.18 Characterization, verification and analysis of endothelial DII1 knockout animals demonstrating that endothelial DII1 is not the major determinant causing adverse remodelling after MI. (A) Scheme of VECad-Cre-ER^{T2}/ROSA26R transgenic mice and characterization of promoter specific Cre expression by lacZ staining. Analysis after induction showing panendothelial activity in major arteries and veins, as well as in capillaries of various mouse tissues (lower panel). Corresponding VeCad-Cre negative controls did not show lacZ activity (upper panel). Scale bar 50μm. (B) Scheme of VECad-Cre-ER^{T2}/DII1^{lox/lox} transgenic mice (termed eDII1 KO after induction). (C) Verification of DII1 downregulation in eDII1 KO conditions 7 days after knockout induction showing decreased RNA levels in heart and aorta, in comparison to respective controls. (D) Kaplan-Meier curve showing unchanged survival of eDII1 KO mice after knockout induction. n=5/7. (E) Infarct size analysis 4 weeks post infarction showing comparable infarct size under control and eDII1 KO conditions. n=10/12; n.s.: not significant.

4. DISCUSSION

Heart, vasculature and immune system development and maintenance are complex processes involving a multitude of signalling pathways; the importance of Notch signalling and its wide variety of sites of action and effects has been proven by several studies.

The aim of this study was to characterize the involvement of the Notch ligand Dll1 in arterial patterning of coronaries in the adult and its role in the ischemic stress response after myocardial infarction.

4.1 Baseline phenotype of Dll1^{+lacZ} mice

4.1.1 Reduced levels of Dll1 do not cause fatal congenital malformations

This study analyzed Dll1^{+lacZ} mice, which were first described by Hrabé de Angelis *et al.* in 1997. As first study providing data from a long-term analysis, our results showed that Dll1 heterozygous animals are viable, fertile and healthy. Animals showed a normal life span (18 months analysis compared to WT), indicating that Dll1 heterozygosity did not cause major and fatal congenital malformations.

4.1.2 Dll1 regulates a heart and coronary artery phenotype

Gravimetric data showed comparable body weight and size, but various analyses demonstrated reduced heart weight and size in Dll1 heterozygous animals, although no gross morphological changes of the heart were observed. Echocardiographic, morphometric and gravimetric analyses showed a consistent picture of the Dll1^{+lacZ} heart: decreased LV mass, smaller LVED area, reduced epicardial circumference, smaller LV wall thickness, decreased septum thickness (young animal analyses) and reduced heart weight (old animal analysis).

In contrast, cardiac function was not impaired in these animals. Data demonstrated that the smaller heart size with concurrent normal body weight is compensated by an elevated

ejection fraction, resulting in a normal stroke volume and cardiac output. This finding elucidates the normal long-term survival of Dll1 heterozygous mice.

In addition, changes in the coronary artery system were evident. In the adult mouse heart, Dll1 was expressed in the endocardium and the coronary endothelium of arteries with a diameter above 20 μm . Adult Dll1 heterozygous animals showed at the heart base a significantly reduced number of vessels bigger than 20 μm (conductance vessels), but an increase of vessels smaller than 20 μm (resistance vessels); the heart apex exhibited reduced vessel numbers of all sizes. The domain supplied by the LAD was significantly smaller.

These data suggest a model where in Dll1 heterozygous mice coronary vessel size is smaller from the start and only a reduced number of vessels will reach more distal heart areas (Figure 4.1).

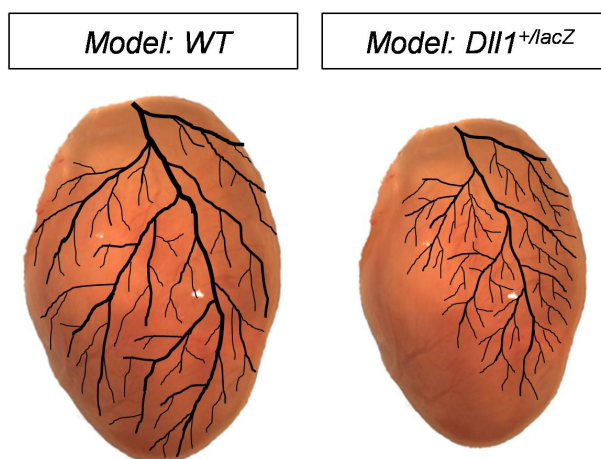


Figure 4.1 Proposed model of the coronary artery phenotype in Dll1 heterozygous mice. Reduced levels of Dll1 impair developmental/neonatal coronary arteriogenesis, becoming evident in the adult by a reduced coronary vessel size in the heart basis and causing a reduced number of vessels reaching more distal heart areas.

However, these data describe a phenotype in the adult, which is generated based on preceding mechanisms. During development, coronary vessels are formed by vasculogenesis and angiogenesis, generating a coronary plexus throughout the heart. Only upon connection to the aorta and corresponding perfusion, arteriogenesis takes place. Arteriogenesis propagates in a proximal-to-distal direction, forming the main coronary arteries first and proceeding to precapillary arterioles; the coronary plexus is remodelled into larger vessels ramifying into smaller branches. After birth, angiogenesis and arteriogenesis continue in order to compensate for the increasing needs of a growing heart

until adulthood (approximately P21 in the mouse) (Luttun and Carmeliet, 2003; Fernández, 2004).

In addition, biomechanical forces resulting from fluid flow also affect vascular development (Darland and D'Amore, 2001). The construction of blood vessels is not only influenced by genetic programs, but blood vessels also underlie basic laws of fluid dynamics. Requirements of effective fluid transport are met by large tubes, while diffusion of nutrients requires slow blood flow. However, if fluid under constant pressure moves from a large-diameter tube to a small-diameter tube, its velocity increases. Consequently, evolution paid its tribute to these physical constraints by the establishment of the hierarchy of the vascular system: many smaller vessels branching out from a larger one. The sum of the cross-sectional area of all branching smaller vessels is greater than that of the larger vessel, thereby decreasing blood flow velocity for effective diffusion (Gilbert, 2006).

Sörensen et al. have shown that Dll1 is expressed in endothelial cells of large arteries, beginning at E13.5 (Sörensen *et al.*, 2009), a time just before perfusion starts and arteriogenesis is initiated (E14). In addition, Sörensen and co-workers used embryos with reduced Dll1 levels and found a reduced lumen of the aorta and other large arteries, but the thickness of the arterial walls was not altered (Sörensen *et al.*, 2009).

Taking all these implications into account, I can only speculate about the underlying relationship leading to the coronary phenotype apparent in the adult Dll1 heterozygous mouse: I suspect that vasculogenesis and angiogenesis are not altered during coronary development, resulting in the same starting situation of the coronary plexus before onset of perfusion and arteriogenesis. Dll1 haploinsufficiency results in an impaired arteriogenesis in the following developmental and neonatal steps, evident in reduced coronary artery growth and vessel size, proceeding in a proximal-to-distal direction. However, Dll1 most probably does not directly influence reduced number of big vessels and at the same time an increased number of small vessels. I suspect the increased number of vessels smaller 20 μm do be a rather indirect effect. Based on fluid dynamic constraints and the fact that the stroke volume is normal, I postulate that due to the general smaller coronary artery lumen in Dll1 heterozygotes, fluid velocity is increased in these vessels and during remodelling of the coronary vascular system this is compensated by the establishment of an increased number of small vessels.

It is evident, that Dll1 haploinsufficiency impairs developmental/neonatal coronary arteriogenesis (the number of large conductance vessels is already decreased in neonates;

data not shown), resulting in an adult phenotype. However, this study did not analyse Dll1 expression during embryonic and neonatal development and no statement is possible regarding the question if there is a threshold of vessel size where Dll1 acts. This question is of importance as to the underlying mechanism which gives rise to reduced vessels bigger than 20 μm , but increased vessel numbers smaller than 20 μm in the adult. Although the basis of the coronary phenotype of Dll1 heterozygous animals lies before adulthood, it is striking that under normal adult conditions Dll1 is expressed in endothelium of vessels bigger than 20 μm , the same vessel category that is actually reduced in Dll1 heterozygotes.

Other studies have shown a role of PDGF-B signaling in coronary arteriogenesis during development (Hellström *et al.*, 1999; Van den Akker *et al.*, 2008). *Pdgf-b^{-/-}* mouse embryos show dilated coronary arteries and reduced number of coronary vSMCs. The group of Van den Akker propose that coronary vessel dilation was based on lack of physical support. They suggest a relationship in which the loss of PDGF-B production in endothelial cells impairs their function of recruitment of stabilizing vSMCs (Van den Akker *et al.*, 2008).

Jag1 and Dll1 are involved in SMC differentiation and maturation. Jag1 and Dll1 on endothelial cells induce SMCs to express Notch3 and Jag1, which subsequently promotes and maintains the differentiation phenotype of SMCs (Kume, 2009).

Sörensen *et al.* provided evidence that endothelial Dll1 activity maintains arterial identity. However, loss of Dll1 activity in fetal vessels and downregulation of arterial markers had surprisingly little effect on vessel morphology. Only reduced arterial lumen, but no changes in wall thickness were evident (Sörensen *et al.*, 2009).

In accordance with data from Sörensen *et al.* (Sörensen *et al.*, 2009), the present study showed reduced coronary vessel size in the adult. In addition, the observed coronary artery phenotype in Dll1 heterozygous animals suggests, that vSMC recruitment is sufficient to maintain their role of physical support and dilation does not occur. Reduced levels of Dll1 in heterozygous animals are either still sufficient for vSMC recruitment and/or effects are sustained by Jag1 function. However, whereas vSMC recruitment is sufficient for vessel support, it seems not to be adequate for normal coronary vessel growth.

Moreover, data indicate a correlation between decreased heart size, coronary vasculature phenotype and smaller cardiomyocyte size in Dll1 heterozygous mice.

Already other studies have posed the question regarding the relationship of endothelial cell mass and organ size. Meaning, is one heart larger than another because it has more vessels

or does it have more vessels because it is larger (Simons, 2005)? Results of studies examining various organs indicate that the former is true, i.e. the vasculature determines organ size (Simons, 2005).

Therefore, altered development of the coronary vasculature due to reduced levels of Dll1 presumably caused reduced heart weight and size. However, the question remains why the cardiomyocytes are smaller. Smaller heart size can be due to smaller cardiomyocytes, but in theory it is also possible that smaller heart size would be based on reduced cardiomyocyte numbers.

Limitations of the study and outstanding questions

One crucial aspect of this study which could not be realized so far due to technical problems, is the visualization of the coronary artery tree. Three-dimensional visualization and comparison of the coronary arteries of WT and Dll1 heterozygous animals could disclose the correctness of the proposed model and give information on the coronary branching pattern.

Furthermore, exact tracing of Dll1 expression in coronary arteries during embryonic development might be able to answer if Dll1 is only expressed in arterial vessels which will grow to become larger than 20 μm in the adult. However, then the new question is raised, about the underlying mechanisms which initiate Dll1 expression in a small vessel supposed to become large, whereas no Dll1 expression takes place in a small vessel destined to remain small. In addition, the question remains why the number of arterial vessels smaller than 20 μm is increased at the heart basis: is this a direct or indirect effect of reduced Dll1 levels?

Another aspect not mentioned so far is tissue ischemia due to reduced perfusion. Although heart function and survival are not impaired in Dll1 heterozygotes, it would be interesting to know if mice exhibit tissue ischemia and if the apex part is more affected than the heart base. To assess tissue ischemia expression of HIF1 α and VEGF could be analyzed.

4.1.3 Dll1 is involved in monocyte generation in the spleen

Monocytes have been shown to constitute a heterogeneous population where Ly-6C^{hi} monocytes exhibit pro-inflammatory functions and Ly-6C^{lo} monocytes are associated with wound healing tasks (Geissmann *et al.*, 2003; Nahrendorf *et al.*, 2007). Moreover, a recent study has identified the spleen as major source of monocytes (Swirski *et al.*, 2009). The

group showed that Ly-6C^{hi} and Ly-6C^{lo} monocytes in the spleen resembled their blood counterparts in morphology, function and differentiation potential. More importantly, the study also showed evidence that after ischemic myocardial injury splenic monocytes exit the spleen en masse, accumulate in injured tissue and participate in wound healing. Splenic monocytes contributed to healing to a much higher extent than bone marrow and blood monocyte pools; without splenic monocytes healing after MI was impaired. However, data also suggested that the spleen does not likely produce monocytes, but rather serves as site for monocyte storage (Swirski *et al.*, 2009).

Dll1 has been shown to be involved in selected steps of B- and T-cell generation. However, a role in monocyte subset generation has not been implicated to date. In this study, monocyte subset analyses revealed that absolute monocyte numbers are significantly decreased in the spleen of Dll1 heterozygous animals. The number of Ly-6C^{hi} monocytes seemed to be decreased in Dll1 heterozygotes, but lower levels just didn't show significance. Yet, the number of Ly-6C^{lo} monocytes was significantly decreased in Dll1 heterozygous mice, compared to WT. Surprisingly however, circulating monocytes in the blood were not altered in Dll1 heterozygous mice.

These data suggest that in the adult Dll1 is involved in monocyte and monocyte subset generation in the spleen. As circulating monocytes in the blood were not altered, results imply that the spleen is involved in monocyte production, in contrast to the finding of Swirski and co-workers which suggest only a monocyte storage function of the spleen (Swirski *et al.*, 2009). Though, if the spleen in fact does not produce monocytes, data would imply selective monocyte recruitment of the spleen in Dll1 heterozygotes.

4.2 Healing after myocardial infarction in Dll1^{+lacZ} animals

4.2.1 Functional LV remodelling in WT animals post infarction

Functional healing processes after myocardial infarction were apparent in WT animals. 1 day after LAD occlusion a moderate initial infarct size was determined. In the following course of time infarct size was stabilized as seen on a slight, but not significant increase of infarct size. In accordance, ejection fraction and stroke volume significantly decreased after MI, but no further long term deterioration was observed.

As expected (acute compensation by the Frank-Starling mechanism), left-ventricular dilation was apparent, but moderate (slight, but significant increase of LVED area and epicardial circumference). Thinning of the left-ventricular free wall was also observed in

WT animals, but significant thinning took place in the first week after infarction probably mainly based on normal cardiomyocyte necrosis and no further thinning was apparent in the following. Therefore, infarct expansion (thinning and elongation of the infarcted area rather associated with myocyte slippage than necrosis) seemed not to be a problem in WT animals. In addition, cardiomyocyte hypertrophy in the remote myocardium is a part of compensatory remodelling, to counteract intensified wall stress. Myocyte hypertrophy in the remote was revealed in WT animals, but the increase of cross-sectional area was moderate, becoming only evident upon 4-week analyses. In accordance, moderate ventricular hypertrophy was evident by a small increase of septum thickness.

Myocardial infarction does not only trigger acute cell death by necrosis (mainly in the infarcted zone), but also by apoptosis at later stages of MI (mainly in the remote and border zone). Analyses revealed a significant increase of apoptotic cells in all heart areas 3 days after infarction. In the following (7 day analysis), cell numbers decreased in the border zone and infarct area in WT animals, but in the remote a further increase of apoptotic cell numbers was observed. 4 weeks after infarction, the apoptotic response had completely subsided in all areas.

Collagen deposition is needed for scar formation and tissue stabilization. A disorganized, immature collagen matrix cannot withstand the cardiac load, leading to dilation and a higher probability of rupture. Deposition of interstitial collagen in the noninfarcted myocardium has a negative influence as it is associated with ventricular stiffness in the remote area. As expected, mature, organized collagen fibres were observed in the infarct area 4 weeks after infarction, but no interstitial fibrosis in the remote was visible.

Analyses of the inflammatory response in WT animals after infarction revealed strong, increasing and persistent leukocyte infiltration in the border zone and infarct. 4 weeks after infarction, leukocyte infiltration had completely ceased. Identification of general macrophages showed infiltration in the infarct area 3 days after infarction and in the following a decline of macrophage numbers. M2 macrophages were already apparent 3 days after infarction in all 3 areas and infiltration was stable until 7 days after MI.

Formation of new blood vessels is critical for supplying the healing myocardium with oxygen and nutrients. Therefore, angiogenesis and arteriogenesis are an essential component of wound healing. Although angiogenesis provides the capillary network for efficient nutrient distribution, only arteriogenesis can provide adequate perfusion necessary for the regeneration after myocardial infarction. Within this regard, of special importance is the border zone, as this area contains the cardiomyocytes at risk which can be rescued by

reperfusion. Angiogenesis in WT animals was demonstrated by an increase in capillary density immediately after infarction, arteriogenesis in the border zone was proven by an increase in numbers of arterial vessels smaller 50 μm .

Taking all these data together, WT animals showed adaptive compensation and healing after myocardial infarction. Obviously, functional remodelling took place in WT animals, explaining the stable long-term survival rate and highlighting the importance of these processes and their control mechanisms.

4.2.2 Dll1 is upregulated after myocardial infarction

Baseline, Dll1 was expressed in arterial endothelium of the heart. RNA and protein analyses revealed an upregulation of Dll1 after myocardial infarction. Expression levels were strongest at day 3 after infarction, but even at day 7 expression levels were still above sham operated levels. LacZ staining revealed baseline Dll1 expression 4 weeks after infarction. Surprisingly, Dll1-lacZ staining and Dll1-immunofluorescence analyses did not show comparable results. Whereas lacZ staining illustrated enhanced Dll1 expression in vascular structures and sporadic single cells in the infarcted area, immunofluorescence did not show baseline Dll1 expression and only single arterial vessels and cells in the border zone stained positive for Dll1.

Preceding studies using the mouse model of Dll1^{+lacZ} (and Dll1^{lacZ/lacZ}) have shown evidence that lacZ identification mimics endogenous Dll1 expression during development and in the adult (Hrabé de Angelis *et al.*, 1997; Beckers *et al.*, 1999; Micely-Libby *et al.*, 2007), and have even been shown to be more sensitive than Dll1 mRNA detection by *in situ*-hybridization (Beckers *et al.*, 1999). Therefore, Dll1 expression analysis by lacZ staining rather illustrated true Dll1 expression, than analyses by immunofluorescence did in this study; differences of detected expression likely reflect the different sensitivities of the two detection techniques. Although the antibody used for Dll1 immunofluorescence has been proven to work in other tissues, like in the hindlimb muscle (Limbourg *et al.*, 2007), it seemed less potent in the heart. Obviously, the low Dll1 expression level and therefore low fluorescence level could not be detected by fluorescence microscopy and only structures expressing Dll1 above a certain threshold level exhibited enough fluorescence intensity to be detectable. Further trials using various Dll1 antibodies showed also positive staining in various tissues, but just not in the heart. This limitation clearly poses a large problem, as a

further characterization of Dll1 positive structures (identified by lacZ) is of major importance for further studies: the present experiments could not reveal if Dll1 upregulation takes only place in arteries, or maybe even in veins, and the allocation of Dll1 single cells to monocytes, macrophages or another inflammatory or non-inflammatory cell type would be of importance as well.

4.2.3 Dll1 heterozygous animals exhibit features of adverse remodelling after myocardial infarction

Analyses of Dll1 heterozygous animals in response to myocardial infarction showed an initial smaller infarct size. Due to the statistical relevance of this finding, this was most probably not caused by operational variations of the LAD ligation (mice analyzed had the same background and were in fact littermates). Instead, the smaller initial infarct size was rather based on the earlier described and discussed developmental/postnatal coronary artery phenotype. As the LAD domain is already smaller in Dll1 heterozygous mice, occlusion of the LAD at the same site as in WT animals affects a smaller heart region. In accordance, the area-at-risk was smaller in Dll1^{+/*lacZ*}, but the infarct fraction of the area-at-risk was the same, demonstrated on a comparable ratio MI/AAR (analyses 1 day after LAD occlusion). This finding suggested that reduced levels of Dll1 during coronary artery development can result in a beneficial effect when the organism suffers a myocardial infarction in adulthood. Surprisingly however, the infarct size demonstrated a drastic increase from day 1 via day 7 to day 28 post infarction in Dll1 heterozygous mice, indicating that the beneficial effect is not retained. In accordance, cardiac analyses revealed a strong functional deterioration in the course of time, illustrated on ejection fraction and stroke volume data.

In addition, Dll1 heterozygous mice showed strong, progressive left-ventricular dilation which was beyond normal infarct compensation, as apparent on the loss of cardiac function. Dilation was demonstrated by a massive increase in LVED area and epicardial circumference. Infarct expansion as indicator of adverse remodelling was observed in Dll1^{+/*lacZ*} mice and evident by the increase of infarct portion of the epicardial circumference and a strong decrease of left-ventricular wall thickness. Furthermore, a strong increase in cross-sectional myocyte area and correspondingly decreased myocytes per field, as well as a significantly increased septum thickness was detected. This strong, progressive cardiomyocyte and ventricular hypertrophy represented further events taking place in Dll1 heterozygotes that are indicators of adverse remodelling.

Surprisingly, characterization of apoptotic cell death in response to MI showed reduced general apoptosis in Dll1 heterozygotes. However, to answer if reduced apoptotic cell numbers are in fact a direct effect of Dll1 heterozygosity or rather based on the initial smaller infarct size, more time points would have to be analyzed. Only with more time points a statement could be made if apoptotic response is rather time-shifted and increases later than in WT, due to smaller infarcts. Though, even if apoptosis is in fact decreased in Dll1 heterozygous mice, obviously massive cell death does occur as apparent on the increase in infarct size. In principle, necrosis and autophagy can contribute to cell death as well. Although necrosis is rather connected with acute cell death in the infarcted area immediately after MI, it is possible that due to impaired arteriogenesis in Dll1 heterozygotes, ischemia is prolonged and necrosis persists. This is especially important for the cardiomyocytes at risk in the border zone and could explain the increase in infarct size. However, persistent ischemia due to impaired arteriogenesis could also cause increased autophagy and corresponding effects on infarct size. Therefore, additional quantification of necrosis and autophagy would be needed to answer which type of cell death is altered in Dll1 heterozygous animals.

4 weeks after infarction, fibrosis analysis revealed mature collagen fibres with increased collagen deposition in Dll1 heterozygotes, but no interstitial fibrosis. Increased collagen deposition (above normal) after infarction is actually associated with LV stiffness and dysfunction, whereas decreased collagen deposition can lead to LV dilation (Jugdutt, 2003). However, although increased collagen is observed in Dll1 heterozygous animals after myocardial infarction, it is not possible to conclude that this is directly related to increased stiffness and dysfunction. As in Dll1 heterozygous mice the final infarct size is bigger than in WT animals, based on the experiments performed it is not possible to tell if collagen deposition is adequate for the corresponding infarct size, or if it is above or below adequate collagen levels. Collagen fibre maturation and organization in the scar seemed not be impaired.

Striking results were also determined with respect to the inflammation response after infarction. Increased leukocyte infiltration 3 days after infarction was especially intriguing with regard to the initial smaller infarct size in Dll1 heterozygotes, indicating a misbalance of inflammation to the corresponding infarct size. Further identification of macrophages revealed delayed, but increased macrophage infiltration in Dll1 heterozygotes. This poses the question which cell types account for the early increased leukocyte infiltration and requires further investigation. In addition, cardiac repair requires the containment of

inflammation into the infarct area; extension into the remote can cause matrix degradation in this area and contribute to adverse remodelling (Frangogiannis, 2008). With this regard, the observed infiltration of F4/80 macrophages in the remote of Dll1 heterozygous infarcted hearts is of special importance and might be a contributor to the increase in infarct size. Staining of M2 macrophages demonstrated highly reduced cell numbers and infiltration ceased even earlier than in WT animals, indicating impaired initiation of healing and repair in Dll1 heterozygotes. Although no direct differentiation of Ly-6C^{lo} monocytes to M2 tissue macrophages has been proven to date, the involvement of both cell types in healing processes have been shown by various studies (Nahrendorf *et al.*, 2007; Swirski *et al.*, 2009; Limbourg *et al.*, *in review*). Furthermore, Swirski and co-workers have proven that splenic monocytes are recruited to the site of ischemic myocardial injury and regulate inflammation (Swirski *et al.*, 2009). Therefore, the observation of reduced basal Ly-6C^{lo} monocyte numbers in Dll1 heterozygous mouse spleen tissue and lower M2 macrophage infiltration after infarction is striking. However, data can only give first hints of processes happening in Dll1 heterozygotes. Clearly more markers distinguishing leukocyte cell types, monocytes, and M1 and M2 macrophages (preferably by FACS analysis which allows quantification) are needed for an informed statement of alterations in inflammatory processes initiated after myocardial infarction in Dll1 heterozygous mice.

Another aspect which should be mentioned at this point is Dll1 expression. As mentioned before, lacZ staining and even immunofluorescence did not only show endothelial Dll1 staining, but also sporadic single cells. Moriyama *et al.* have demonstrated Dll1 expression on a considerable fraction of macrophages in the spleen (Moriyama *et al.*, 2008). In this heart study, however, sporadic single Dll1 positive cells in the myocardium did not resemble the massive monocyte/macrophage infiltration observed, highlighting again the importance of characterization of Dll1 positive structures.

Characterization of angiogenesis showed a comparable, but delayed increase in capillary density. Probably the delay is a direct effect of the smaller initial infarct size. This result is in correspondence with unimpaired angiogenesis in a setting of hindlimb ischemia in Dll1 heterozygotes by Limbourg and co-workers. The group demonstrated Dll1-independent regulation of microvascular angiogenesis, possibly through Dll4 which is expressed in adult microvessels (Limbourg *et al.*, 2007). Analogous to impaired arteriogenesis in the same setting of hindlimb ischemia (Limbourg *et al.*, 2007), analyses of arteriogenesis after myocardial infarction in this study revealed that diminished levels of Dll1 caused a complete lack of arteriogenic response, as illustrated by the complete absence of vessel

growth. As the importance of postnatal arteriogenesis for the restoration of blood flow and rescue of an ischemic organ has been proven by various studies (Limbourg *et al.*, 2007; Deindl and Schaper, 2005; Simons, 2005), impaired arteriogenesis after MI in Dll1 heterozygotes adds yet another aspect to the obvious adverse remodelling that is taking place in these animals.

Clearly, this study could provide evidence for adverse remodelling processes taking place after myocardial infarction in Dll1 heterozygous animals, leading to progressive mortality. However, survival was just followed 4 weeks after LAD occlusion. Longer follow-up would be needed to support the theory of adverse remodelling, demonstrating proceeding dysfunction and progressive heart failure in Dll1 heterozygous mice.

As adverse remodelling is demonstrably not caused by the initial infarct size in Dll1 heterozygous mice, infarct healing must be affected in these animals. Although no clear statement about cause-effect relationship can be done based on the present data, other studies have shown an involvement of Dll1 and Notch signalling in arteriogenesis and inflammation (Limbourg *et al.*, 2007; Moriyama *et al.*, 2008; Limbourg *et al.*, *in review*). I suggest that impaired arteriogenesis and altered inflammation are direct causes of reduced Dll1 levels; other factors like infarct expansion, increased dilation and increased hypertrophy are rather indirect effects caused by impaired arteriogenesis and altered inflammation, altogether leading to adverse remodelling, increasing infarct size and corresponding progressive dysfunction.

Nevertheless, one major limitation of the study is the initial smaller infarct size in Dll1 heterozygotes which is based on the confounding developmental coronary artery phenotype. This bias makes the exact comparison of infarction-induced processes difficult with respect to timing and absolute data; only the general trend can be compared between WT and Dll1^{+lacZ} animals. To solve this problem a general, inducible Dll1 knockout would have to be analyzed.

4.2.4 Not endothelial Dll1 is the major determinant in infarct healing

As basal expression and upregulation of Dll1 after MI was most apparent in arterial endothelium, the most obvious hypothesis implicated that endothelial Dll1 contributed to

the observed adverse remodelling phenotype after infarction. Therefore, an inducible, panendothelial Dll1 knockout mouse model which also brought about the advantage of absence of the confounding developmental coronary artery phenotype was evaluated. Surprisingly however, adverse remodelling could not be reproduced in these mice, as apparent on a comparable infarct size 4 weeks after LAD occlusion (compared to infarcted controls). Obviously, endothelial Dll1 is not the major determinant causing the adverse remodelling phenotype observed in Dll1 heterozygous animals. However, only endpoint infarct size was determined in this study. Further analyses especially of Dll1 expression and arteriogenesis, but also of inflammation, dilation, hypertrophy and cardiac function would be needed to elucidate exact differences of MI response in Dll1^{+lacZ} and eDll1 KO animals.

Besides, no other studies have detected Dll1 in infarcted hearts and cardioprotective Notch signalling in stressed hearts has been rather associated with Notch1/Jag1 signalling (Gude *et al.*, 2008; Croquelois *et al.*, 2008; Kratsios *et al.*, 2010). Apart from endothelial staining, this study only detected Dll1 in sporadic single cells which did not reflect massive inflammatory infiltration. It is questionable if under normal conditions Dll1 expressing cells enter the infarcted myocardium and activate present Notch receptors but cannot be detected by the methods applied in this study. First data shown in this study indicate another possibility: Dll1 acts outside the heart by regulating monocyte/macrophage differentiation. This regulation might occur directly in the spleen, although our data contradict data of another study which identifies only a storage role of the spleen (Swirski *et al.*, 2009). Therefore, detailed analysis of the site and mode of action of Dll1 after myocardial infarction will be a main task of future studies.

5. CONCLUSION

This study provides evidence that the Notch ligand Dll1 is involved in developmental/neonatal coronary arteriogenesis. Dll1 regulates coronary artery growth and number, thereby directly influencing heart size. In addition, first evidence is apparent of Dll1 engagement in monocyte generation in the spleen.

In response to myocardial infarction, data demonstrate the importance of Dll1 for correct compensation and functional remodelling to preserve ventricular function. Reduced levels of Dll1 cause adverse remodelling, progressive infarct size enlargement and ventricular dysfunction rather based on altered infarct healing mechanisms, than on the extent of the ischemic incident. I suggest direct effects of diminished Dll1 levels leading to impaired arteriogenesis and enhanced inflammation, whereas infarct expansion, and progressive dilation and hypertrophy are rather downstream effects.

Dll1 is selectively expressed in the heart in arterial endothelium of large coronary arteries and Dll1 expression is upregulated after infarction. However, at least in a setting of permanent myocardial infarction by permanent LAD occlusion, this study provides first data showing that not endothelial Dll1 is the major determinant causing adverse remodelling effects upon reduction/absence. Data rather point to an extravascular role of Dll1 in infarct healing, adumbrating a role in the monocyte/macrophage system, but the exact site and mode of action remains an open question which will have to be addressed by future studies.

6. REFERENCES

Adams RH. Molecular control of arterial-venous blood vessel identity. *J Anat* 202:105-112 (2003)

Al Haj Zen A, Madeddu P. Notch signalling in ischemia-induced angiogenesis. *Biochem Soc Trans* 37:1221-1227 (2009)

Alva JA, Zovein AC, Monvoisin A, Murphy T, Salazar A, Harvey NL, Carmeliet P, Iruela-Arispe ML. VE-Cadherin-Cre-Recombinase Transgenic Mouse: A Tool for Lineage Analysis and Gene Deletion in Endothelial Cells. *Dev Dynamics* 235:759-767 (2006)

Apelqvist A, Li H, Sommer L, Beatus P, Andersonk DJ, Honjo T, Hrabé de Angelis M, Lendahl U, Edlund H. Notch signalling controls pancreatic cell differentiation. *Nature* 400:877-881 (1999)

Artavanis-Tsakonas S, Rand MD, Lake RJ. Notch Signaling: Cell Fate Control and Signal Integration in Development. *Science* 284:770-776 (1999)

Beckers J, Clark A, Wünsch K, Hrabé De Angelis M, Gossler A. Expression of the mouse Delta1 gene during organogenesis and fetal development. *Mech Dev* 84:165-168 (1999)

Benedito R, Duarte A. Expression of Dll4 during mouse embryogenesis suggests multiple developmental roles. *Gene Expr Patterns* 5(6):750-755 (2005)

Bodi V, Sanchis J, Nunez J, Mainar L, Minana G, Benet I, Solano C, Chorro FJ, Llacer A. Uncontrolled immune response in acute myocardial infarction: unraveling the thread. *Am Heart J* 156:1065-1073 (2008)

Borggreffe T, Oswald E. The Notch signaling pathway: Transcriptional regulation at Notch target genes. *Cell Mol Life Sci* 66:1631-1646 (2009)

Bray SJ. Notch signaling: a simple pathway becomes complex. *Nat Rev Mol Cell Bio* 7:678-689 (2006)

Brooker R, Hozumi K, Lewis J. Notch ligands with contrasting functions: Jagged1 and Delta1 in the mouse inner ear. *Development* 133:1277-1286 (2006)

Buckingham M, Meilhac S, Zaffran S. Building the mammalian heart from two sources of myocardial cells. *Nat Rev Genet* 6(11):826-835 (2005)

Campa VM, Gutiérrez-Lanza R, Cerignoli F, Díaz-Trelles R, Nelson B, Tsuji T, Barcova M, Jiang W, Mercola M. Notch activates cell cycle reentry and progression in quiescent cardiomyocytes. *J Cell Biol* 183(1):129-41 (2008)

-
- Carmeliet P.** Mechanisms of angiogenesis and arteriogenesis. *Nature Medicine* 6(3):389-395 (2000)
- Carmeliet P, De Smet F, Loges S, Mazzone M.** Branching morphogenesis and antiangiogenesis candidates: tip cells lead the way. *Nat Rev Clin Oncol* 6:315-326 (2009)
- Carmeliet P, Ng YS, Nuyens D, Theilmeier G, Brusselmans K, Cornelissen I, Ehler E, Kakkar VV, Stalmans I, Mattot V, Perriard JC, Dewerchin M, Flameng W, Nagy A, Lupu F, Moons L, Collen D, D'Amore PA, Shima DT.** Impaired myocardial angiogenesis and ischemic cardiomyopathy in mice lacking the vascular endothelial growth factor isoforms VEGF164 and VEGF188. *Nat Med* 5:495-502 (1999)
- Chen JN, Cowan DB, Mably JD.** Cardiogenesis and the Regulation of Cardiac-Specific Gene Expression. *Heart Fail Clin* 1(2):157-170 (2005)
- Collesi C, Zentilin L, Sinagra G, Giacca M.** Notch1 signaling stimulates proliferation of immature cardiomyocytes. *J Cell Biol* 183(1):117-28 (2008)
- Cordes R, Schuster-Gossler K, Serth K, Gossler A.** Specification of vertebral identity is coupled to Notch signalling and the segmentation clock. *Development* 131:1221-1233 (2004)
- Croquelois A, Domenighetti AA, Nemir M, Lepore M, Rosenblatt-Velin N, Radtke F, Pedrazzini T.** Control of the adaptive response of the heart to stress via the Notch1 receptor pathway. *J Exp Med* 205(13):3173-85 (2008)
- Darland DC, D'Amore PA.** Cell-Cell Interactions in Vascular Development. *Curr Top Dev Biol* 52:107-149 (2001)
- Deindl E, Schaper W.** The Art of Arteriogenesis. *Cell Biochemistry and Biophysics* 43:1-15 (2005)
- Domenga V, Fardoux P, Lacombe P, Monet M, Maciazek J, Krebs LT, Klonjowski B, Berrou E, Mericskay M, Li Z, Tournier-Lasserre E, Gridley T, Joutel A.** Notch3 is required for arterial identity and maturation of vascular smooth muscle cells. *Genes Dev* 18(22):2730-2735 (2004)
- Dorn GW II, Diwan A.** The rationale for cardiomyocyte resuscitation in myocardial salvage. *J Mol Med* 86:1085-1095 (2008)
- Dreyer WJ, Michael LH, Nguyen T, Smith CW, Anderson DC, Entman ML, Rossen RD.** Kinetics of C5a release in cardiac lymph of dogs experiencing coronary artery ischemia-reperfusion injury. *Circ Res* 71:1518-1524 (1992)
- Duarte A, Hirashima M, Benedito R, Trindade A, Diniz P, Bekman E, Costa L, Henrique D, Rossant J.** Dosage-sensitive requirement for mouse Dll4 in artery development. *Genes Dev* 18(20):2474-2478 (2004)
- Dyczynska E, Sun D, Yi H, Sehara-Fujisawa A, Blobel CP, Zolkiewska A.** Proteolytic processing of delta-like 1 by ADAM proteases. *J Biol Chem* 282(1):436-44 (2007)
-

-
- Eble JA, Niland S.** The Extracellular Matrix of Blood Vessel. *Curr Pharmaceutical Design* 15:1385-1400 (2009)
- Fernández B.** Embryonic Development of Collateral Arteries. In *Arteriogenesis, edited by Schaper W and Schaper J, 1st edition, Springer Netherlands* (2004)
- Ferrari R, Ceconi C, Campo G, Cangiano E, Cavazza C, Secchiero P, Tavazzi L.** Mechanisms of Remodelling – A Question of Life (Stem Cell Production) and Death (Myocyte Apoptosis) – *Circ J* 73:1973-1982 (2009)
- Fortini ME.** Notch Signaling: The Core Pathway and Its Posttranslational Regulation. *Dev Cell* 16:633-647 (2009)
- Frangogiannis NG.** The Mechanistic Basis of Infarct Healing. *Antioxidants & Redox Signaling* 8:1907-1939 (2006)
- Frangogiannis NG.** The immune system and cardiac repair. *Pharmacological Research* 58:88-111 (2008)
- Frantz S, Bauersachs J, Ertl G.** Post-infarct remodelling: contribution of wound healing and inflammation. *Cardiovasc Res* 81:474-481 (2009)
- Fuchs M, Hilfiker A, Kaminski K, Hilfiker-Kleiner D, Guener Z, Klein G, Podewski E, Schieffer B, Rose-John S, Drexler H.** Role of interleukin-6 for LV remodeling and survival after experimental myocardial infarction. *FASEB J* 17:2118-2120 (2003)
- Gale NW, Dominguez MG, Noguera I, Pan L, Hughes V, Valenzuela DM, Murphy AJ, Adams NC, Lin HC, Holash J, Thurston G, Yancopoulos GD.** Haploinsufficiency of delta-like 4 ligand results in embryonic lethality due to major defects in arterial and vascular development. *Proc Natl Acad Sci USA* 101(45):15949-15954 (2004)
- Geissmann F, Jung S, Littman DR.** Blood Monocytes Consist of Two Principal Subsets with Distinct Migratory Properties. *Immunity* 19:71-82 (2003)
- Gerhardt H, Golding M, Fruttiger M, Ruhrberg C, Lundkvist A, Abramsson A, Jeltsch M, Mitchell C, Alitalo K, Shima D, Betsholtz C.** VEGF guides angiogenic sprouting utilizing endothelial tip cell filopodia. *J Cell Biol* 161(6):1163-77 (2003)
- Gerwins P, Sköldenberg E, Claesson-Welsh L.** Function of fibroblast growth factors and vascular endothelial growth factors and their receptors in angiogenesis. *Crit Rev Onc Hem* 34:185-194 (2000)
- Gessler M.** Dll1 and Dll4: similar, but not the same. *Blood* 113(22):5375-5376 (2009)
- Gilbert SF.** *Developmental Biology, 8th edition, Sinauer Associates Inc.* (2006)
- Gordon S, Taylor PR.** Monocyte and macrophage heterogeneity. *Nature Rev Immunol* 5:953-964 (2005)

-
- Gory S, Vernet M, Laurent M, Dejana E, Dalmon J, Huber P.** The *Vascular Endothelial-Cadherin* Promoter Directs Endothelial-Specific Expression in Transgenic Mice. *Blood* 93(1):184-192 (1999)
- Grego-Bessa J, Luna-Zurita L, del Monte G, Bolós V, Melgar P, Arandilla A, Garratt AN, Zang H, Mukoyama YS, Chen H, Shou W, Ballestar E, Esteller M, Rojas A, Pérez-Pomares JM, de la Pompa JL.** Notch signaling is essential for ventricular chamber development. *Dev Cell* 12(3):415-429 (2007)
- Gude NA, Emmanuel G, Wu W, Cottage CT, Fischer K, Quijada P, Muraski JA, Alvarez R, Rubio M, Schaefer E, Sussman MA.** Activation of Notch-mediated protective signaling in the myocardium. *Circ Res* 102(9):1025-35 (2008)
- Hainaud P, Contreres JO, Villemain A, Liu LX, Plouet J, Tobelem G, Dupuy E.** The role of the vascular endothelial growth factor-Delta-like4 ligand/Notch4-ephrin B2 cascade in tumor vessel remodelling and endothelial functions. *Cancer Res* 66:8501-8510 (2006)
- Hamada Y, Kadokawa Y, Okabe M, Ikawa M, Coleman JR, Tsujimoto Y.** Mutation in ankyrin repeats of the mouse Notch2 gene induces early embryonic lethality. *Development* 126(15):3415-3424 (1999)
- Hatcher CJ, Diman NY, Kim MS, Pennisi D, Song Y, Goldstein MM, Mikawa T, Basson CT.** A role for Tbx5 in proepicardial cell migration during cardiogenesis. *Physiol Genomics* 18:129-140 (2004)
- Heil M, Eitenmüller I, Schmitz-Rixen TS, Schaper W.** Arteriogenesis versus angiogenesis: similarities and differences. *J Cell Mol Med* 10:45-55 (2006)
- Hellström M, Kalén M, Lindahl P, Abramsson A, Betsholtz C.** Role of PDGF-B and PDGFR-beta in recruitment of vascular smooth muscle cells and pericytes during embryonic blood vessel formation in the mouse. *Development* 126:3047-2055 (1999)
- Hellström M, Phng LK, Hofmann JJ, Wallgard E, Coultas L, Lindblom P, Alva J, Nilsson AK, Karlsson L, Gaiano N, Yoon K, Rossant J, Iruela-Arispe ML, Kalén M, Gerhardt H, Betsholtz C.** Dll4 signalling through Notch1 regulates formation of tip cells during angiogenesis. *Nature* 445:776-780 (2007)
- High FA, Epstein JA.** The multifaceted role of Notch in cardiac development and disease. *Nature Reviews Genetics* 9:49-61 (2008)
- High FA, Lu MM, Pear WS, Loomes KM, Kaestner KH, Epstein JA.** Endothelial expression of the Notch ligand Jagged1 is required for vascular smooth muscle development. *Proc Natl Acad Sci USA* 105(6):1955-1959 (2008)
- Hill JH, Ward PA.** The phlogistic role of C3 leukotactic fragments in myocardial infarcts of rats. *J Exp Med* 133:885-900 (1971)
- Hiratochi M, Nagase H, Kuramochi Y, Koh CS, Ohkawara T, Nakayama K.** The Delta intracellular domain mediates TGF-beta/Activin signaling through binding to Smads and has an important bi-directional function in the Notch-Delta signaling pathway. *Nucleic Acids Res* 35(3):912-22 (2007)
-

-
- Hofmann JJ, Iruela-Arispe ML.** Notch Signaling in Blood Vessels: Who Is Talking to Whom About What? *Circ Res* 100:1556-1568 (2007)
- Hori M, Nishida K.** Oxidative stress and left ventricular remodelling after myocardial infarction. *Cardiovasc Res* 81:457-464 (2009)
- Horowitz A, Simons M.** Branching Morphogenesis. *Circ Res* 103:784-795 (2008)
- Hozumi K, Negishi N, Suzuki D, Abe N, Sotomaru Y, Tamaoki N, Mailhos C, Ish-Horowicz D, Habu S, Owen MJ.** Delta-like 1 is necessary for the generation of marginal zone B cells but not T cells *in vivo*. *Nature Immunology* 5(6):638-644 (2004)
- Hrabé de Angelis M, McIntyre J, Gossler A.** Maintenance of somite borders in mice requires the *Delta* homologue *Dll1*. *Nature* 386:717-721 (1997)
- Huether SE, McCance KL.** Understanding Pathophysiology. 2nd edition, C.V. Mosby (2000)
- Iso T, Hamamori Y, Kedes L.** Notch Signaling in Vascular Development. *Arterioscler Thromb Vasc Biol* 23:543-553 (2003)
- Jugdutt BI.** Ventricular Remodeling After Infarction and the Extracellular Collagen Matrix: When Is Enough Enough? *Circulation* 108:1395-1403 (2003)
- Karsan A.** The role of notch in remodeling and maintaining the vasculature. *Can J Physiol Pharmacol* 83:14-23 (2005)
- Kirby ML, Waldo KL.** Molecular Embryogenesis of the Heart. *Pediatr Dev Pathol* 5(6):516-543 (2002)
- Kopan R, Ilagan MXG.** The Canonical Notch Signaling Pathway: Unfolding the Activation Mechanism. *Cell* 137:216-233 (2009)
- Kratsios P, Catela C, Salimova E, Huth M, Berno V, Rosenthal N, Mourkioti F.** Distinct roles for cell-autonomous notch signaling in cardiomyocytes of the embryonic and adult heart. *Circ Res* 106(3):559-72 (2010)
- Krebs LT, Xue Y, Norton CR, Shutter JR, Maguire M, Sundberg JP, Gallahan D, Closson V, Kitajewski J, Callahan R, Smith GH, Stark KL, Gridley T.** Notch signaling is essential for vascular morphogenesis in mice. *Genes Dev* 14(11):1343-1352 (2000)
- Krebs LT, Iwai N, Nonaka S, Welsh IC, Lan Y, Jiang R, Saijoh Y, O'Brien TP, Hamada H, Gridley T.** Notch signaling regulates left-right asymmetry determination by inducing Nodal expression. *Genes Dev* 17(10):1207-12 (2003)
- Krebs LT, Shutter JR, Tanigaki K, Honjo T, Stark KL, Gridley T.** Haploinsufficient lethality and formation of arteriovenous malformations in Notch pathway mutants. *Genes Dev* 18(20):2469-2473 (2004)
- Kume T.** Novel insights into the differential functions of Notch ligands in vascular formation. *J Angiogenesis Res* 1:8 (2009)
-

-
- Kwee L, Baldwin HS, Shen HM, Stewart CL, Buck C, Buck CA, Labow MA.** Defective development of the embryonic and extraembryonic circulatory systems in vascular cell adhesion molecule (VCAM-1) deficient mice. *Development* 121:489-503 (1995)
- Lai EC.** Keeping a good pathway down: transcriptional repression of Notch pathway target genes by CSL proteins. *EMBO reports* 3(9):840-845 (2002)
- Lai EC.** Notch signaling: control of cell communication and cell fate. *Development* 131:965-973 (2004)
- Laflamme MA, Murry CE.** Regenerating the heart. *Nature Biotechnology* 23(7):845-856 (2005)
- LaVoie MJ, Selkoe DJ.** The Notch ligands, Jagged and Delta, are sequentially processed by alpha-secretase and presenilin/gamma-secretase and release signaling fragments. *J Biol Chem* 278(36):34427-37 (2003)
- Lawson ND, Scheer N, Pham VN, Kim CH, Chitnis AB, Campos-Ortega JA, Weinstein BM.** Notch signaling is required for arterial-venous differentiation during embryonic vascular development. *Development* 128:3675-3683 (2001)
- Lawson ND, Vogel AM, Weinstein BM.** Sonic hedgehog and vascular endothelial growth factor act upstream of the Notch pathway during arterial endothelial differentiation. *Dev Cell* 3:127-136 (2002)
- Limbourg A, Ploom M, Elligsen D, Sørensen I, Ziegelhoeffer T, Gossler A, Drexler H, Limbourg FP.** Notch Ligand Delta-Like 1 Is Essential for Postnatal Arteriogenesis. *Circ Res* 100:363-371 (2007)
- Limbourg A, Napp CL, Winter C, Hu L, Elligsen D, Airik M, Woiterski J, Lozanovski V, Getzin T, Meier M, Larmann J, Sadoni N, Adams S, Theilmeier G, Drexler H, Adams RH, Limbourg FP.** The Balance between Vascular Regeneration and Chronic Inflammation is Regulated by Macrophage Notch Signalling. *in review* February 2010
- Limbourg FP, Takeshita K, Radtke F, Bronson RT, Chin MT, Liao JK.** Essential Role of Endothelial Notch1 in Angiogenesis. *Circulation* 111:1826-1832 (2005)
- Liu H, Kennard S, Lilly B.** Notch3 expression is induced in mural cells through an autoregulatory loop that requires endothelial-expressed Jagged1. *Circ Res* 104:466-475 (2009)
- Loomes KM, Underkoffler LA, Morabito J, Gottlieb S, Piccoli DA, Spinner NB, Baldwin HS, Oakey RJ.** The expression of Jagged1 in the developing mammalian heart correlates with cardiovascular disease in Alagille syndrome. *Hum Mol Genet* 8(13):2443-2449 (1999)
- Loomes KM, Taichman DB, Glover CL, Williams PT, Markowitz JE, Piccoli DA, Baldwin HS, Oakey RJ.** Characterization of Notch receptor expression in the developing mammalian heart and liver. *Am J Med Genet* 112(2):181-189 (2002)
-

- Luttun A, Carmeliet P.** De novo vasculogenesis in the heart. *Cardiovasc Res* 58:378-389 (2003)
- Mailhos C, Modlich U, Lewis J, Harris A, Bicknell R, Ish-Horowicz D.** Delta4, an endothelial specific notch ligand expressed at sites of physiological and tumor angiogenesis. *Differentiation* 69:135-144 (2001)
- Markkanen JE, Rissanen TT, Kivelä A, Ylä-Herttuala S.** Growth factor-induced therapeutic angiogenesis and arteriogenesis in the heart – gene therapy. *Cardiovasc Res* 65:656-664 (2005)
- McCright B.** Notch signaling in kidney development. *Curr Opin Nephrol Hypert* 12:5-10 (2003)
- McCright B, Gao X, Shen L, Lozier J, Lan Y, Maguire M, Herzlinger D, Weinmaster G, Jiang R, Gridley T.** Defects in development of the kidney, heart and eye vasculature in mice homozygous for a hypomorphic Notch2 mutation. *Development* 128:491-502 (2001)
- Miele L.** Notch Signaling. *Clin Cancer Res* 12(4):1074-1079 (2006)
- Mishra-Gorur K, Rand MD, Perez-Villamil B, Artavanis-Tsakonas S.** Down-regulation of Delta by proteolytic processing. *J Cell Biol* 159(2):313-24 (2002)
- Monvoisin A, Alva JA, Hofmann JJ, Zovein AC, Lane TF, Iruela-Arispe ML.** VE-cadherin-CreER^{T2} Transgenic Mouse: A Model for Inducible Recombination in the Endothelium. *Dev Dynamics* 235:3413-3422 (2006)
- Morabito CJ, Kattan J, Bristow J.** Mechanisms of embryonic coronary artery development. *Curr Opin Cardiol* 17:235-241 (2002)
- Moriyama Y, Sekine C, Koyanagi A, Koyama N, Ogata H, Chiba S, Hirose S, Okumura K, Yagita H.** Delta-like 1 is essential for the maintenance of marginal zone B cells in normal mice but not in autoimmune mice. *Int Immunol* 20(6):763-773 (2008)
- Morrow D, Guha S, Sweeney C, Birney Y, Walshe T, O'Brien C, Walls D, Redmond EM, Cahill PA.** Notch and Vascular Smooth Muscle Cell Phenotype. *Circ Res* 103:1370-1382 (2008)
- Mosser DM, Edwards JP.** Exploring the full spectrum of macrophage activation. *Nature Rev Immunol* 8:958-969 (2008)
- Nahrendorf M, Swirski FK, Aikawa E, Stangenberg L, Wurdinger T, Figueiredo J-L, Libby P, Weissleder R, Pittet M.** The healing myocardium sequentially mobilizes two monocyte subsets with divergent and complementary functions. *J Exp Med* 204:3037-3047 (2007)
- Nemir M, Pedrazzini T.** Functional role of Notch signaling in the developing and postnatal heart. *J Mol Cell Cardiol* 45:495-504 (2008)
- Niessen K, Karsan A.** Notch signaling in the developing cardiovascular system. *Am J Physiol Cell Physiol* 293:1-11 (2007)

-
- Niessen K, Karsan A.** Notch Signaling in Cardiac Development. *Circ Res* 102:1169-1181 (2008)
- Nijjar SS, Crosby HA, Wallace L, Hubscher SG, Strain AJ.** Notch receptor expression in adult human liver: a possible role in bile duct formation and hepatic neovascularization. *Hepatology* 34(6):1184-1192 (2001)
- Oyama J, Blais C Jr, Liu X, Pu M, Kobzik L, Kelly RA, Bourcier T.** Reduced myocardial ischemia-reperfusion injury in toll-like receptor 4-deficient mice. *Circulation* 109:784-789 (2004)
- Patel NS, Li JL, Generali D, Poulson R, Cranston DW, Harris AL.** Upregulation of delta-like 4 ligand in human tumor vasculature and the role in basal expression in endothelial cell function. *Cancer Res* 65:8690-8697 (2005)
- Phng L-K, Gerhardt H.** Angiogenesis: A Team Effort Coordinated by Notch. *Dev Cell* 16:196-208 (2009)
- Phng LK, Potente M, Leslie JD, Babbage J, Nyqvist D, Lobov I, Ondr JK, Rao S, Lang RA, Thurston G, Gerhardt H.** Nrarp coordinates endothelial Notch and Wnt signaling to control vessel density in angiogenesis. *Dev Cell* 16(1):70-82 (2009)
- Pfeffer JM, Pfeffer MA, Fletcher PJ, Braunwald E.** Ventricular Performance in Rats with Myocardial Infarction and Failure. *Am J Med* 76(5B):99-103 (1984)
- Pfeffer MA.** Left Ventricular Remodeling After Acute Myocardial Infarction. *Annu Rev Med* 46:455-466 (1995)
- Pfeffer MA, Braunwald E.** Ventricular remodeling after myocardial infarction. Experimental observations and clinical implications. *Circulation* 81:1161-1172 (1990)
- Pfeffer MA, Pfeffer JM, Fishbein MC, Fletcher PJ, Sparado J, Kloner RA, Braunwald E.** Myocardial infarct size and ventricular function in rats. *Circ Res* 44:503-512 (1979)
- Pfister S, Przemeck GK, Gerber JK, Beckers J, Adamski J, Hrabé de Angelis M.** Interaction of the MAGUK family member Acvrin1 and the cytoplasmic domain of the Notch ligand Delta1. *J Mol Biol* 333(2):229-35 (2003)
- Pinckard RN, Olson MS, Giclas PC, Terry R, Boyer JT, O'Rourke RA.** Consumption of classical complement components by heart subcellular membranes in vitro and in patients after acute myocardial infarction. *J Clin Invest* 56:740-750 (1975)
- Przemeck GKH, Heinzmann U, Beckers J, Hrabé de Angelis M.** Node and midline defects are associated with left-right development in Delta1 mutant embryos. *Development* 130:3-13 (2003)
- Porter KE, Turner NA.** Cardiac fibroblasts: At the heart of myocardial remodeling. *Pharmacology & Therapeutics* 123:255-278 (2009)
-

- Qi H, Rand MD, Wu X, Sestan N, Wang W, Rakic P, Xu T, Artavanis-Tsakonas S.** Processing of the notch ligand delta by the metalloprotease Kuzbanian. *Science* 283:91-94 (1999)
- Reese DR, Mikawa T, Bader DM.** Development of the Coronary Vessel System. *Circ Res* 91:761-768 (2002)
- Riad A, Jäger S, Sobirey M, Escher F, Yaulema-Riss A, Westermann D, Karatas A, Heimesaat MM, Bereswill S, Dragun D, Pauschinger M, Schultheiss HP, Tschöpe C.** Toll-like receptor-4 modulates survival by induction of left ventricular remodeling after myocardial infarction in mice. *J Immunol* 180:6954-6961 (2008)
- Risau W.** Mechanisms of angiogenesis. *Nature* 386:671-674 (1997)
- Risau W, Flamme I.** Vasculogenesis. *Annu Rev Cell Dev Biol* 11:73-91 (1995)
- Roca C, Adams RH.** Regulation of vascular morphogenesis by Notch signaling. *Genes Dev* 21:2511-2524 (2007)
- Rossen RD, Michael LH, Kagiya A, Savage HE, Hanson G, Reisberg MA, Moake JN, Kim SH, Self D, Weakley S.** Mechanism of complement activation after coronary artery occlusion: evidence that myocardial ischemia in dogs causes release of constituents of myocardial subcellular origin that complex with human C1q in vivo. *Circ Res* 62:572-584 (1988)
- Rossen RD, Michael LH, Hawkins HK, Youker K, Dreyer WJ, Baughn RE, Entman ML.** Cardiolipin-protein complexes and initiation of complement activation after coronary artery occlusion. *Circ Res* 75:546-555 (1994)
- Rubio-Aliaga I, Soewarto D, Wagner S, Kluft M, Fuchs H, Kalaydjiev S, Busch DH, Klempt M, Rathkolb, Wolf E, Abe K, Zeiser S, Przemeck GKH, Beckers J, Hrabé de Angelis M.** A Genetic Screen for the Modifiers of the Delta1-Dependent Notch Signaling Function in the Mouse. *Genetics* 175:1451-1463 (2007)
- Salto-Tellez M, Yung Lim S, El-Oakley RM, Tang TP, Almsherqi ZA, Lim SK.** Myocardial infarction in the C57BL/6J mouse: a quantifiable and highly reproducible experimental model. *Cardiovasc Pathol* 13(2):91-97 (2004)
- Schaper W.** Theory of Arteriogenesis. In *Arteriogenesis, edited by Schaper W and Schaper J, 1st edition, Springer Netherlands* (2004)
- Schuster-Gossler K, Cordes R, Gossler A.** Premature myogenic differentiation and depletion of progenitor cells cause severe muscle hypotrophy in Delta1 mutants. *Proc Natl Acad Sci USA* 104(2):537-542 (2007)
- Shishido T, Nozaki N, Yamaguchi S, Shibata Y, Nitobe J, Miyamoto T, Takahashi H, Arimoto T, Maeda K, Yamakawa M, Takeuchi O, Akira S, Takeishi Y, Kubota I.** Toll-like receptor-2 modulates ventricular remodeling after myocardial infarction. *Circulation* 108:2905-2910 (2003)

-
- Shutter JR, Scully S, Fan W, Richards WG, Kitajewski J, Deblandre GA, Kintner CR, Stark KL.** Dll4, a novel Notch ligand expressed in arterial endothelium. *Genes Dev* 14(11):1313-1318 (2000)
- Siekman AF, Lawson ND.** Notch signalling limits angiogenic cell behaviour in developing zebrafish arteries. *Nature* 445:781-784 (2007)
- Simons M.** Angiogenesis: Where Do We Stand Now? *Circulation* 111:1556-1566 (2005)
- Six E, Ndiaye D, Laabi Y, Brou C, Gupta-Rossi N, Israel A, Logeat F.** The Notch ligand Delta1 is sequentially cleaved by an ADAM protease and gamma-secretase. *Proc Natl Acad Sci USA* 100(13):7638-43 (2003)
- Smart N, Dubé KN, Riley PR.** Coronary vessel development and insights towards neovascular therapy. *Int J Exp Path* 90:262-283 (2009)
- Smart N, Risebro CA, Melville AA, Moses K, Schwartz RJ, Chien KR, Riley PR.** Thymosin beta4 induces adult epicardial progenitor mobilization and neovascularization. *Nature* 445:177-182 (2007)
- Soriano P.** Generalized *lacZ* expression with the ROSA26 Cre reporter strain. *Nature Genetics* 21:70-71 (1999)
- Sörensen I, Adams RH, Gossler A.** DLL1-mediated Notch activation regulates endothelial identity in mouse fetal arteries. *Blood* 113(22):5680-5688 (2009)
- Stavrou D.** Neovascularization in wound healing. *J Wound Care* 17:298-302 (2008)
- Suchting S, Freitas C, le Noble F, Benedito R, Bréant C, Duarte A, Eichmann A.** The Notch ligand Delta-like 4 negatively regulates endothelial tip cell formation and vessel branching. *Proc Natl Acad Sci USA* 104(9):3225-3230 (2007)
- Swiatek PJ, Lindsell CE, del Arno FF, Weinmaster G, Gridley T.** Notch1 is essential for postimplantation development in mice. *Genes Dev* 8:707-719 (1994)
- Swift MR, Weinstein BM.** Arterial-Venous Specification During Developmet. *Circ Res* 104:576-588 (2009)
- Swirski FK, Nahrendorf M, Etzrodt M, Wildgruber M, Cortez-Retamozo V, Panizzi P, Figueiredo JL, Kohler RH, Chudnovskiy A, Waterman P, Aikawa E, Mempel TR, Libby P, Weissleder R, Pittet MJ.** Identification of splenic reservoir monocytes and their deployment to inflammatory sites. *Science* 325:612-616 (2009)
- Takagawa J, Zhang Y, Wong ML, Sievers RE, Kapasi NK, Wang Y, Yeghiazarians Y, Lee RJ, Grossmann W, Springer ML.** Myocardial infarct size measurement in the mouse chronic infarction model: comparison of area- and length-based approaches. *J Appl Physiol* 102:2104-2111 (2007)
- Texas Heart Institute.** http://www.texasheart.org/HIC/ProjH/images/coronary_arteries.gif (website as at February 2010)
-

-
- Tien A-C, Rajan A, Bellen HJ.** A Notch updated. *J Cell Biol* 184:621-629 (2009)
- Timmerman LA, Grego-Bessa J, Raya A, Bertrán E, Pérez-Pomares JM, Díez J, Aranda S, Palomo S, McCormick F, Izpisua-Belmonte JC, de la Pompa JL.** Notch promotes epithelial-mesenchymal transition during cardiac development and oncogenic transformation. *Genes Dev* 18(1):99-115 (2004)
- Tiyyagura SR, Pinney SP.** Left Ventricular Remodeling after Myocardial Infarction: Past, Present, and Future. *The Mount Sinai Journal of Medicine* 73:840-851 (2006)
- Tomanek RJ.** Formation of the coronary vasculature during development. *Angiogenesis* 8:273-284 (2005)
- Tomanek RJ, Zheng W.** Role of growth factors in coronary morphogenesis. *Tex Heart Inst J* 29:250-254 (2002)
- Torres-Vázquez J, Kamei M, Weinstein BM.** Molecular distinction between arteries and veins. *Cell Tissue Res* 314:43-59 (2003)
- Van den Akker NM, Winkel LC, Nisancioglu MH, Maas S, Wisse LJ, Armulik A, Poelmann RE, Lie-Venema H, Betsholtz C, Gittenberger-de Groot AC.** PDGF-B signaling is important for murine cardiac development: its role in developing atrioventricular valves, coronaries, and cardiac innervation. *Dev Dyn* 237:494-503 (2008)
- van Royen N, Piek JJ, Schaper W, Bode C, Buschmann I.** Arteriogenesis: Mechanisms and modulation of coronary artery development. *J Nucl Cardiol* 8:687-693 (2001)
- Villa N, Walker L, Lindsell CE, Gasson J, Iruela-Arispe ML, Weinmaster G.** Vascular expression of Notch pathway receptors and ligands is restricted to arterial vessels. *Mech Dev* 108:161-164 (2001)
- Visual Sonics.** Manual: Vevo 770[®] Standard Measurements and Calculations, Rev 1.5.
- Wang HU, Chen ZF, Anderson DJ.** Molecular distinction and angiogenic interaction between embryonic arteries and veins revealed by ephrin-B2 and its receptor EphB4. *Cell* 93:741-753 (1998)
- Watt AJ, Battle MA, Li J, Duncan SA.** GATA4 is essential for formation of the proepicardium and regulates cardiogenesis. *Proc Natl Acad Sci USA* 101:12573-12578 (2004)
- Whelan RS, Mani K, Kitsis RN.** Nipping at cardiac remodeling. *J Clin Inv* 117:2751-2753 (2007)
- Whittaker P, Kloner RA, Boughner DR, Pickering JG.** Quantitative assessment of myocardial collagen with picosirius red staining and circularly polarized light. *Basic Res Cardiol* 89:397-410 (1994)
- Whittaker P.** Collagen organization in wound healing after myocardial injury. *Basic Res Cardiol* 93:Suppl 3, 23-25 (1998)
-

Xue Y, Gao X, Lindsell CE, Norton CR, Chang B, Hicks C, Gendron-Maguire M, Rand EB, Weinmaster G, Gridley T. Embryonic lethality and vascular defects in mice lacking the Notch ligand Jagged1. *Hum Mol Genet* 8(5):723-730 (1999)

Yasojima K, Schwab C, McGeer EG, McGeer PL. Human heart generates complement proteins that are upregulated and activated after myocardial infarction. *Circ Res* 83:860-869 (1998)

You LR, Lin FJ, Lee CT, DeMayo FJ, Tsai MJ, Tsai SY. Suppression of Notch signalling by the COUP-TFII transcription factor regulates vein identity. *Nature* 435:98-104 (2005)

Zaffran S, Frasch M. Early Signals in Cardiac Development. *Circ Res* 91:457-469 (2002)

Zhong TP, Rosenberg M, Mohideen MA, Weinstein B, Fishman MC. gridlock, an HLH gene required for assembly of the aorta in zebrafish. *Science* 287:1820-1824 (2000)

Zhong TP, Childs S, Leu JP, Fishman MC. Gridlock signalling pathway fashions the first embryonic artery. *Nature* 414:216-220 (2001)

Zornoff LAM, Paiva SAR, Duarte DR, Spadaro J. Ventricular Remodeling after Myocardial Infarction: Concepts and Clinical Implications. *Arq Bras Cardiol* 92:150-156 (2009)

APPENDIX

Publications

Publications in review/in preparation

Limbourg A, Napp LC, Winter C, Hu L, Elligsen D, Airik M, Woiterski J, Lozanovski V, Getzin T, Meier M, Larmann J, Sadoni N, Adams S, Theilmeyer G, Drexler H, Adams RH, Limbourg FP.

The Balance between Vascular Regeneration and Chronic Inflammation is Regulated by Macrophage Notch Signalling.

Manuscript in review

Woiterski J, Limbourg A, Schnabel S, Napp LC, Korf-Klingebiel M, Wollert K, Drexler H, Limbourg FP.

Regulation of adverse cardiac remodelling by the Notch ligand Delta-like 1.

Manuscript in preparation

Augustynik M, Napp LC, Woiterski J, Limbourg A, Drexler H, Limbourg FP.

Regulation of arterial branching morphogenesis by Delta-like 1.

Manuscript in preparation

Conference participations

Abstract presentations

Jeschke J, Limbourg A, Schnabel S, Napp LC, Sauer PTD, Wollert K, Drexler H, Limbourg FP.

Essential role of Notch ligand Delta-like 1 in coronary arteriogenesis and cardiac recovery after myocardial infarction.

European Society of Cardiology Congress 2008, Munich, Germany; August/September 2008

Jeschke J, Limbourg A, Schnabel S, Napp LC, Sauer PTD, Wollert K, Drexler H, Limbourg FP.

Essential role of Notch ligand Delta-like 1 in coronary arteriogenesis and cardiac recovery after myocardial infarction.

Heart Failure 2008, Milan, Italy; June 2008 – Young Investigator Award Session

Jeschke J, Limbourg A, Schnabel S, Templin C, Adams RH, Drexler H, Limbourg FP.

Notch Signalling in Coronary Arteries: Notch Ligand Delta-like1 Regulates Coronary Artery Numbers and is Protective in Myocardial Infarction.

American Heart Association Scientific Sessions 2007, Orlando, USA; November 2007

Jeschke J, Schantz J-T, Chong WS, Foo TT, Pua CM, Hutmacher DW.
Development and Evaluation of a Spherical, Bi-Axial Rotating Bioreactor for Bone Tissue Engineering.
2nd World Congress on Regenerative Medicine, Leipzig, Germany; May 2005

Poster presentation

Woiterski J, Limbourg A, Schnabel S, Napp LC, Korf-Klingebiel M, Wollert K, Drexler H, Limbourg FP.
Essential role of Notch ligand Delta-like 1 in coronary arteriogenesis and cardiac recovery after myocardial infarction.
Deutsche Gesellschaft für Kardiologie - Jahrestagung 2009, Mannheim, Germany; April 2009

Acknowledgements

First I would like to thank Prof. Kispert, Prof. Schlegelberger and Prof. Scheper for their willingness to act as examiner of this thesis.

Mainly, I owe Dr. Florian Limbourg a large debt of gratitude for supervision and guidance throughout my studies. I thank him for all valuable discussions and advice, as well as for teaching fundamental basics of how to structure and carry out evidence based research in the life sciences. His encouraging words, personal commitment and enthusiasm for scientific research and Notch signalling helped a lot when no experiment seemed to work.

In addition, I thank Dr. Anne Limbourg for teaching most of the skills needed for this project: from mouse work over cryosectioning until staining. She always had some good advice on how to improve a protocol and helped with practical skills when needed.

Furthermore, I am very thankful to Sabine Schnabel for performing the LAD ligation operations and Dr. Mortimer Korf-Klingebiel for performing the echocardiographies (and patient answering of all related questions), thereby providing so essential data for this thesis. I thank Christine Winter for providing the FACS data on monocyte subsets and valuable discussions on this issue.

My warmest thanks also to my colleagues and friends Dr. Merlin Airik, Jennifer Bonse and Dr. Christian Napp. Lab life would not have been the same without you and your support.

I also thank Anja Quint, Anna Kanwischer and Eva Brinkmann from the Wollert' lab for their friendship and helping out with chemicals and reagents.

To all research staff of the cardiology department: your support, friendship, heart lifting humour, and most funny lunches added to a daily lab life that was never dreary.

Not to forget, I would like to thank my parents and brothers for their love, never ending support, and encouragement which has always accompanied my life.

Lastly, to my husband Roman and my little son Arne. No words can express my deep gratitude for your unconditional love, support, and understanding. You always remind me of the things most important in life.

Curriculum Vitae

Personal Details

<i>Name</i>	Jeanette Woiterski, née Jeschke
<i>Date and Place of Birth</i>	3 August 1981, Frankfurt (Oder), Germany
<i>Family status</i>	Married, 1 child
<i>Nationality</i>	German
<i>Languages</i>	German, English, Spanish

Education

<i>University</i>	Graduate studies Leibniz University Hannover, Hannover, Germany since April 2008 Degree: Master of Science in Biotechnology Mannheim University of Applied Sciences, Mannheim, Germany March 2005 – September 2006 Degree: Bachelor of Science with Honours in Biotechnology Mannheim University of Applied Sciences, Mannheim, Germany October 2001 – February 2005
<i>High School</i>	Abitur Carl-Friedrich-Gauss-Gymnasium, Frankfurt (Oder), Germany August 1994 – July 2001

Work Experience

<i>Dissertation</i>	Hannover Medical School, Hannover, Germany Institute of Cardiology and Angiology, Limbourg Lab October 2006 – June 2009 Title: “Essential role of the Notch ligand Delta-like 1 in coronary arteriogenesis and cardiac recovery after myocardial infarction.”
<i>Master-Thesis</i>	Max-Planck-Institute for Heart and Lung Research, Bad Nauheim, Germany April 2006 – September 2006 Title: “Generation of Lenti- and Adenoviral Gene Expression Systems for In Vivo and In Vitro Applications on Amphibian Newt Heart Tissue”
<i>Bachelor-Thesis</i>	National University of Singapore – Tissue Engineering Laboratory and Singapore Polytechnic – Technology Centre for Life Sciences, Singapore September 2004 – February 2005 Title: “Evaluation of a Spherical, Bi-Axial Rotating Bioreactor for Tissue Engineering Applications”
<i>Traineeship</i>	Biobest Laboratories Ltd, Edinburgh, Great Britain August 2003 – February 2004 Position: Assistant Virologist

Lab Projects Mannheim University of Applied Sciences, Mannheim, Germany
January 2006 – March 2006
Institute of Molecular and Cell Biology
Project II: “Cloning and Expression of Four Huntingtin-JRed Fusion Proteins for
Aggregational Studies in Huntington’s Disease”

Mannheim University of Applied Sciences, Mannheim, Germany
August 2005 – November 2005
Institute of Molecular and Cell Biology
Project I: “Neuronal Differentiation and Optimization of Transfection of the Cell
Lines NTERA-2 cl.D1, PC-12 and SH-SY5Y”

Miscellaneous maternity leave since July 2009